Electric Field Distribution and Neuron Electrodynamics for Deep Brain Stimulation

Thomas Tarnaud

Supervisors: Prof. dr. ir. Wout Joseph, Prof. dr. ir. Luc Martens
Counsellors: Prof. dr. ir. Emmeric Tanghe, Dr. ir. Günter Vermeeren

Master's dissertation submitted in order to obtain the academic degree of
Master of Science in Engineering Physics

Department of Information Technology
Chair: Prof. dr. ir. Daniël De Zutter
Faculty of Engineering and Architecture
Academic year 2015-2016

UNIVERSITEIT GENT

Electric Field Distribution and Neuron Electrodynamics for Deep Brain Stimulation

Thomas Tarnaud

Supervisors: Prof. dr. ir. Wout Joseph, Prof. dr. ir. Luc Martens
Counsellors: Prof. dr. ir. Emmeric Tanghe, Dr. ir. Günter Vermeeren

Master's dissertation submitted in order to obtain the academic degree of
Master of Science in Engineering Physics

Department of Information Technology
Chair: Prof. dr. ir. Daniël De Zutter
Faculty of Engineering and Architecture
Academic year 2015-2016

UNIVERSITEIT GENT

Acknowledgments

First, I would like to thank my counsellor, prof. dr. ir. Emmeric Tanghe, for guiding me through the process of this master thesis. He always took the time to discuss results and to answer my questions. He came up with some important key insights, without which this thesis would certainly not have been the same. Furthermore he gave me the freedom to research my own interests in the interesting subject of electromagnetic neurostimulation.

I would like to thank dr. ir. Günter Vermeeren and ir. Amine Samoudi for taking the time to answer my technical and theoretical questions on the Sim4life software, that was used to simulate the electromagnetic field distribution in this thesis. I would also like to thank my supervisors, prof. dr. ir. Wout Joseph and prof. dr. ir. Luc Martens.

Thomas Tarnaud, May 2016.

Copyright statement

Abstract

The electric field distribution excited by a Medtronic lead (Mo. 3389, Medtronic Inc., Minneapolis, MN, USA) in deep brain stimulation was simulated by the low-frequency electroquasistatic (FEM) solver in Sim4life (Sim4life, ZMT Zurich MedTech AG). The simulations are performed in the high-resolution head and neck model, called MIDA. The dependency of electric field distribution on the frequency of the applied stimulus current was studied and it was found that the distribution is approximately independent of frequency. An approximation for the assessment of the electric field distribution excited by a biphasic square-wave is then proposed.

The simulated electromagnetic field was subsequently used to calculate the transmembrane voltage and gate-parameters during two square-wave periods on the neurons of the lenticular fasciculus (LF) and macaca fascicularis (MF). For this end a program was written in Matlab (MATLAB 8.6, The MathWorks Inc., Natick, MA, 2000). The neurons were modelled as straight multi-compartmental fibers. In this way different specialised neuronal models can be used for different parts of the neuron. The resulting differential equations were discretised by the Crank-Nicolson scheme and iterated in the Matlab program. The percentage of activated neurons ($\%AN$) was also determined by the Matlab code. A comparison was made for the $\%AN$ in the LF and MF for two stimulation set-ups in deep brain stimulation.

The Matlab code was first tested for several more simple configurations. The stimulation of a single straight neuron and a neuron bending at a specific location were studied and compared for both cathode-make and anode-make stimulation. The different mechanisms by which neuronal activation occurs is subsequently discussed. Matlab was furthermore programmed to calculate the mean propagation velocity of the action potential. Also some simple bundles of multiple neurons were simulated and the influence of the distance between the bundle and the electrode on the neuronal activation was assessed.

Keywords: electric field distribution, transmembrane voltage, gate-parameters, neuronal activation, deep brain stimulation

Electric Field Distribution and Neuron Electrodynamics for Deep Brain Stimulation

Thomas Tarnaud

Supervisors: Prof. dr. ir. Wout Joseph, Prof. dr. ir. Luc Martens
Counsellors: Prof. dr. ir. Emmeric Tanghe, Dr. ir. Günter Vermeeren

Abstract—**In this work, a program in Matlab (MATLAB 8.6, The MathWorks Inc., Natick, MA, 2000) was written to solve for the membrane-voltage and gate-parameters in a general multi-compartmental neuron and in bundles of multiple neurons. The Matlab-program was coupled with electromagnetic simulations in Sim4life (Sim4life, ZMT Zurich MedTech AG), to obtain the neuronal response to an electromagnetic field distribution that is excited by one or more electrodes. Simulations on single neurons are done to determine the influence of the electrode configuration and neuronal boundary conditions on the membrane-voltage and gate-parameters. Furthermore electromagnetic simulations in a high-resolution head and neck model (MIDA) are coupled with the calculation in Matlab of the percentage of activated neurons in the lenticular fasciculus and macaca fascicularis, to mimic a typical DBS-configuration.**

Keywords— **electric field distribution, transmembrane voltage, gate-parameters, neuronal activation, deep brain stimulation**

I. Introduction

In deep brain stimulation (DBS) an electrode or lead is surgically placed in the brain of the patient. An electromagnetic field, that will stimulate the surrounding neuronal tissue, is subsequently excited around the electrode. This will lead to increased or decreased firing in the bundles of neurons, neighbouring the electrode. The goal is to reduce symptoms in patients suffering from a wide range of neurological disorders, f.i. Parkinson disease (Benabid et al.,2003 [1]), essential tremor (Benabid et al,1996 [2]), dystonia (Kupschl et al.,2006 [3]), treatment-resistant depression (Maybergh et al.,2005 [4]), obsessive-compulsive disorder (Nuttin et al.,2003 [5]) and epilepsy (Hodaie et al.,2002 [6]).

To study electromagnetic neurostimulation a program was written in Matlab (MATLAB 8.6, The MathWorks Inc., Natick, MA, 2000) that will solve a multi-compartmental neuron, that is exposed to an electric field distribution, for the membrane-voltage and gate-parameters. The electromagnetic field distribution will first be simulated in Sim4life (Sim4life, ZMT Zurich MedTech AG) and will subsequently be exported to Matlab, to be used as a source-term in the neuronal models. In total six different neuronal models were implemented in Matlab[1]. This way it is possible to describe each structure of the neuron with the most appropriate neuron model. For instance, for the nodes of Ranvier the CRRSS-model was chosen, while for the synapse a (warm) Hodgkin-Huxley model was applied. An overview of the different neuron models is given in Rattay (2005) [7]. The differential equations of each neuronal model were discretized by a Crank-Nicholson scheme and the resulting matrix-equations can subsequently be iterated in Matlab.

[1] Passive (transmissionline) model, Hodgkin-Huxley (HH) model, Frankenhaeuser-Huxley (FH) model, Chiu-Ritchie-Rogert-Stagg-Sweeney (CRRSS) model, Schwarz-Eikhof (SE) model and Scwharz-Reid-Bostock (SRB) model

First, some simulation results on isolated neurons will be discussed in section II. Secondly, simulations on bundles of multiple neurons are presented in section III.

II. Simulations on single neurons

In this section we will discuss results of simulations that are done on single isolated neurons[2], stimulated by a spherical electrode in homogeneous tissue. These simulations are relatively simple, but allow to draw some general conceptual conclusions. For example, these simulations allow to determine the influence of different factors on the membrane-voltage, gate-parameters and neuronal activation. Different factors and parameters that were varied in order to study their influence on the neuron will be briefly discussed in this section: the distance d_{elec} between the neuron and the electrode (subsection II-B), the location of the electrode along the neuron (subsection II-D), the electrode-voltage (subsection II-C and subsection II-A), the applied neuronal boundary conditions (subsection II-F) and the angle over which the neuron bends (subsection II-E).

A. Anode-make versus cathode-make stimulation

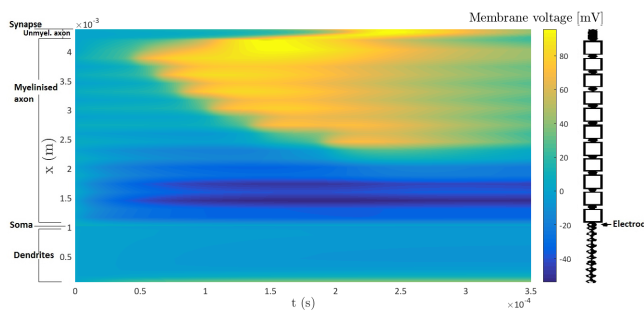

Fig. 1. Anode-make stimulation by a spherical electrode (60 V) at $2mm$ from the soma of a straight neuron. A colour map of the reduced membrane voltage is shown.

From theoretical considerations (Roth, 1993 [8]) it follows that the neuronal membrane right under the electrode will tend to hyperpolarise,[3] when the spherical stimulation electrode is an anode (i.e. a positive electrode-potential is applied). In other

[2] The electric and geometric parameters of the used multi-compartmental neuron are obtained from Rattay (2005) [7]

[3] The reduced membrane voltage $\tilde{V}$ is defined as: $\tilde{V} = V_i - V_e - V_r$. Here V_i is the intercellular potential, V_e is the extracellular potential, and V_r is the rest (Nernst) potential of the membrane. We say that the neuronal membrane depolarizes, if $\tilde{V} > 0$. Conversely, the membrane hyperpolarizes if $\tilde{V} < 0$.

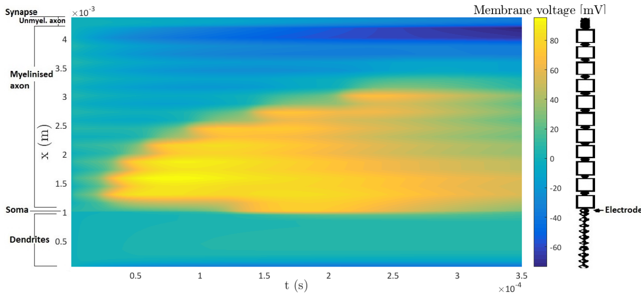

Fig. 2. Cathode-make stimulation by a spherical electrode (-60 V) at $2mm$ from the soma of a straight neuron. A colour map for the reduced membrane voltage $\tilde{V}$ is shown.

words, the of hyperpolarisation (RoH) on the neuron, is localized at the anode-position. Furthermore the neuron will tend to depolarise at the so-called "virtual" cathodes. There are two virtual cathodes: one at both sides of the anode. Ofcourse, the exact manifestation of this theory is dependent on the electrical parameters of the neuron.

Analogously, if the spherical stimulation electrode is a cathode, the neuron will tend to depolarize at the cathode. Two regions where the neuron tends to hyperpolarize are localized at the virtual anodes.

Stimulation by a spherical cathode, is called "cathode-make" (CM) stimulation, if the neuron is stimulated because the cathode is turned on[4]. Analogously we speak of anode-make (AM) stimulation when the spherical electrode is an anode.

Furthermore we notice that in the AM-stimulation the actionpotential will reach the synapse (at $x = 4.4mm$), which is not the case for CM-stimulation. This is due to the fact that in the latter case, the actionpotential is initiated at the beginning of the axon, and consequentially has a longer distance to travel to reach the synapse than in the case of AM-stimulation. Furthermore in CM-stimulation a region of hyperpolarization is present at the end of the axon, impeding the actionpotential in its way to the synapse.

In this section we will only compare the colour maps for the reduced membrane voltage produced by the Matlab program. However also plots for the spatial and temporal distribution of the voltage and gate-parameters (m, n, h and p) are generated by Matlab and can be compared. As an example we refer to a colour map for the m-gate parameter (Fig. 10) and a spatial distribution plot (Fig. 9) of the membrane voltage, in the appendix. These plots were generated in the simulation of AM-stimulation by a spherical electrode at $2mm$ from the soma. When an actionpotential is initiated, natrium-channels in the neuronal membrane will open. This is reflected by the m-gate parameter, that will increase towards unity. Note that the m-gate parameter will only increase on the active compartments (i.e. nodes of Ranvier, soma, the unmyelinated axon and the synapse) and will remain zero on passive compartments (f.i. myelinated internodes on the axon). This is a consequence of the fact that no natrium-gates are present in the myelinated parts of the neuron.

[4]In contrast, in cathode-break stimulation, the neuron is stimulated because the cathode is turned off (Roth (1993) [8])

B. Distance between the electrode and the neuron

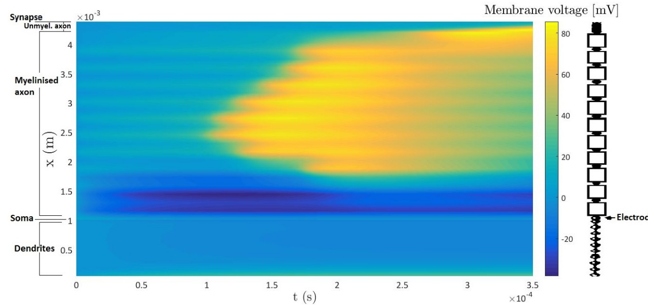

Fig. 3. Anode-make stimulation by a spherical electrode (10 V) at $1mm$ from the soma of a straight neuron. A colour map for the reduced membrane voltage $\tilde{V}$ is shown.

Secondly, we examine the role of the distance between the electrode and the neuron d_{elec}. For this end, we compare the results of AM-stimulation with an electrode at $2mm$ and at $1mm$ from the soma (Fig. 1 and Fig. 3 respectively). We observe that the distance d_{elec} determines the shape of the spatial distribution of the reduced voltage map. For instance the width of the RoH increases, with increasing d_{elec}. This result could be anticipated from a theoretical perspective: the distance between the anode and virtual cathodes can be calculated and increases with increasing d_{elec}.

C. Electrode-potential

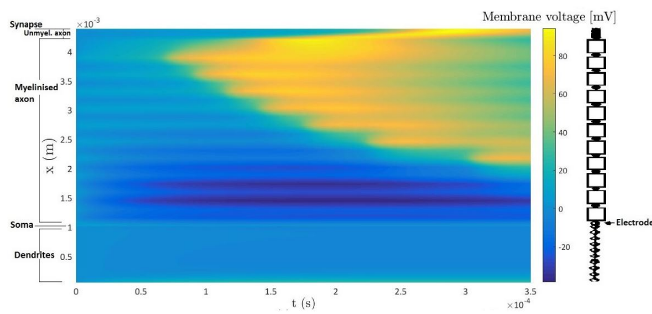

Fig. 4. Anode-make stimulation by a spherical electrode (40 V) at $2mm$ from the soma of a straight neuron. A colour map for the reduced membrane voltage $\tilde{V}$ is shown.

Note in the previous subsection (subsection II-B), that the electrode potential was also changed from $60V$ for AM-stimulation at $2mm$ (Fig. 1) to $10V$ for AM-stimulation at $1mm$ (Fig. 3)[5]. Nevertheless we observed for activated neurons, that the electrode-potential has little influence on the spatial distribution of the reduced membrane voltage. For instance, we compare anode-make stimulation by an electrode at $2mm$ from the soma of a neuron, at $40V$ (Fig. 4) and at $60V$ (Fig. 1).

[5]The idea is to approximately equalize the amount of power incident on the neuron. For instance, AM-stimulation at $2mm$ from the soma at an electrode-potential of $10V$ was also simulated. The neuron was however not activated in this case.

Both neurons are clearly activated and by comparing the voltage maps we conclude that the spatial distribution of the voltage was not significantly influenced by the electrode-potential. Also, a higher electrode potential will not lead to stronger depolarisation of the neuronal membrane. This is due to the fact that the system of equations to determine the membrane voltage $\tilde{V}$ is non-linear: as observed in literature (f.i. De Geeter, 2014 [9]) an all-or-nothing principle applies for the actionpotential. In contrast, the spatial distribution of the membrane voltage can qualitatively be predicted by the activation function f, defined in Rattay (2005) [7]. This activation function is linear in the electrode-potential, explaining the result that the spatial distribution of the membrane-voltage was maintained, while altering the electrode-potential.

The only difference between the result for AM-stimulation at $40V$ and AM-stimulation at $60V$, is a shift in time: a higher stimulus ($60V$), results in a faster initiation of the action potential.

We conclude that the spatial distribution of the membrane voltage is determined by d_{elec}, for an activated neuron. Lowering the electrode-potential will not alter the spatial distribution, but will delay the time of neuronal activation. If the electrode-potential is too low, no neuronal activation will occur at all during the simulation time.

D. Location of the electrode along the neuron

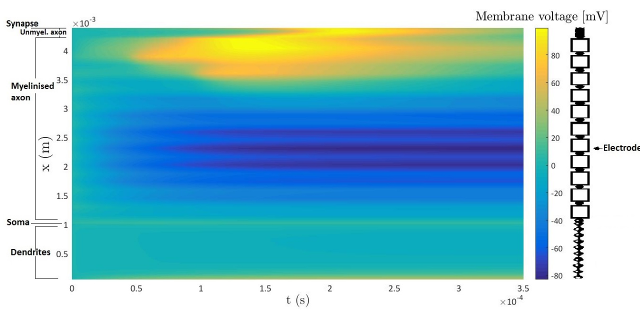

Fig. 5. Anode-make stimulation by a spherical electrode (60 V) at $2mm$ from the centre of a straight neuron. A colour map for the reduced membrane voltage $\tilde{V}$ is shown.

We will now briefly discuss the influence of the location of the electrode along the neuron. For this end, an AM-stimulation (60 V) at $2mm$ from the neuron is shown in Fig. 5, but now the electrode is placed at the centre of the neuron, instead of at the soma, as in Fig. 1.

We observe that the RoH has shifted with the electrode, to the centre of the neuron. This could be anticipated, because the region of hyperpolarisation is expected to be located at the anode-position. The position of the virtual cathode is now located at the end of the axon, leaving only a small region in which the actionpotential can freely propagate.

E. Straight neuron versus bending neuron

It is interesting to study the impact of neuronal bendings on the distribution of the membrane voltage. In literature it is observed, both from an experimental as from a theoretical perspective, that neuronal activation is likely to occur at neuronal terminations and bendings. Depending on the direction of the bending, increased hyperpolarisation or increased depolarisation is expected (Roth, 1993 [8]). As an example, AM-stimulation by a spherical electrode (60 V; electrode at $2mm$ from the centre of the neuron) of a neuron, that bends at the centre over $15°$ is shown in Fig. 6. This simulation corresponds with the simulation for a straight neuron from the previous subsection (see Fig. 5). The bending will promote depolarisation of the neuronal membrane. Because the bending is located at the centre of the RoH, no net depolarisation will occur at the bending. Instead, the RoH is split into two parts: the membrane at the bending is less hyperpolarised than it would have been if the neuron were straight.

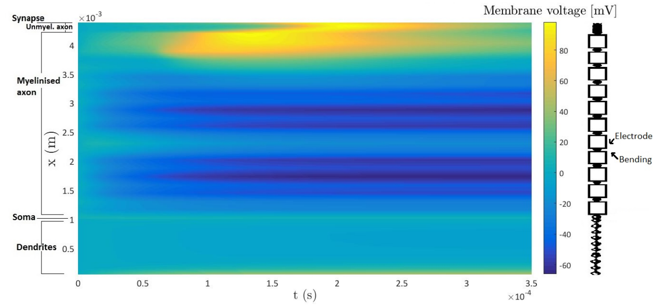

Fig. 6. Anode-make stimulation by a spherical electrode (60 V) at $2mm$ from the centre of a neuron, that bends at the centre over $15°$. A colour map for the reduced membrane voltage $\tilde{V}$ is shown.

F. Sealed-end versus voltage-clamped boundary conditions

Until now all simulations were done with sealed-end boundary conditions. This means that no current can leave the neuron (the neuron terminals are "sealed"). To determine the influence of the boundary conditions on the distribution of the voltage, some simulations were done with voltage-clamped boundary conditions (i.e. the neuron terminals are clamped to constant voltage). By comparing the results, we observed that the boundary conditions do not alter the global distribution of the membrane-voltage and gate-parameters significantly. Because of this, the colour maps for the voltage and gate-parameters are similar for both types of boundary conditions. However, in a very small region close to the neuronal terminations, the voltage and gate-parameters will strongly depend on the applied boundary conditions. This is difficult to see on the colour maps, but can for instance be visualized by plotting the voltage and gate-parameters at the synapse for both types of boundary conditions.

III. Simulations on bundles of multiple neurons

In this section simulations on bundles of multiple neurons are considered. The influence of the stimulation parameters on the percentage of neurons that are activated in the bundle ($\%AN$; percentage of activated neurons) and the percentage of neurons in the bundle for which the synapse was activated ($\%AS$; percentage of activated synapses) can be determined. For example, we mention the influence of the distance between a spherical electrode and a simple straight bundle in subsection III-A.

	$01xx$-stimulation		$10xx$-stimulation	
	Lenticular fasciculus (GPi-Th)	Macaca fascicularis (STN-GPi)	Lenticular fasciculus (GPi-Th)	Macaca fascicularis (STN-GPi)
$\%AN$	10	19.6	6	14.4
$\%AS$	6	14.4	4	9.28

Tabel 1: $\%AN$ and $\%AS$ in the lenticular fasciculus (GPi-Th) and macaca fascicularis (STN-GPi) for $01xx$- and $10xx$-stimulation.

Finally, simulations resembling a DBS-configuration were performed (subsection III-B). For this end, a realistic DBS-lead was modeled in Sim4life, based on specifications provided by Medtronic (Mo. 3389, Medtronic Inc., Minneapolis, MN, USA). A typical biphasic square-wave was applied on the Medtronic lead ($65Hz$, pulse duration $60\mu s$). The electromagnetic field distribution was subsequently simulated in a high-resolution head and neck model MIDA (Iacono et al., 2015 [10]) for different electrode-configurations.

A. Dependency of percentage of activated neurons in bundle on electrode-bundle distance

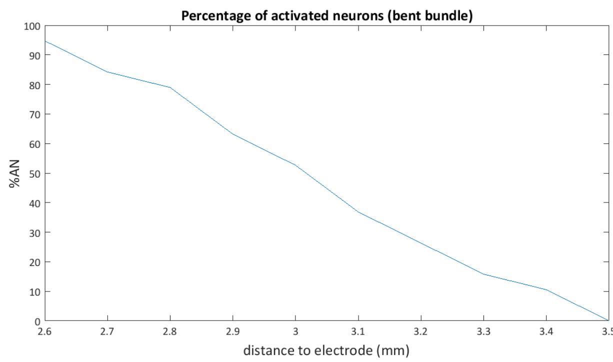

Fig. 7. The relation between the percentage of activated neurons $\%AN$ and the distance between the electrode and the centre of the neuronbundle is shown. The neurons in the bundle contain a central bending over $15°$.

Some general simulations on bundles of multiple neurons were done. We discuss the example of the dependency of the percentage of activated neurons ($\%AN$) in the bundle on the distance between the electrode and the centre of the bundle d_{be}. A bundle of 19 neurons, bending at the centre over $15°$ was considered. The distance between the electrode and the centre of the bundle was increased in steps of $\Delta x = 0.1mm$ from $2.6mm$ to $3.5mm$. For each distance the membrane-voltage and gate-parameters for all neurons in the bundle was calculated. Subsequently each neuron was evaluated for neuronal activation, by the Matlab code, and the $\%AN$ was determined. The result is shown in Fig. 7.

We observe that the $\%AN$ decreases, with increasing d_{be}. This is ofcourse expected, because for higher distances d_{be} and the same electrode potential, less power will reach the neuron bundle. A similar result was obtained for a straight neuronbundle. We note that the relation between the $\%AN$ and d_{be} seems continuous. However, this is probably due to the low resolution of the spatial step Δx. For high spatial resolution, $\%AN(d_{be})$ is expected to be a staircase function.

B. Deep brain stimulation in MIDA-head phantom

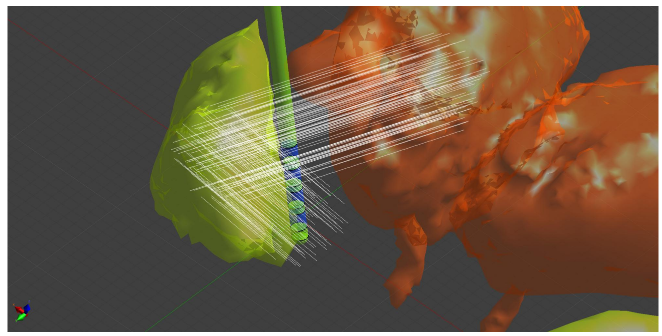

Fig. 8. Representation of the two considered neuronbundles (lenticular fasciculus and macaca fascicularis). The thalamus (Th) is shown in orange and the globus pallidus internus (GPi) in yellow. The tracts of the individual neurons are shown as white lines. Also the Medtronic DBS lead is shown (insulation in yellow and electrodes in blue).

We will now discuss a simulation, that is meant to resemble a realistic DBS-configuration. A Medtronic DBS-lead (Mo. 3389) was modeled in Sim4life and was placed at the subthalamic nucleus (STN) of the high resolution head and neck MIDA model. The azimuthal and polar angles of the DBS-lead were set to $7°$ and $20°$ respectively. Simulations were done with two types of bipolar electrode-configurations: a $01xx$-stimulation and a $10xx$-stimulation[6]

For the treatment of Parkinson's disease, two distinct neuronal bundles are often stimulated: projection neurons (macaca fascicularis; MF) of the STN and the output fibers (lenticular fasciculus; LF) of the globus pallidus internus (GPi). These two neuronal tracts were roughly approximated and modeled as straight neurons, randomly connecting the relevant brain structures (thalamus, STN, GPi). This is shown in figure 8: the white lines represent the two neuronal tracts (LF and MF). The thalamus is shown in orange and the globus pallidus in yellow. The electromagnetic field distribution was simulated in Sim4life and subsequently used for the assessment of the $\%AN$ and $\%AS$ in Matlab.

The result is shown in table 1. Some observations can be made. First, the activation percentages are always higher for

[6]The Medtronic DBS-lead contains four electrodes, that are numbered 0 to 3. The electrode closest to the tip of the lead is the zeroth electrode. In the $01xx$-stimulation, the zeroth electrode is set to $0V$. For the first electrode a typical biphasic square-wave ($65Hz$, pulse duration $60\mu s$) is used with amplitude of $1V$. The voltage on the second and third electrode is left floating with the environment (Neumann-conditions). Analogously, for the $10xx$-stimulation the role of the zeroth and first electrode is reversed.

$01xx$-stimulation than for $10xx$-stimulation. This is a result of the fact that the first electrode tends to be closer to the axon of a random neuron in both bundles, than the zeroth electrode. Furthermore initiation of an actionpotential often occurs at the axon. Secondly, the activation percentages are higher in the MF, compared to the LF. This can be explained in a similar way, by noting that the neurons of the macaca fascicularis are closer to the active electrodes.

Finally it is interesting to note that not all neurons, on which an actionpotential is generated, will be activated at the synapse. This is observed by comparing the $\%AN$ and $\%AS$ values in the table. In other words, not every actionpotential will reach the synapse. By plotting the colour maps for the voltage and gate-parameters, we observed that this can be explained by noting that the RoH can impede the propagation of the actionpotential.

IV. Conclusion

Electromagnetic simulations were done in Sim4life in a homogeneous medium and in the high resolution MIDA model. The resulting field distribution is coupled to a program in Matlab, that was written to solve for the membrane-voltage and gate-parameters in a multi-compartmental neuron and in bundles of multiple neurons. First, simulations on single neurons resulted in general conceptual conclusions about neurostimulation. Secondly, simulations on bundles of neurons were done, resembling a DBS-configuration.

V. Appendix

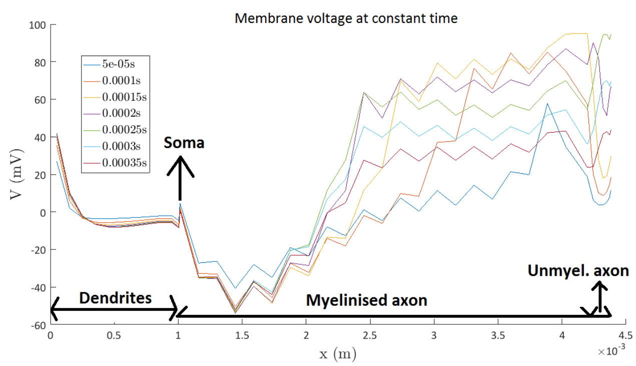

Fig. 9. Anode-make stimulation by a spherical electrode (60 V) at $2mm$ from the soma of a straight neuron. The spatial distribution of the reduced membrane voltage $\tilde{V}$ at 7 subsequent times is shown.

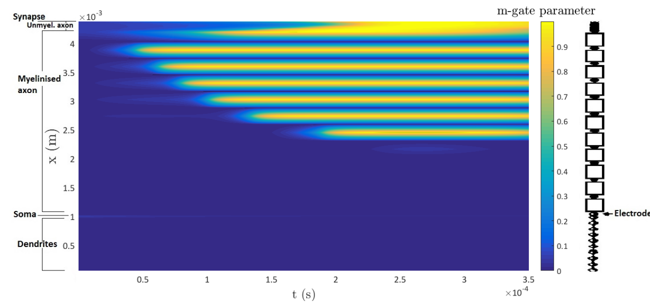

Fig. 10. Anode-make stimulation by a spherical electrode (60 V) at $2mm$ from the soma of a straight neuron. A colour map for the m-gate parameter is shown.

References

1. Benabid, A. L. Deep brain stimulation for Parkinsons disease. *Current opinion in neurobiology, Elsevier.*
2. Benabid, A. L. *et al.* Chronic electrical stimulation of the ventralis intermedius nucleus of the thalamus as a treatment of movement disorders. *Journal of neurosurgery* **84,** 203–214 (1996).
3. Kupsch, A. *et al.* Pallidal deep-brain stimulation in primary generalized or segmental dystonia. *New England Journal of Medicine* **355,** 1978–1990 (2006).
4. Mayberg, H. S. *et al.* Deep brain stimulation for treatment-resistant depression. *Neuron* **45,** 651–660 (2005).
5. Nuttin, B. J. *et al.* Long-term electrical capsular stimulation in patients with obsessive-compulsive disorder. *Neurosurgery* **52,** 1263–1274 (2003).
6. Hodaie, M., Wennberg, R. A., Dostrovsky, J. O. & Lozano, A. M. Chronic anterior thalamus stimulation for intractable epilepsy. *Epilepsia* **43,** 603–608 (2002).
7. Rattay, F. *Functional Electrical Stimulation of the Central Nervous System: Analysis of the Primarily Excited Structures* PhD thesis (Medical University of Vienna).
8. Roth, B. J. Mechanisms for electrical stimulation of excitable tissue. *Critical reviews in biomedical engineering* **22,** 253–305 (1993).
9. Geeter, N. D. *A Diffusion Tensor-Based Computational Model for Transcranial Magnetic Stimulation: from Macroscopic Fields to Neuronal Membrane Potentials* PhD thesis (University of Ghent, Technologiepark 913 9052 Zwijnaarde, Belgium, 2014-2015).
10. Iacono, M. I. *et al.* MIDA: a multimodal imaging-based detailed anatomical model of the human head and neck. *PloS one* **10,** e0124126 (2015).

Contents

List of Figures

List of Tables

List of symbols

Scalars, vectors and matrices

ϕ	Scalar
$\mathbf{u}, \bar{A}$	Vector
$\overline{\overline{A}}$	Matrix

Mathematical symbols

$\cdot$	dot product
∇	Gradient
$\nabla\cdot$	Divergence
i	Imaginary unit

Latin letters

$\#AC_f, \#AC_b$	Number of active compartments over which the actionpotential has propagated (forward or backward direction)
$\%AN$	Percentage of activated neurons
$\%AS$	Percentage of activated synapses
$\overline{\overline{A_1}}, \overline{\overline{A_2}}, \overline{\overline{B}}, \overline{\overline{C_E}}, \overline{\overline{C_V}}$	Crank-Nicolson matrices
A_1, A_2, A_3	Activation mechanisms
c_m	Membrane capacitance per unit length $[\frac{F}{m}]$
C_m^*	Compartmental capacity $[F]$
d	Diameter of the neuron
d_{be}	Bundle-electrode distance

d_{elec}	Distance between electrode and neuron
$\mathbf{E}$	Electric field intensity $[\frac{V}{m}]$
E_l	Electric field intensity component along the neural trajectory: $E_l = \mathbf{E} \cdot \mathbf{u_l}$
f	Activating function
F	Faraday constant $F = 96485\frac{C}{mol}$
G_a^*	Compartmental axial conductance $[S]$
$G_{a,f}^*, G_{a,b}^*$	Axial conductance between compartments in forward and backward direction $[S]$
g_{Na}, g_K, g_L	Membrane's conductance per unit length for the sodium, potassium and leakage channels $[\frac{A}{m}]$
h	h gate-parameter [-]
$h_0, h_0^{HH}, \dots$	rest-value for h gate-parameter [-]
I_a	Axonal current $[A]$
$I_a^{(l-\Delta l)\to l}, I_a^{(l+\Delta l)\to l}$	Axonal current flowing to the compartment at $x = l$ from the previous/next compartment $[A]$
$I_a^{cons}, I_a^{non-cons}$	Conservative and non-conservative part of axonal current $[A]$
I_C	Current through the membrane capacitance $[A]$
I_{elec}	Electrode current $[A]$
i_m	Membrane's current per unit length $[\frac{A}{m}]$
$i_{K,fast}, i_{K,slow}$	Fast and slow potassium membrane current $[\frac{A}{m}]$
i_{Na}, i_K, i_L, i_P	Sodium, potassium, leakage and non-specific membrane current $[\frac{A}{m}]$
i_s	Membrane current through the neuronal channels and loss current per unit length $[\frac{A}{m}]$
$I_s, I_s^{HH}, I_s^L, \dots$	Membrane current through the neuronal channels and loss current $[\frac{A}{m}]$
$k, k_\alpha, k_\beta, \dots$	Temperature factor [-]
Δl	Spatial discretisation step $[m]$
l	Local space parameter along the neural trajectory [m]
m	m gate-parameter [-]
$m_0, m_0^{HH}, \dots$	rest-value for m gate-parameter [-]

$MSOA, MSOA_f, MSOA_b$	Mean speed of activation pulse (forward or backward direction)
n	n gate-parameter [-]
$n_0, n_0^{HH}, \dots$	rest-value for n gate-parameter [-]
$[Na]_i, [Na]_0, [K]_i, [K]_0$	Sodium and potassium concentrations $[\frac{mol}{l}]$
p	p gate-parameter [-]
$p_0, p_0^{HH}, \dots$	rest-value for p gate-parameter [-]
P_{Na}, P_K, P_p	Permeabilities $[\frac{m}{s}]$
R	Universal gas constant $R = 8.314\frac{J}{molK}$
r_a	Axial resistance per unit length $[\frac{\Omega}{m}]$
r_m	Membrane resistance times unit length $[\Omega m]$
$\mathbb{S}, \tilde{\mathbb{S}}$	Set of points on the neuron, where an actionpotential is locally generated.
Δt	Temporal discretisation step $[s]$
t	time [s]
T	Temperature $[K]$ or $[°C]$
T_{pulse}	Pulse duration $[s]$
T_{sim}	Simulation time [s]
$\mathbf{u_l}$	Unit vector along the neural trajectory
V, V^{ES}	Transmembrane voltage (ES = Electroquasistatic) $[V]$
$\tilde{V}$	Membrane voltage with respect to the rest voltage: $\tilde{V} = V_i - V_e - V_r$ $[V]$
V_e, V_e^{ES}	Neuronal external potential (ES = electroquasistatic) $[V]$
V_{elec}	Electrode voltage $[V]$
V_f	Final electrode voltage for neuron at rest $[V]$
V_i, V_i^{ES}	Neuronal internal potential (ES=electroquasistatic) $[V]$
V_{Na}, V_K, V_L	Nernst equilibrium potential for the sodium, potassium and leakage channels $[V]$
v_{prop}	propagation velocity of actionpotential $[\frac{m}{s}]$
$V_r, V_r^{HH}, V_r^{CRRSS}, \dots$	Transmembrane rest voltage $[V]$
V_{thresh}	Threshold voltage $[V]$
$\bar{V}^*$	Crank-Nicholson vector

Greek letters

ϵ	Electric permittivity $[\frac{F}{m}]$
ϵ_0	Electric vacuum permittivity $[\frac{F}{m}]$
ϵ_r	Electric relative permitivity [-]
θ	Angle (f.i. between neuron and electric field)
λ	Space constant of the neural membrane [m]
ρ, ρ_i, ρ_e	Internal/external resistivity $[\Omega m]$
σ	Electric conductivity $[\frac{S}{m}]$
τ	Time constant of the neural membrane [s]
ϕ	Electric potential $[\frac{V}{C}]$
ω	Angular frequency $[\frac{rad}{s}]$
$\Omega_{HH}, \Omega_{FH}, \ldots$	Set of x values described by HH, FH, $\ldots$ model

List of abbreviations

$\%AN$	Percentage of activated neurons
$\%AS$	Percentage of activated synapses
AM	Anode-make stimulation
CM	Cathode-make stimulation
CRRSS	Chiu-Ritchie-Rogert-Stagg-Sweeney model
DBS	Deep brain stimulation
FEM	Finite-element method
FH	Frankenhaeuser-Huxley model
GM	Gray matter
GPi	Globus pallidus internus
HF	Harmonic frequency
HH	Hodgkin-Huxley model
K	Kalium
LF	Lenticular fasciculus
MF	Macaca fascicularis
MIDA	multimodel imaging-based detailed anatomical computer model of the human head and neck
$MSOA$	mean speed of activation pulse
$MSOA_b$	mean speed of activation pulse (backward)
$MSOA_f$	mean speed of activation pulse (forward)
Na	Natrium
NRMV	Non-reduced membrane voltage
RoH	Region of hyperpolarisation
S4L	Sim4life
SE	Schwarz-Eikhof model
SRB	Schwarz-Reid-Bostock model
STN	Subthalamic nucleus
Th	Thalamus
TMS	Transcranial magnetic stimulation
$\%VTA$	Percentage of volume of tissue activated
WM	White matter

Introduction

In deep brain stimulation an electromagnetic field distribution is excited around an electrode or lead, that has been surgically placed in the brain of the patient. This electromagnetic field will stimulate the surrounding neuronal tissue, which is therapeutically beneficial for patients suffering of a wide range of neurological disorders, as Parkinson disease (Benabid et al.,2003 [1]; Benabid et al.,1994 [2]; Deuschl et al.,2006 [3]; Obeso et al., 2001 [4]), essential tremor (Benabid et al,1996 [5]), dystonia (Kupschl et al.,2006 [6]; Vidailhet et al.,2005 [7]), treatment-resistant depression (Maybergh et al.,2005 [8]), obsessive-compulsive disorder (Nuttin et al.,2003 [9]) and epilepsy (Hodaie et al.,2002 [10]). The goal of this thesis is to simulate the electric field distribution in the brain of the patient and to subsequently use the field distribution to obtain a measure of neuronal activation.

The simulation of the electromagnetic field excited by the electrode or DBS lead was done in the Sim4life (S4L) software (Sim4life, ZMT Zurich MedTech AG). In Sim4life a low-frequency electroquasistatic (FEM) solver was used to obtain the field distribution. Different electrode shapes and stimulation current waveforms can be used for these simulations. In this thesis, we first used a spherical electrode in a homogeneous medium for simple simulations, intended to verify certain concepts. Secondly, to obtain a more accurate picture of deep brain stimulation, more realistic simulations were done in the high-resolution head and neck MIDA-phantom (Iacono et al.; 2015 [11]). A biphasic square-wave stimulus current is then applied on a Medtronic DBS lead (Mo. 3389, Medtronic Inc., Minneapolis, MN, USA), to obtain a realistic field distribution. The methodology for the different simulations of the electromagnetic field in the brain of the patient is discussed in chapter 1.

The simulated electromagnetic field distribution is exported from S4L and imported in Matlab (MATLAB 8.6, The MathWorks Inc., Natick, MA, 2000). For this thesis several neuronal models have been implemented in Matlab, that solve for the transmembrane voltage V and gate-parameters (m, n, p and h). These gate-parameters specify the state of the neuronal membrane. Each model consists of a set of coupled non-linear differential equations in V and the gate-parameters. The applied electromagnetic field is included in the model as a source term. The implemented neuronal models (a passive transmissionline model, the Hodgkin-Huxley (HH) model, Frankenhaeuser-Huxley (FH) model, Chiu-Ritchie-Rogert-Stagg-Sweeney (CRRSS) model, Schwarz-Eikhof (SE) model, Scwharz-Reid-Bostock (SRB) model) are discussed in chapter 2.

The Matlab code is first verified by reproducing some simulations from literature (Rattay, 2005 [12]). These simulations still have an exact analytic solution for the excited electromagnetic field distribution, and can thus be carried out only using Matlab (i.e. without the need of the S4L FEM solver). Furthermore the simulation is restricted to one completely straight neuron, without bifurcations. The Matlab-code and the comparison with results from literature is discussed in chapter 3. In chapter 4 some more general simulations are studied, now using the imported electromagnetic field distribution simulated in Sim4life, although still a spherical electrode in a homogeneous medium is used. The field distribution is now obtained by a FEM simulation, and can't be be derived analytically anymore. Although we still study single neurons without bifurcations in this chapter, the neurons are now allowed to bend. We will use these simple simulations on a single neuron to draw some general conclusions, f.i. about the influence of neuronal bendings on activation and about the difference between anode-make and cathode-make stimulation.

After finishing the simulation of the transmembrane voltage and the gate-parameters, we are able to determine if the neuron has been activated. A check for neuronal activation has been implemented in Matlab: the code will look after activation of the neuron (i.e. the propagation of an actionpotential over the neuronal axon), and it will generate a table listing all the positions and times on the neuron where activation has occurred. In section 4.3 we will discuss the heuristics by which neuronal activation is determined in the Matlab code. The activation table will also list the speed by which the activation pulse will propagate over the neuron. A distinction is made between the forward propagating speed $MSOA_f$ (mean speed of activation pulse in forward direction) which represents orthodromic propagation, from the backward propagating speed $MSOA_b$ (mean speed of the activation pulse in backward direction), which represents the antidromic propagation of the activation potential. In other words propagation is defined as forward propagation, if it occurs in the direction of the synapse (orthodromic). In contrast, backward propagation (antidromic) is in the direction of the soma.

In chapter 4 it is observed that neuronal bendings and terminations play an important role in the initiation of an action potential. This effect is also observed in experiments (Maccabee et al.,1993 [13]; Nagarajan et al.,1993 [14]). The important influence of bendings and terminations on the locus of activation is described by Roth et al. (1993) [15]. A similar discussion will be presented in chapter 5.

In part III of this thesis, the Matlab code is generalised to enable us to simulate bundles of multiple neurons. In chapter 6 we will discuss some simulations of simple neurons bundles. The membrane voltage and gate-parameters on each individual neuron of the bundle can then be examined. Furthermore the global response of the neuron bundle on the applied stimulus, is studied by the percentage of activated neurons ($\%AN$). Subsequently, we will discuss the dependency of the $\%AN$ on the electrode-bundle distance d_{elec}.

Finally in chapter 7 we try to mimic a realistic DBS-setup. The electric field distribution is simulated in S4L in the high-resolution head and neck MIDA-model (Iacono et al.,2015 [11]). The fields are excited by a representation of a Medtronic lead (Mo. 3389, Medtronic Inc., Minneapolis, MN, USA), that was modelled in Sim4life. We study the activation of two neuronal pathways, that are important in practice for deep brain stimulation: the lenticular fasciculus

(LF) and macaca fascicularis (MF). The former neuron bundle connects the globus pallidus internus (GPi) with the thalamus (Th). The latter neuron bundle connects the subthalamic nucleus (STN) with the GPi. Some approximations were made to model the geometry and electrical parameters of the neurons in both pathways. Nevertheless the results of the simulations can give some conceptual insight in the mechanisms of deep brain stimulation. It was noticed that not all neurons that were activated, i.e. neurons on which an action potential starts to propagate, will be stimulated at the synapse. In other words, not all action potentials will reach the end of the neuron. This phenomenon was studied through membrane voltage plots of individual neurons in the bundle. It was noticed that electric stimulation induces a region of hyperpolarisation (RoH) on the neuron, that can effectively stop the propagation of the action potential. Finally we observed that the freedom of stimulation-configurations (the DBS-lead consists of four independent electrodes) can be used to alter the volume of activated tissue ($\%VTA$).

Part I

Methodology

Chapter 1

Simulation of the electromagnetic field

Our goal is to determine the neuronal response to an applied electrode stimulus current. The first step to reach this goal, is to determine the distribution of the electromagnetic field around the electrode. This electromagnetic field distribution will be simulated in Sim4life, and will subsequently be exported to Matlab, where it will be used as source to determine the neuronal response (see chapter 2). The electromagnetic simulation will depend on the electrode shape, the surrounding medium (homogeneous or heterogeneous, isotropic or anisotropic), the discretisation grid, boundary conditions, the applied waveform of the stimulationcurrent, ... The simulation however won't depend on the surrounding neuron geometries, as long as they don't affect the electric properties of the medium. Because of this we can reuse one electromagnetic simulation when determining its effect on various neuronal geometries. In this section we will discuss the electromagnetic simulation set-ups we used in the thesis.

1.1 Spherical electrode in homogeneous medium

The most simple simulation we considered, consists of a spherical electrode in a completely homogeneous and isotropic medium (i.e. constant permittivity ϵ). This electromagnetic simulation will be used to obtain the results in chapter 4. The simulation geometry is shown in figure 1.1, which is a screenshot of the Sim4life software after the geometry was defined. In chapter 4 the electrode will be a sphere of radius $0.1mm$. The electrode is displayed in figure 1.1 as a small purple sphere in a green cube. The purple cube determines the simulation domain. At the end of the simulation domain, Dirichlet-conditions are applied for the electric potential. In the purple cube the medium is completely homogeneous and isotropic. The used grid however is not homogeneous, but it is cartesian. The green cube, shown in figure 1.1 is only used as a grid mask to define the inhomogeneous Sim4life grid and has no electromagnetic properties. On the electrode we then use Dirichletconditions to define the applied electrode voltage V_{elec}.

The simulation will result in a file that determines the electromagnetic field on a specific inhomogeneous cartesian grid. Subsequently this field is exported to Matlab (MATLAB 8.6, The

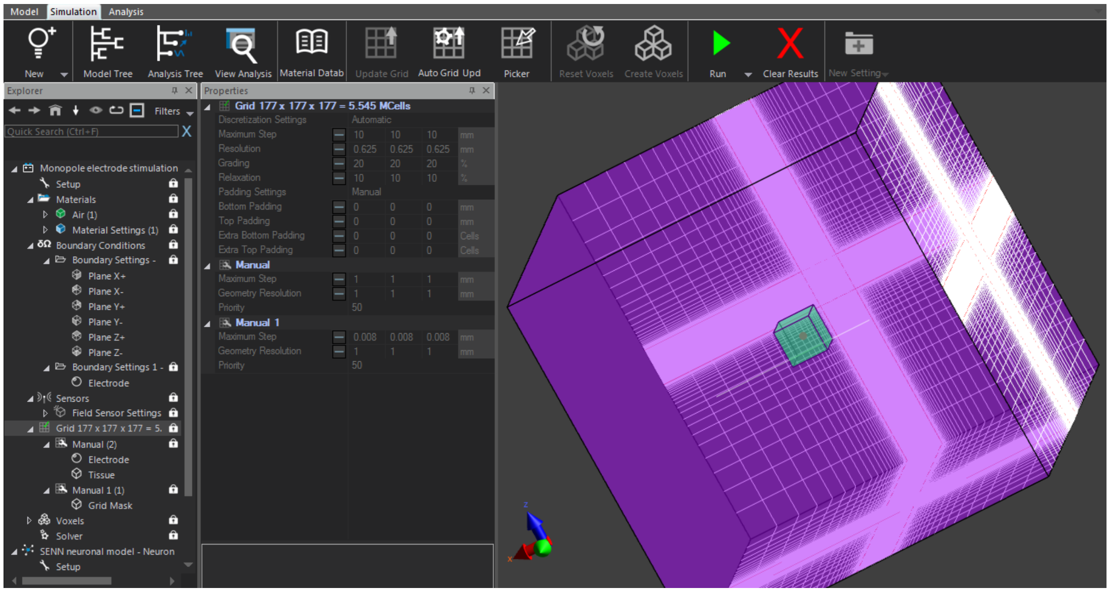

Figure 1.1: Simulation geometry of a spherical electrode in a homogeneous medium in Sim4life.

MathWorks Inc., Natick, MA, 2000), where it will be used to determine the neuronal response. However the used grid to discretise the neuron(s) in Matlab will in general not match with the S4L-grid used to obtain the electric field. Consequentially it is necessary to convert the electromagnetic field from the S4L-grid to the Matlab-grid. This is achieved by three-dimensional interpolation between the S4L-grid and Matlab-grid.

1.2 Medtronic electrode in head phantom

A more realistic virtual electrode was created based on the specifications of a Medtronic DBS lead (Mo. 3389,Medtronic Inc.,Minneapolis, MN, USA). This approach of simulating the electromagnetic field excited by a virtual electrode based on the specifications of a Medtronic DBS lead, using a FEM-method, and subsequently coupling the fields with a compartmental neuron-model, has been widely used in literature (Chaturvedi et al.,2012 [16]; Schmidt et al.,2012 [17]; Butson et al,2005 [18]; Sotiropoulos et al. [19]).

A model of the Medtronic 3389 DBS lead was made in Sim4life, as is shown in figure 1.2. The Medtronic DBS lead contains four platinum-iridium electrodes (shown in blue), the outer jacket tubing (shown in yellow) in between the electrodes is made of polyurethane. In our model the electrodes were modelled using Dirichlet-boundary conditions (approximating the platinum-iridium as a perfect conductor) and the polyurethane jacket was modelled as a perfect insulator, using Neumann-boundary conditions for the voltage. Furthermore, one or more electrodes can also be left floating with the environmental potential, by applying Neumann-conditions on these electrodes. In this thesis we will number the electrodes from 0 to 3, where electrode 0 is closest to the tip of the DBS-lead. This convention is also often used in literature.

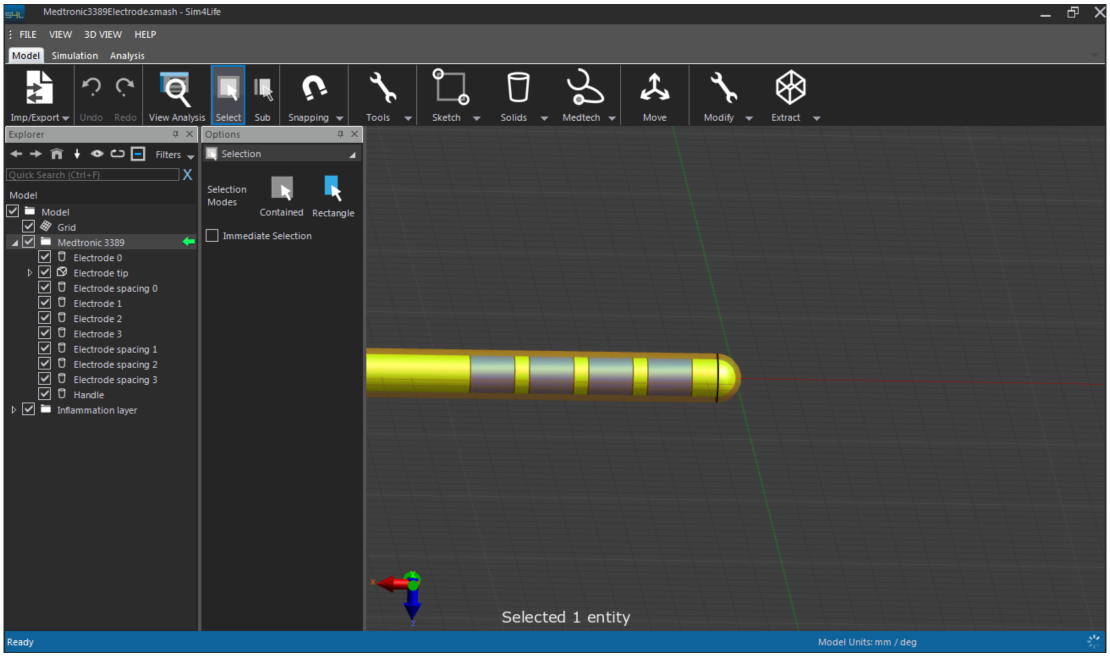

Figure 1.2: Virtual electrode based on the specifications of the Medtronic 3389 DBS lead, modelled in Sim4life.

Due to the inflammatory response of the body to the DBS-implant, an encapsulation layer will enclose the Medtronic lead, some weeks after the operation (Schmidt et al.,2012 [17]; Yousif and Liu, 2009 [20]; Grant et al.,2010 [21]; Butson et al.,2006 [22]). This inflammation layer will influence the electromagnetic fields in the tissue and is included in the Sim4life model, shown in figure 1.2, as a transparent yellow layer of thickness $0.2mm$. However for our simulations with the MIDA-model in chapter 7 we will omit the inflammation layer, mimicking the conditions of acute DBS.

As mentioned, the electric simulations with the virtual Medtronic lead, will be done in the MIDA-head phantom (Iacono et al,2015 [11]), in chapter 7. The DBS-lead was placed under azimuthal and polar angles of respectively 7° and 20°, referring to room axes (the same orientation parameters of the DBS lead are used in Schmidt et al.,2012 [17]). For therapeutic applications, the DBS-lead is typically located in the region of the subthalamic nucleus (STN) (Limousin et al.; 1998 [23],Hamel et al;2003 [24], Nowinkski et al.;2005 [25],Saint-Cyr et al.;2002 [26],Starr et al.;2002 [27]),Voges et al.; 2002 [28], Yelnik et al.;2003 [29]; Zonenshayn et al.; 2004 [30]). Because of this we chose the STN as the location of preference for the DBS-lead. First, the location of the subthalamic nucleus was estimated, relative to the thalamus. Electrode 0 was subsequently placed at the estimated position of the subthalamic nucleus. The resulting model is shown in figure 1.3.

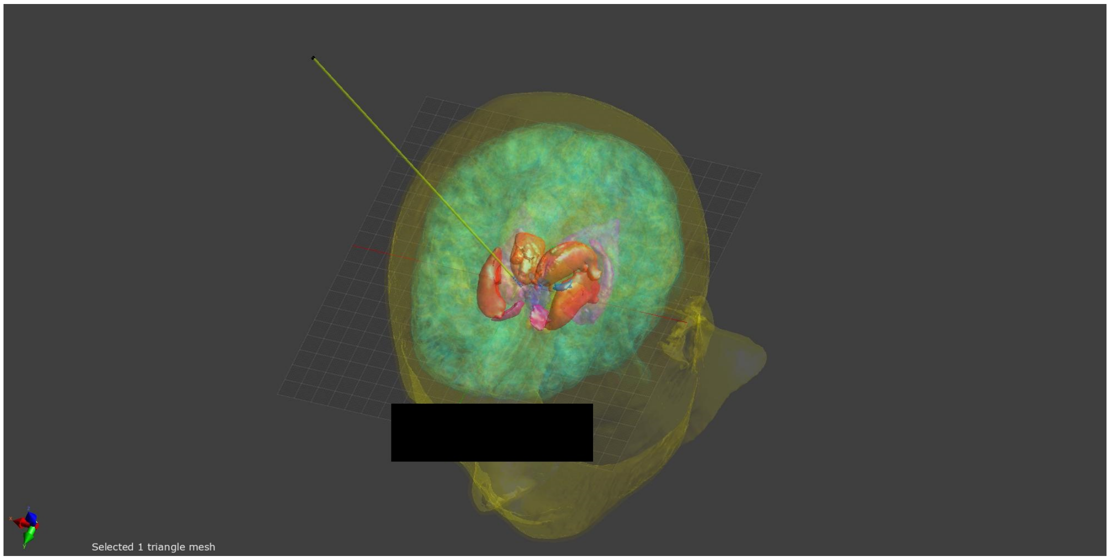

Figure 1.3: MIDA-head model with implanted DBS-lead at the subthalamic nucleus. The regions of the brain, important for deep brain stimulation, were made less transparent than the surrounding tissue.

The Sim4life software will now calculate the electric field distribution in the MIDA-head phantom. We notice that the full set of Maxwell equations can be simplified to the electroquasistatic equation, under conditions that are fulfilled for the spatial dimensions of the brain and the corresponding tissue types (Bossetti et al.,2007 [31]):

$$\nabla \cdot ((\sigma + i\omega\epsilon_r\epsilon_0)\nabla\phi) = 0 \tag{1.1}$$

For the most important frequencies relevant in DBS and for the electrical properties of brain tissue the electroquasistatic equation can be simplified to the stationary-currents equation, using $i\omega\epsilon_r\epsilon_0 \ll \sigma$ (Bossetti et al.,2007 [31]):

$$\nabla \cdot (\sigma\nabla\phi) = 0 \tag{1.2}$$

Equation (1.2) can subsequently be solved in Sim4life, while applying Dirichlet-boundary conditions at the end of the simulationdomain.

For deep brain stimulation the Medtronic electrode is typically stimulated by a square-wave biphasic pulse with a duration of $60\mu s$ and frequency of $65Hz$ (Gimsa et al.,2005 [32]). To calculate the electric field excited by a square-wave stimulation potential, in general the fourierspectrum of the square-wave has to be determined. Subsequently FEM-simulations at several harmonic frequencies have to be carried out. To determine which harmonic frequencies need to be simulated, the subsequent fourierapproximations of a biphasic square-wave were calculated in Matlab (the same was done for a monophasic square-wave by Gimsa et al. (2005) [32]). The result is shown in figure 1.4. A zoomed-in version on a single pulse is shown in figure 1.5.

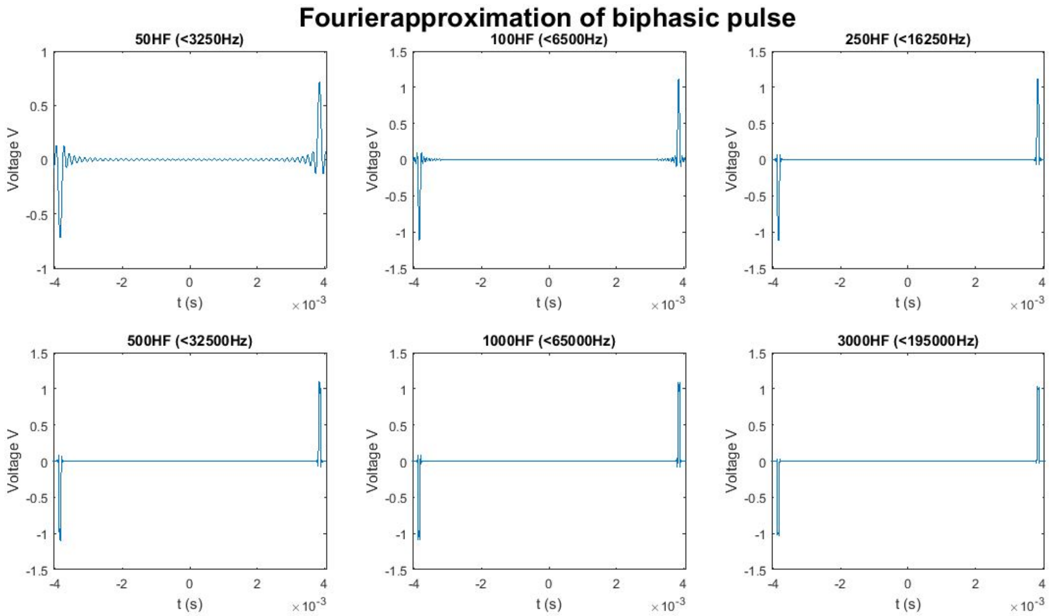

Figure 1.4: Fourierapproximations of a biphasic square-wave for different amounts of harmonic frequencies (HF). The corresponding frequency range is mentioned in each subplot.

We notice from figure 1.5 that a good approximation of the biphasic square-wave is obtained after summation of 1000 harmonic frequencies (HF), which is equivalent to considering frequencies in the range $0Hz - 65kHz$. The conductivity used in equation (1.2) depends strongly on frequency in this range. To illustrate this, conductivities for gray matter and white matter brain tissue were extracted from Sim4life, which makes use of the IT'IS anatomical tissue database [33]. (figure 1.6 and 1.7).

However, while the conductivity depends strongly on frequency, the electric field distribution around the DBS-lead does not vary that much with frequency. To establish this dependency of the field distribution on frequency, the electromagnetic field was simulated in Sim4life for 41 frequencies, that were logarithmically distributed in the range $10Hz - 100kHz$. The field distribution was excited by two types of electrode stimulation. We abbreviate the first simulation set-up as $10xx$-stimulation. Here the 1 refers to the zeroth electrode, on which a sinusoidal voltage with unit amplitude was applied. The 0 refers to the first electrode, on which a zero-potential is applied[1]. In the notation ($10xx$) the x denotes that the second and third electrode are left floating with the surrounding tissue (i.e. Neumann-conditions are used). Analogously, also a $10xx$-stimulation set-up was used.

Subsequently the variation in the field distributions of the simulated fields was observed. To do this, we denote the electric field at the ground frequency as $\mathbf{E_1} = \mathbf{E}(65Hz)$. The field excited

[1] Dirichlet-conditions are applied on the end of the simulation domain. As such, the end of the simulation domain acts as reference for all potentials

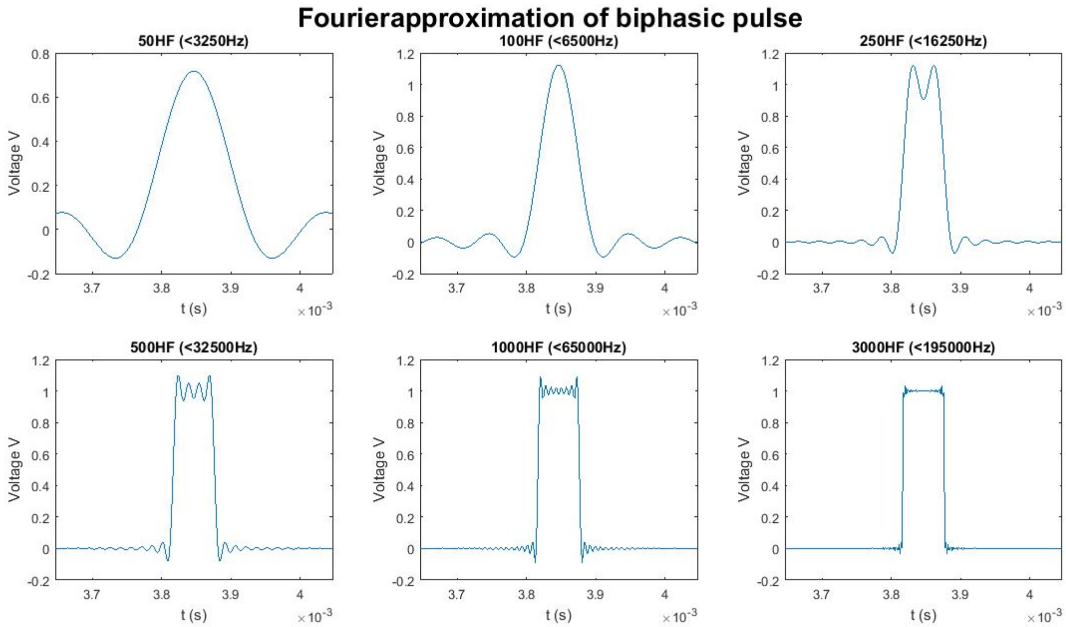

Figure 1.5: Subsequent fourierapproximations of a biphasic square-wave. A zoomed-in version on a single pulse is shown. The amount of harmonic frequencies (HF) that need to be summed is shown in each subplot.

at frequency f is denoted by $\mathbf{E_f}$. To measure the deviation in the distribution between $\mathbf{E_1}$ and $\mathbf{E_f}$, the normalised inner product is used:

$$\frac{< \mathbf{E_1}, \mathbf{E_f} >}{||\mathbf{E_1}||||\mathbf{E_f}||} = \frac{\int_V dV \mathbf{E_1} \cdot \mathbf{E_f}}{\sqrt{\int_V dV \mathbf{E_1} \cdot \mathbf{E_1}}\sqrt{\int_V dV \mathbf{E_f} \cdot \mathbf{E_f}}} \tag{1.3}$$

The result for the $01xx$-stimulation is shown in figure 1.8 and for the $10xx$-stimulation in figure 1.9.

We notice that the normalised inproduct in figure 1.8 and figure 1.9 is necessarily lower or equal than one, by the Cauchy-Schwarz theorem. The normalised inproduct will reach unity at the groundfrequency of $65Hz$. For $01xx$-stimulation the normalised inproduct will deviate at most approximately 0.2% from unity. For the $10xx$-stimulation setup the maximum deviation of the normalised inproduct from unity is approximately 4.5%. This deviation is reached at three frequencies. However for other frequencies the deviation from unity is much lower. We conclude that the electric field distribution doesn't seem to depend much on frequency. However the norm of the electric field could still vary with frequency. To establish the dependency of the norm of the field distribution with frequency, we define the ratio $r(f)$:

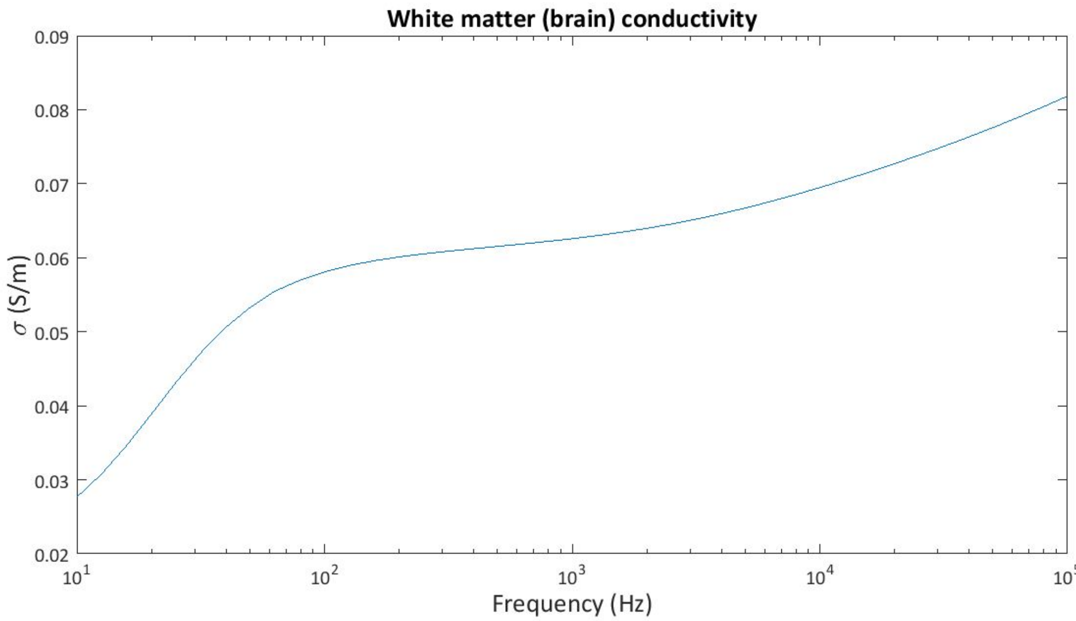

Figure 1.6: White matter conductivity versus frequency

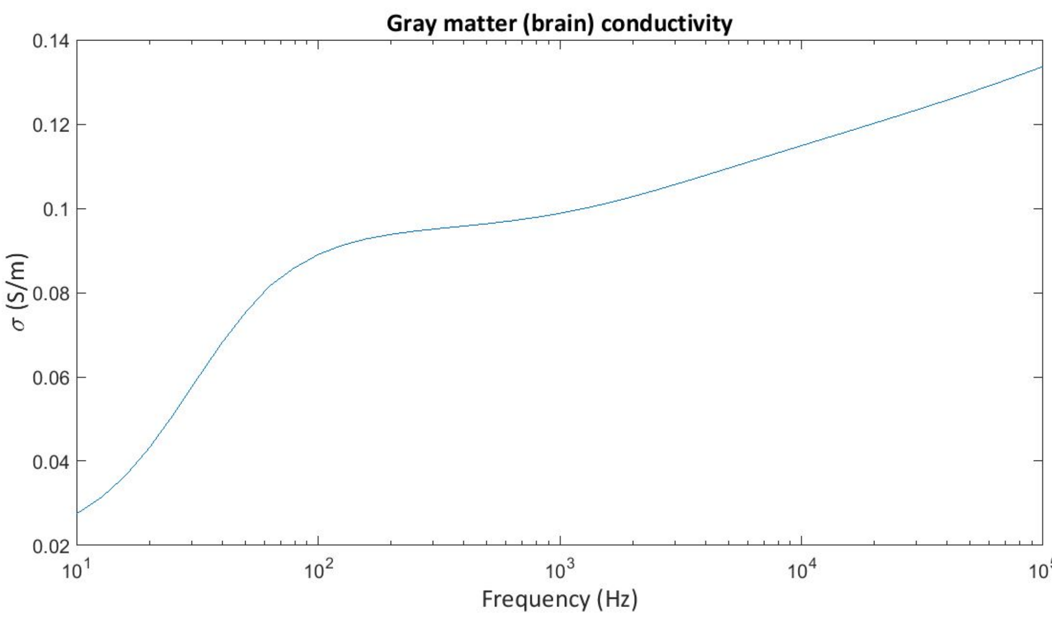

Figure 1.7: Gray matter conductivity versus frequency

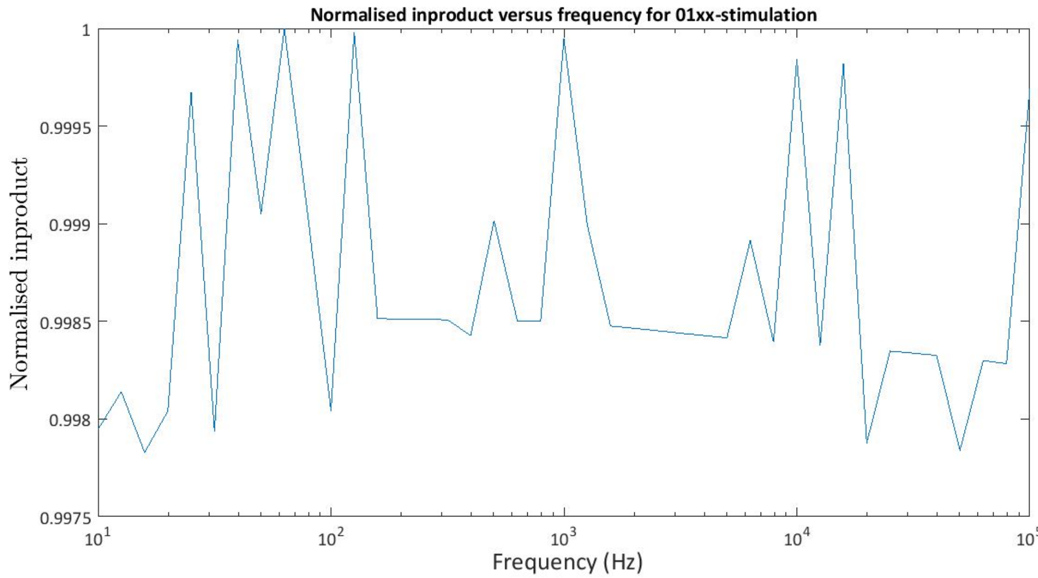

Figure 1.8: Normalised inproduct between $\mathbf{E_f}$ and $\mathbf{E_1}$ versus frequency for $01xx$-stimulation

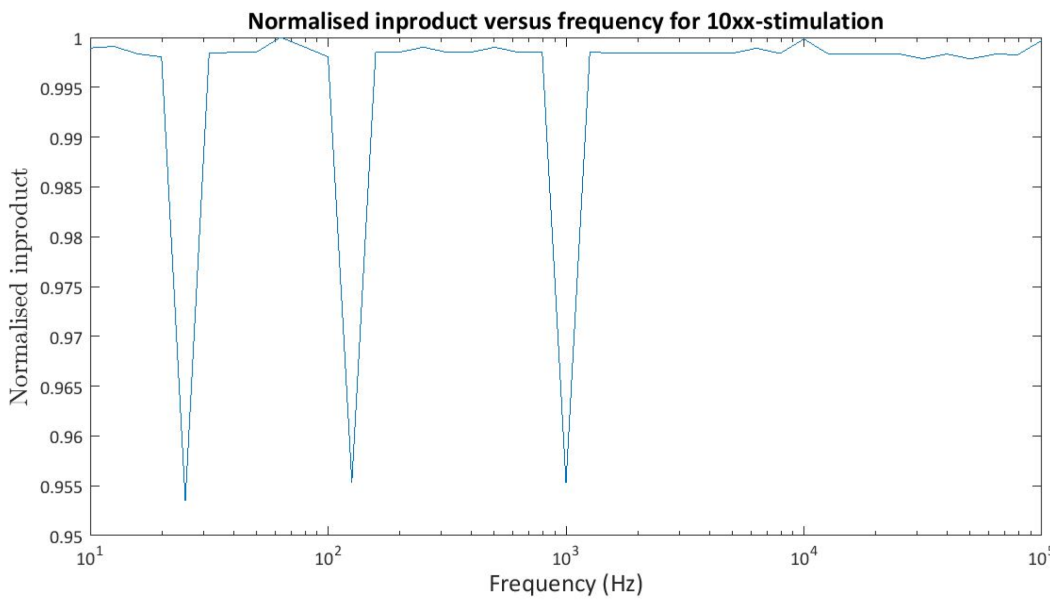

Figure 1.9: Normalised inproduct between $\mathbf{E_f}$ and $\mathbf{E_1}$ versus frequency for $10xx$-stimulation

$$r(f) = \frac{||E_f||}{||E_1||} = \frac{\sqrt{\int_V dV ||\mathbf{E_f}(\mathbf{r})||^2}}{\sqrt{\int_V dV ||\mathbf{E_1}||^2}} \tag{1.4}$$

This ratio $r(f)$ is shown for $10xx$-stimulation and $01xx$-stimulation in figure 1.10 and figure 1.11 respectively. We notice that for both stimulation-setups the ratio is approximately equal to one. Indeed for $01xx$-stimulation $r(f)$ deviates at most 0.2% from unity. For the $10xx$-stimulation the deviation is again somewhat larger, but still deviates at most 0.5% from unity. We notice that $r(f)$ peaks at the same frequencies, as the normalised inproduct in $10xx$-stimulation. We conclude that the field distribution does not depend much on frequency. Because of this we will approximate the field distribution excited by a biphasic square-wave by assuming that the transfer function does not depend on frequency. This allows us to simplify the computational complexity: instead of carrying out 1000 FEM simulations, we only need a single simulation to determine the transfer function. This simulation was done at the groundfrequency of $65Hz$.

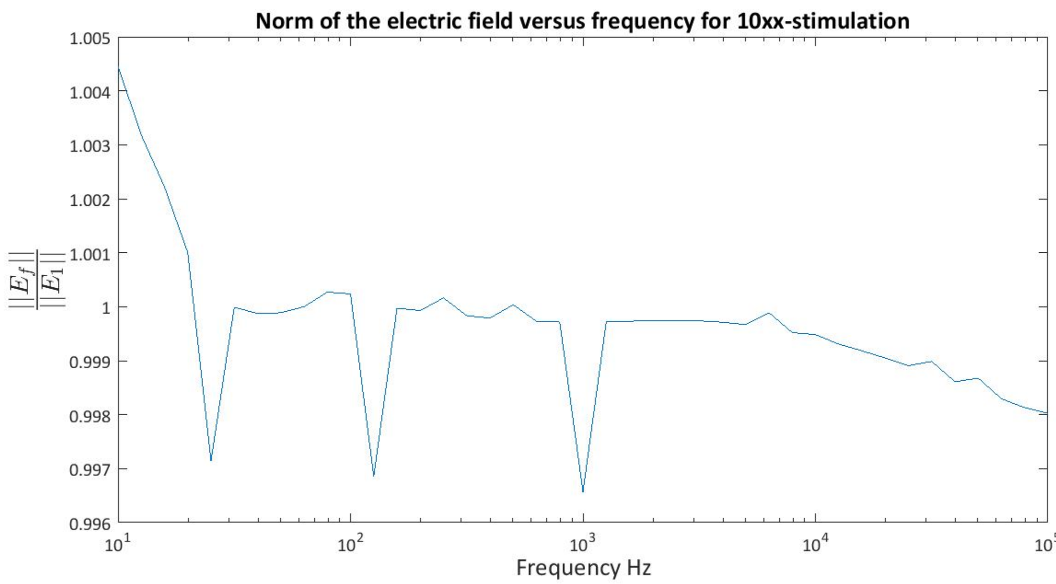

Figure 1.10: Ratio $r(f)$ between the norm of the electric field distribution at frequency f and the norm of the electric field distribution at the ground frequency ($65Hz$) for $10xx$-stimulation.

The field distribution seems mostly independent of frequency for both $10xx$- and $01xx$-stimulation, although the white-matter and gray-matter conductivities do depend strongly on frequency, as was noticed from figure 1.7 and figure 1.6. We notice that also the mutual ratio of the conductivities does depend strongly on frequency, as can be seen in figure 1.12.

For the independency of the field distribution with frequency, we propose as explanation that the field distribution will be very localized. This is naturally the case, because in deep brain stimulation only a very localized region has to be stimulated. This is illustrated in figure 1.13, where a slice of the electric field distribution is shown. Some important brain structures are shown as well: the thalamus is shown in orange, the GPi in yellow. We notice that indeed the field dimishes very fast (the black colour means that the field has dimished by more than $50dB$). This means that the conductivity is locally approximately constant, in a zeroth order approximation.

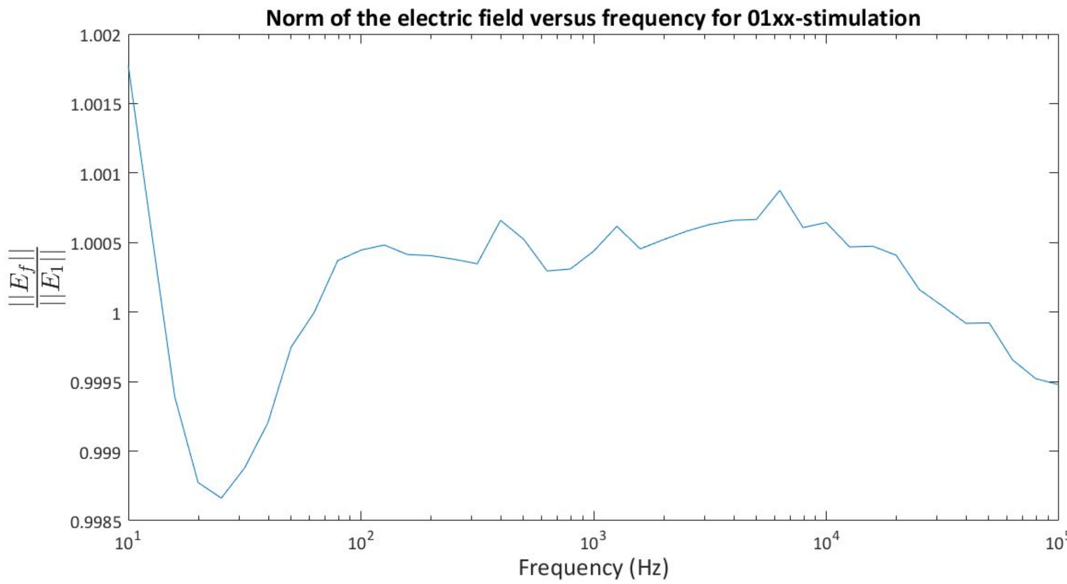

Figure 1.11: Ratio $r(f)$ between the norm of the electric field distribution at frequency f and the norm of the electric field distribution at the ground frequency ($65Hz$) for $01xx$-stimulation.

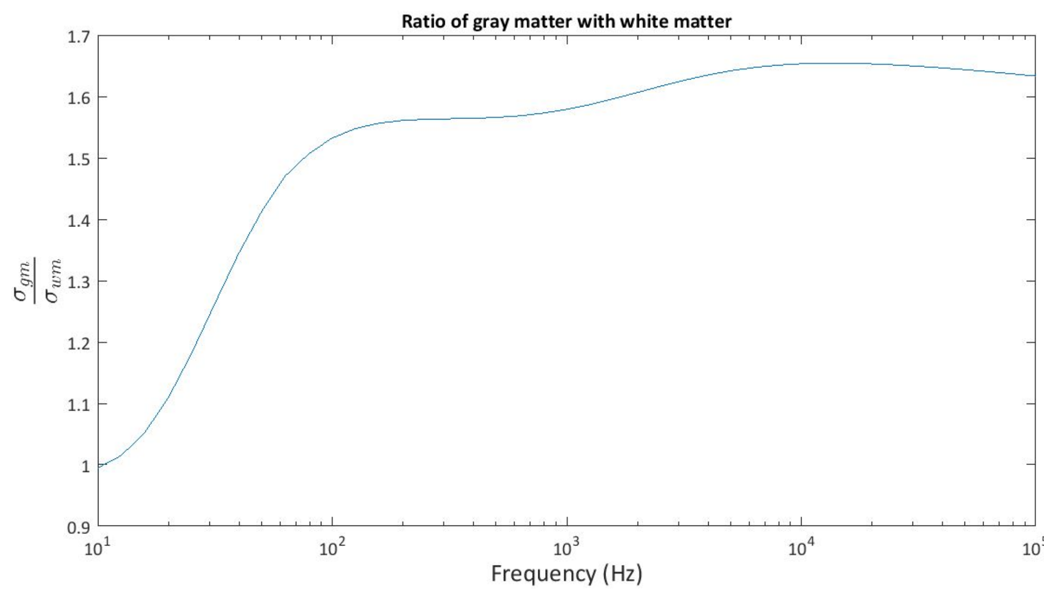

Figure 1.12: Dependency on frequency of the ratio of the conductivity in gray matter with the conductivity in white matter.

In this approximation the stationary-currents equation would reduce to a Laplace-equation, which is indeed independent of frequency:

$$\nabla^2 \phi = 0 \tag{1.5}$$

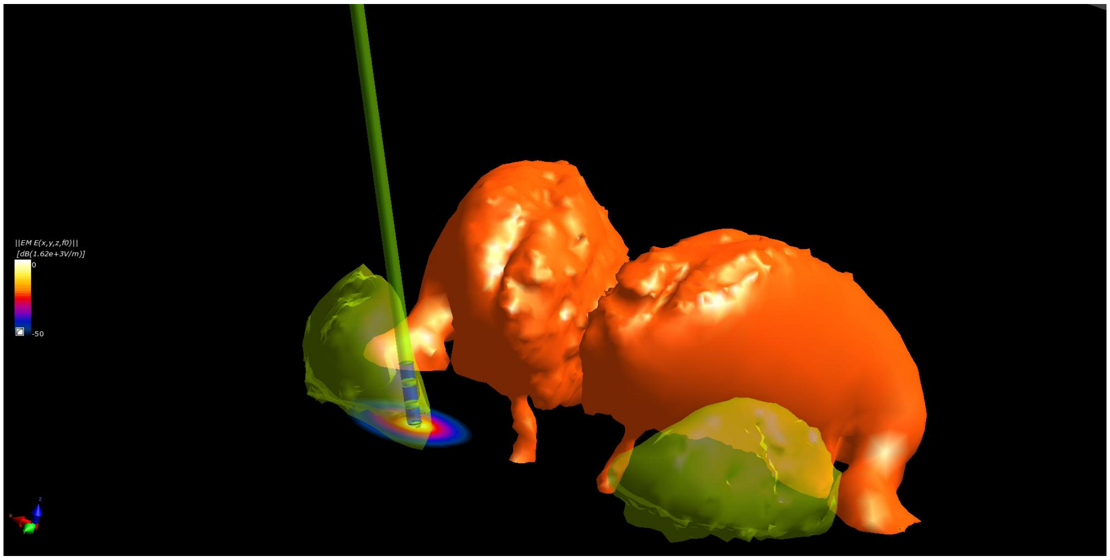

Figure 1.13: Slice view of the RMS-value of the electric field distribution in the MIDA-head phantom. Two important brain structures are shown as well: the thalamus (orange) and globus pallidus (yellow).

Chapter 2

Discussion of some neuronal models

The electromagnetic field distribution excited by an electrode can be simulated in Sim4life, as discussed in chapter 1. In this section we will discuss how this field distribution can subsequently be used as a source term, to obtain the neuronal response.

The structure of a generic neuron is depicted in figure 2.1. For the calculation of the neuronal response, the neuron is divided into compartments with different electric properties. Active and passive neuronal compartments can subsequently be distinguished by the presence of a myelin layer. For instance parts of the axon are myelinated (myelinated internodes) and the neuronal dendrites might be myelinated too. Because of this myelin layer, the neuronal membrane will only admit a loss current due to conduction by electrons. Active transport of electrolytes through neuronal gates is impossible, due to the insulating properties of myelin. Compartments surrounded by a myelin layer are thus electrically passive.

The nodes of Ranvier, the soma and the synapse however are not insulated by myelin. Their behaviour is electrically active: the membrane current is now determined by electronic conduction like in the passive case, but also by the transport of electrolytes (f.i. natrium and kalium) through the gates in the neuronal membrane. The state of these neuronal gates is determined by parameters m, n, h and p (or a subset of these, depending on the neuronal model). These are dimensionless numbers between 0 and 1 that indicate the resistance to conduction of a specific type of electrolyte. The exact meaning of the gate-parameters depends on the neuronal model.

In Matlab the simulated electromagnetic field will be used to determine the neuronal response on the stimulation. For this end a solver was programmed, to determine the transmembrane voltage and gate-parameters on the neuron in time, for a general multi-compartmental neuron. This means that the neuron is segmentated into different compartments for the dendrites, soma, nodes of Ranvier, synapse, initial segment and myelinated internodes. On each compartment a specific neuronal model was chosen, for the calculation of the voltage and gate-parameters. The program will then iterate for V and m, n, h and p, after combining all neuronal models on the multi-compartmental neuron in a single matrix equation. First we will give an overview of the different neuronal models that were programmed, and their properties, in this chapter[1]

[1] A similar overview of the active compartments discussed in this chapter, is also given in Rattay (2005) [12].

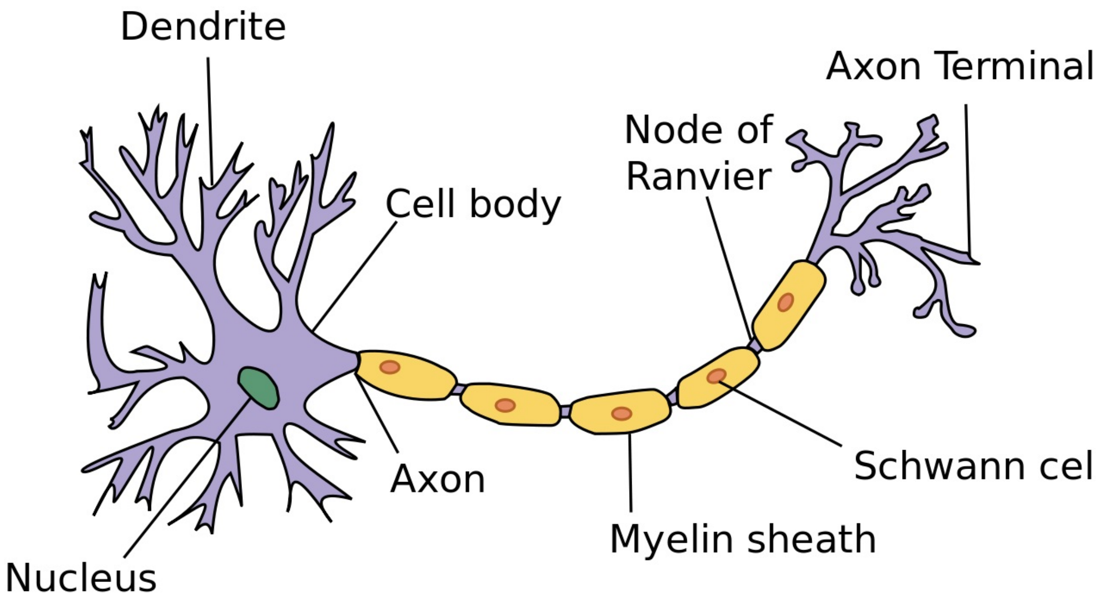

Figure 2.1: Schematic representation of the neuronal structure. Figure reproduced from Wikimedia Commons [35].

2.1 Passive transmissionline model

When the compartment (f.i. the internodes or the dendrites) is myelinated, there is no transport of electrolytes through the membrane-gates. The only possible current through the membrane is thus seen to be the electroncurrent. The passive compartment can then be replaced by an equivalent electric circuit, as shown in figure 2.2. We obtain for the membrane current i_m:

$$i_m = c_m \frac{\partial V}{\partial t} + \frac{V - V_r}{r_m} \tag{2.1}$$

The membrane current i_m is expressed per unit length, c_m is capacitance per unit length and r_m is the membrane resistance times unit length. A rest potential term V_r is added both to equation (2.1) and to the electric equivalent circuit (figure 2.2), to account for the diffusion of electrons through the neuronal membrane. This diffusion is due to the non-equilibrium of the intracellular and the extracellular system. This rest voltage can be obtained by the Nernst-equation or by experiment.

Furthermore we can express the membrane current i_m as:

$$i_m = -\frac{\partial I_a}{\partial l} = \frac{1}{r_a}\left(\frac{\partial^2 V}{\partial l^2} - \frac{\partial E_l}{\partial l}\right) \tag{2.2}$$

An overview of the properties of the passive transmissionline model and Hodgkin-Huxley model is for instance also given in De Geeter (2014) [34]. There is also specialised literature for each neuronal model.

Here we used Kirchoff-current law for the first equality and Ohm's law for the second. I_a is the axial current and r_a the axial resistance per unit length.

Because this electric model of the passive compartment is just a transmissionline-model, we recover the transmissionline equation (Roth and Basser,1990 [36]; Rattay, 1989 [37]), by combining equation (2.1) and equation (2.2):

$$\lambda^2 \frac{\partial^2 V}{\partial l^2} - (V - V_r) = \tau \frac{\partial V}{\partial t} + \lambda^2 \frac{\partial E_l}{\partial l} \tag{2.3}$$

We defined a space constant $\lambda = \sqrt{\frac{r_m}{r_a}}$ and a time constant $\tau = r_m c_m$. Equation (2.3) describes the transmembranevoltage V, defined as the difference of the intracellular and extracellular potential, by a partial differentialequation. This equation can then be solved for the transmembranevoltage V, when the electric field distribution $E_l = \mathbf{E} \cdot \mathbf{u_l}$ is known, which occurs as source term in the differential equation. Only the derivative of the projection of the electric field on the neurondirection $\mathbf{u_l}$ seems to be important as activation mechanism when solving for V. The derivation of the transmissionline equation assumes straight and long transmissionlines though, neglecting charge accumulation at neuronal bends and terminations. These additional activation mechanisms are directly proportional to E_l, and will be discussed in section 5.

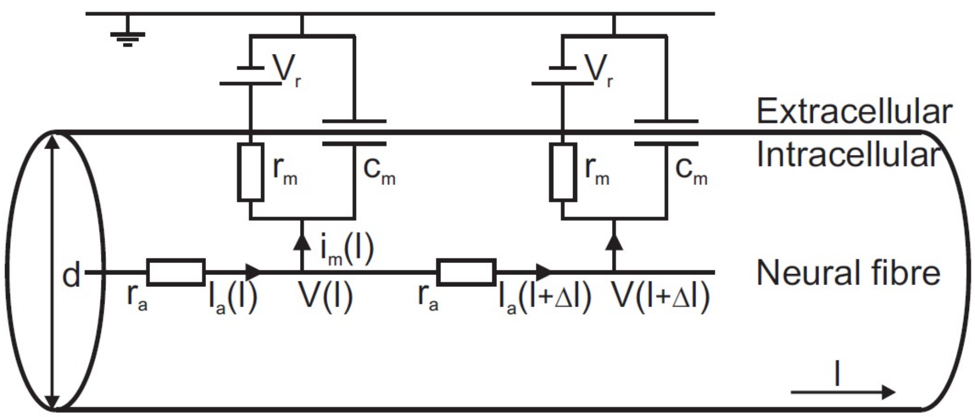

Figure 2.2: Equivalent electrical circuit for a passive compartment. Figure reproduced from De Geeter (2014) [34].

2.2 Active models

An active model is used when there is no myelin layer: the active membrane-gates are now important as well. There are several different types of active models, that are used for different types of compartments. For example, for this thesis the CRRSS-model is generally used to describe the nodes of Ranvier and the initial segment, while a a warm Hodgkin-Huxley method is used to describe the soma. There is a vast amount of literature describing different active neuronal models, for different types of cells. We refer to Varghese (1995) [38] for a summary of these models. In this thesis we only discuss five important active neuronal models, that have been implemented in Matlab. For a similar overview of these active models, we refer to Rattay[2] (2005) [12].

2.2.1 Hodgkin-Huxley model

The Hodgkin-Huxley model (Hodgkin and Huxley, 1952[39]; De Geeter [34],2014; Rattay, 2005 [12]; Nelson, 2004 [40]) was developed in 1952 by Hodgkin and Huxley based on voltage-clamp experiments on the homogeneous non-myelinated giant squid axon. The model includes two additional membrane currents, due to transport of natrium and kalium electrolytes.

$$i_m = c_m \frac{\partial V}{\partial t} + i_{Na} + i_K + i_L \tag{2.4}$$

The currents are again expressed per unit length: i_L is the loss current due the electronic conduction, i_{Na} the active natrium current, and i_K the active kalium current. Ofcourse one may also express the currents and capacitance per unit surface, as is done in Rattay (2005) [12] for active models.

Only the electronic current i_L is passive, and can be expressed as in the passive model by Ohm's law:

$$i_L = g_L(V - V_L) \tag{2.5}$$

Here g_L is the conductance per unit length, which is a constant. The currents i_{Na} and i_K can be expressed similarly:

$$i_{Na} = g_{Na} m^3 h(V - V_{Na}) \tag{2.6}$$

The total conductance per unit length $g_{Na}m^3h$ is no longer constant, and is seperated in a constant conductance g_{Na} and time-dependent gate-parameters m and h, that determine the state of the Na gates. Analogously we have:

$$i_K = g_K n^4(V - V_K) \tag{2.7}$$

With n the gate-parameter for kalium transport. Combining equation 2.4, 2.5, 2.6 and 2.7 we obtain:

$$i_m = c_m \frac{\partial V}{\partial t} + g_{Na} m^3 h(V - V_{Na}) + g_K n^4(V - V_K) + g_L(V - V_L) \tag{2.8}$$

As for the passive model (section 2.1), we can use equation (2.2) to obtain a partial differential-equation in the transmembrane voltage V with the electromagnetic field distribution E_l as source term. Because the model is now active, the differential equation will depend on time-dependent, yet unknown, prefactors m, n, h.

To solve equation (2.8), we need additional differential equations for the gate-parameters m, h and n:

$$\frac{dm}{dt} = k(\alpha_m(1 - m) - \beta_m m) \tag{2.9}$$

[2]The choice of the active neuronal models that were implemented in Matlab, is based on this publication.

$$\frac{dh}{dt} = k(\alpha_h(1-h) - \beta_h h) \tag{2.10}$$

$$\frac{dn}{dt} = k(\alpha_n(1-n) - \beta_n n) \tag{2.11}$$

The coefficients α and β depend non-linearly on the voltage V. The expressions for the different α and β coefficients can be obtained by fitting to measurements. We refer to Rattay (2005) [12] for their mathematical expressions. The constant k is a temperature factor: $k = 3^{0.1T-0.63}$. The temperature is expressed in $°C$. The factor k corrects for temperatures different than $T = 6.3°C$, for which the experiments were performed.

Equation 2.8, 2.9, 2.10, 2.11 form a set of coupled non-linear differential equations in V, m, h and n, called the Hodgkin-Huxley equations. Because the Hodgkin-Huxley equation in the membranevoltage, equation 2.8, can still be considered linear in V with time-dependent coefficients, it is still straightforward to apply a Crank-Nicholson discretisation scheme on the HH-equations. This will be discussed in chapter 3. This type of linearity is no longer present in the FH, SE and SRB model, making application of a Crank-Nicholson scheme more difficult (see section 3).

2.2.2 Chiu-Ritchie-Rogert-Stagg-Sweeney model

The CRRSS model (Chiu et al.,1979 [41];Sweeney et al.,1987 [42];Rattay 2005[12]) was obtained by voltage-clamp experiments on myelinated rabbit nerve fibers at $14°C$. The results were subsequently extrapolated to $37°C$. The model is similar to the HH-model; however there is now no kalium transport.

$$i_m = c_m \frac{\partial V}{\partial t} + g_{Na} m^2 h(V - V_{Na}) + g_L(V - V_L) \tag{2.12}$$

The gate-parameters m and h, are described analogously to the Hodgkin-Huxley case:

$$\frac{dm}{dt} = k(\alpha_m(1-m) - \beta_m m) \tag{2.13}$$

$$\frac{dh}{dt} = k(\alpha_h(1-h) - \beta_h h) \tag{2.14}$$

The temperature constant k is now introduced to describe temperatures different from $37°C$: $k = 3^{0.1T-3.7}$. The α and β coefficients are again non-linear in V (Rattay, 2005 [12]). A Crank-Nicholson scheme can now be applied to solve the discretised version of the CRRSS-equations for V, m and h.

2.2.3 Frankenhaeuser-Huxley model

The Frankenhaeuser-Huxley model (Frankenhaeuser, 1960 [43]) was developed on the frog axon node as the first myelinated fiber model. It differs from the more linear HH and CRRSS models in that the ion current is no longer expressed as function of V by Ohm's law, but is derived from the Nernst-Planck equation. This makes discretising the equations by Crank-Nicholson more tedious. The FH-equation for the membranevoltage is:

$$i_m = c_m \frac{\partial V}{\partial t} + i_{Na} + i_K + i_L + i_P \tag{2.15}$$

Where a non-specific current density i_P was added. The current densities are given by:

$$i_{Na} = P_{Na} m^2 h \frac{VF^2}{RT} \frac{[Na]_0 - [Na]_i \exp\{\frac{VF}{RT}\}}{1 - \exp\{\frac{VF}{RT}\}} \tag{2.16}$$

$$i_K = P_K n^2 \frac{VF^2}{RT} \frac{[K]_0 - [K]_i \exp\{\frac{VF}{RT}\}}{1 - \exp\{\frac{VF}{RT}\}} \tag{2.17}$$

$$i_p = P_p p^2 \frac{VF^2}{RT} \frac{[Na]_0 - [Na]_i \exp\{\frac{VF}{RT}\}}{1 - \exp\{\frac{VF}{RT}\}} \tag{2.18}$$

For the values of the constants we refer to Rattay (2005) [12] (currents and capacitance are expressed per unit surface). We notice that we defined the transmembrane voltage as $V = V_i - V_e$, with V_i the internal potential and V_e the external potential. The equations are different if the membrane voltage is defined with respect to the rest-voltage (i.e. $V = V_i - V_e - V_r$), as is done in f.i. Rattay (2005) [12]. In this thesis we will always define V as the difference between the internal and external potential: $V = V_i - V_e$. We will call the membrane voltage defined with respect to the rest-voltage, the reduced membrane voltage $\tilde{V} = V_i - V_e - V_r$. Both definitions will be used through this thesis: for instance for plots the reduced membrane voltage $\tilde{V}$ is more appropriate, while for calculations the non-reduced membrane voltage V is useful.

The electronic loss current is again given by Ohm's law:

$$i_L = g_L(V - V_L) \tag{2.19}$$

and the gate-parameters m, n, h and p are described by differential equations:

$$\frac{dm}{dt} = k_{\alpha_m} \alpha_m (1 - m) - k_{\beta_m} \beta_m m \tag{2.20}$$

$$\frac{dh}{dt} = k_{\alpha_h} \alpha_h (1 - h) - k_{\beta_h} \beta_h h \tag{2.21}$$

$$\frac{dn}{dt} = k_{\alpha_n} \alpha_n (1 - n) - k_{\beta_n} \beta_n n \tag{2.22}$$

$$\frac{dp}{dt} = k_{\alpha_p} \alpha_p (1 - p) - k_{\beta_p} \beta_p p \tag{2.23}$$

We notice the more general temperature dependency in these gate-parameters equations.

The FH-equations form a set of coupled non-linear differential equations and can be solved numerically, as will be described in chapter 3.

2.2.4 Schwarz-Eikhof model

The SE-model (Scwharz-Eikhof, 1987 [44]; Rattay, 2005 [12]) is a neural model of the Frankenhaeuser-Huxley type. It is obtained by voltage-clamp experiments on rat nodes. The SE-equation for the membrane voltage is given by a FH-like equation, without the non-specific current density:

$$i_m = c_m \frac{\partial V}{\partial t} + i_{Na} + i_K + i_L \tag{2.24}$$

with current densities given by:

$$i_{Na} = P_{Na} m^3 h \frac{VF^2}{RT} \frac{[Na]_0 - [Na]_i \exp\{\frac{VF}{RT}\}}{1 - \exp\{\frac{VF}{RT}\}} \tag{2.25}$$

$$i_K = P_K n^2 \frac{VF^2}{RT} \frac{[K]_0 - [K]_i \exp\{\frac{VF}{RT}\}}{1 - \exp\{\frac{VF}{RT}\}} \tag{2.26}$$

The equations for the loss current i_L and the gate-parameters m, n, h are analogous to the FH-model.

2.2.5 Schwarz-Reid-Bostock model

The SRB-model (Schwarz, Reid, Bostock, 1995 [45]) provides a set of equations of the FH-type, without the non-specific current density and where the kalium current density has been separated in fast and slow kalium transport $i_K = i_{K,fast} + i_{K,slow}$. The model was obtained in 1995 by experiments on human nerve fibers at room temperature.

$$i_m = c_m \frac{\partial V}{\partial t} + i_{Na} + i_{K,fast} + i_{K,slow} + i_L \tag{2.27}$$

The gate-parameters are m, n, h and p and are again described by the usual differential equations. The natrium current density is obtained from the Nernst-Planck equation:

$$i_{Na} = P_{Na} m^3 h \frac{VF^2}{RT} \frac{[Na]_0 - [Na]_i \exp\{\frac{VF}{RT}\}}{1 - \exp\{\frac{VF}{RT}\}} \tag{2.28}$$

The kalium-transport is described by:

$$i_{K,fast} = g_{K,fast} n^4 (V - V_K) \tag{2.29}$$

$$i_{K,slow} = g_{K,slow} p (V - V_K) \tag{2.30}$$

The loss current i_L is described as in equation (2.5). This set of coupled differential equations will be discretised and iterated over time in Matlab to obtain a solution for the voltage and gate-parameters, as will be described in the next chapter.

Chapter 3

Implementation in Matlab

In this chapter we discuss the implementation in Matlab of the different neuronal models (see chapter 2). The idea is to solve these models for V and the gate-parameters on single neurons without bifurcations. The generalisation to neuronbundles will be discussed in chapter 6. To numerically solve the sets of coupled differential equations, we have to apply a discretisation scheme, as discussed in section 3.1. Furthermore the discretised equations need to be completed by the appropriate boundary conditions, as will be discussed in section 3.2. The discretised equations will then be iterated over time and be solved by Matlab. Subsequently the program is verified by comparing some results with literature in section 3.3.

3.1 Discretisation of the neuronal model

We combine equation (2.4) with equation (2.2), to obtain the differential-equation that describes the membrane voltage in the Hodgkin-Huxley case:

$$\frac{1}{r_a}(\frac{\partial^2 V}{\partial l^2} - \frac{\partial E_l}{\partial l}) = c_m \frac{\partial V}{\partial t} + i_{Na} + i_K + i_L \tag{3.1}$$

This equation can easily be generalised: when we denote i_s as the part of the membrane current, that does not include the current through the membrane capacitance, we find:

$$\frac{1}{r_a}(\frac{\partial^2 V}{\partial l^2} - \frac{\partial E_l}{\partial l}) = c_m \frac{\partial V}{\partial t} + i_s \tag{3.2}$$

Equation (3.2) is valid for all neuronal models described in chapter 2. It describes the evolution of the membrane voltage, with the electric field E_l as source term. For each neuronal model a different expression of i_s is used. We now discretise the spatial coordinate l along the neuron with separation Δl[1], we obtain:

$$G_a^*(V(l-\Delta l) - 2V(l) + V(l+\Delta l) + \Delta l E(l-\Delta l) - \Delta l E(l)) = C_m^* \frac{\partial V(l)}{\partial t} + I_s(l) \tag{3.3}$$

[1] A similar discussion of the Crank-Nicholson discretisation of the neuronal models is given in De Geeter (2014) [34]

Here we multiplied equation (3.2) with Δl and introduced the axial conductance and capacitance per compartment: $G_a^* = \frac{1}{r_a \Delta l}$ and $C_m^* = c_m \Delta l$. We also defined the current I_s: $I_s = \Delta l i_s$. We now apply a Crank-Nicholson discretisation scheme (De Geeter (2014) [34]), f.i.:

$$I_s(l) \rightarrow \frac{I_s(l,t) + I_s(l,t+\Delta t)}{2} \tag{3.4}$$

And the time derivative:

$$\frac{\partial V(l)}{\partial t} \rightarrow \frac{V(l,t+\Delta t) - V(l,t)}{\Delta t} \tag{3.5}$$

We can simplify the equations, including a staggered time grid:

$$f(t + \frac{\Delta t}{2}) = \frac{f(t) + f(t+\Delta t)}{2} \tag{3.6}$$

So we finally obtain:

$$\begin{aligned} &\frac{2C_m^*}{\Delta t}(V(l,t+\frac{\Delta t}{2}) - V(l,t)) + I_s(l,t+\frac{\Delta t}{2}) \\ &= G_a^*(V(l-\Delta l,t+\frac{\Delta t}{2}) - 2V(l,t+\frac{\Delta t}{2}) + V(l+\Delta l,t+\frac{\Delta t}{2}) + \Delta l E(l-\Delta l,t+\frac{\Delta t}{2}) - \Delta l E(l,t+\frac{\Delta t}{2})) \end{aligned} \tag{3.7}$$

Equation (3.7) implicitly determines $\bar{V}(t + \frac{\Delta t}{2})$ as function of $\bar{V}(t)$, $\bar{E}_l(t + \frac{\Delta t}{2})$ and $\bar{I}_s(t + \frac{\Delta t}{2})$. We will use the notation $\bar{X}$ to refer to the vector obtained by discretising the spatial parameter l along the neuron, while $\bar{\bar{\bar{X}}}$ refers to a matrix.

We will in general use the electric field distribution E_l as source to determine the membrane-voltage, because the electric field can be obtained from S4L-simulations as discussed in chapter 1. Sometimes it is however easier to use the corresponding potential $E_l = -\frac{\partial V_e}{\partial l}$, f.i. when an analytic expression exists for V_e, as in the case that will be discussed in section 3.3. Note that writing the electric field E_l as the derivative of a potential V_e, implicitly implies that the electric field has to be conservative, excluding the case of magnetic stimulation. The electric field is conservative however for the case of deep brain stimulation. In this case equation (3.7) is rewritten as:

$$\begin{aligned} &\frac{2C_m^*}{\Delta t}(V(l,t+\frac{\Delta t}{2}) - V(l,t)) + I_s(l,t+\frac{\Delta t}{2}) \\ &\qquad = G_a^*(V(l-\Delta l,t+\frac{\Delta t}{2}) - 2V(l,t+\frac{\Delta t}{2}) + V(l+\Delta l,t+\frac{\Delta t}{2}) \\ &\qquad\qquad + V_e(l-\Delta l,t+\frac{\Delta t}{2}) - 2V_e(l,t+\frac{\Delta t}{2}) + V_e(l+\Delta l,t+\frac{\Delta t}{2})) \end{aligned} \tag{3.8}$$

Because we defined the transmembranevoltage V as $V = V_i - V_e$, equation (3.8) can be rewritten as function of the internal potential:

$$\begin{aligned} &\frac{2C_m^*}{\Delta t}(V(l,t+\frac{\Delta t}{2}) - V(l,t)) + I_s(l,t+\frac{\Delta t}{2}) \\ &\qquad = G_a^*(V_i(l-\Delta l,t+\frac{\Delta t}{2}) - 2V_i(l,t+\frac{\Delta t}{2}) + V_i(l+\Delta l,t+\frac{\Delta t}{2})) \end{aligned} \tag{3.9}$$

Equation (3.9) is not very useful when solving for the transmembranevoltage V, because the internal potential V_i is not known. The Matlab code will thus make use of equation (3.7) or equation (3.8) to determine $V(x,t)$, because the source term in these equations (E_l or V_e) can be simulated or calculated. However, equation (3.9) is easy to physically interpret: it gives conservation of current at the compartment with $x = l$. Indeed, equation (3.9) can be rewritten as:

$$I_C(l) + I_s(l) = I_a^{(l-\Delta l)\to l} + I_a^{(l+\Delta l)\to l} \tag{3.10}$$

$I_C(l) = \frac{2C_m^*}{\Delta t}(V(l, t+\frac{\Delta t}{2}) - V(l,t))$ is the current that flows through the membrane-capacitance of compartment $x = l$. I_s denotes the membrane-current of the compartment that is due to electronic losses and ionic current through the membrane-gates. The current that flows through the neuronal membrane is compensated by axially flowing current: $I_a^{(l-\Delta l)\to l} = G_a^*(V_i(l-\Delta l, t+\frac{\Delta t}{2}) - V_i(l, t+\frac{\Delta t}{2}))$ is the current that flows axially from the compartment at $x = l - \Delta l$ to the compartment at $x = l$. Analogously we have that $I_a^{(l+\Delta l)\to l} = G_a^*(V_i(l+\Delta l, t+\frac{\Delta t}{2}) - V_i(l, t+\frac{\Delta t}{2}))$ represents the current flowing from the compartment at $x = l+\Delta l$ to the compartment at $x = l$. We see that equation (3.10), and consequently equation (3.9), equation (3.8) and equation (3.7) can be seen as conservation of current (Kirchoff current law).

The interpretation of the Crank-Nicholson discretised differential-equation for the membrane-voltage (i.e. equations (3.7) and (3.8)) is useful, when trying to generalize the discretised equations. In general a neuron has non-homogeneous electric parameters: the membrane-capacitance per unit length c_m and the axial resistance per unit length r_a are both functions of the spatial parameter l. These functions are smooth and continuous in each compartment. They are discontinuous however on the boundary between two different compartments (for instance when going from the dendrites to the soma, from the soma to the axon, etc.). This is important, because the derivation of the discretised equation (3.7) is no longer valid if r_a depends on l (we can neglect this effect however in one compartment, but a generalisation is needed on the boundaries between compartments). This is due to the fact that equation (2.2), makes use of:

$$I_a = \frac{1}{r_a(l)}(-\frac{\partial V}{\partial l} + E_l) \tag{3.11}$$

When r_a is a function of l, we obtain a generalisation of equation (2.2):

$$i_m = -\frac{\partial I_a}{\partial l} = -\frac{\partial}{\partial l}\frac{1}{r_a(l)}(-\frac{\partial V}{\partial l} + E_l) \tag{3.12}$$

The generalised version of equation (3.7) and (3.8) is implemented in Matlab, by defining the compartmental conductances $G_{a,f}^*(l)$ and $G_{a,b}^*(l)$, denoting the forward conductance between the compartment at $x = l$ and at $x = l + \Delta l$ and the backward conductance between the compartments at $x = l$ and at $x = l - \Delta l$ respectively[2]. We obtain:

$$\frac{2C_m(l)^*}{\Delta t}(V(l,t+\frac{\Delta t}{2}) - V(l,t)) + I_s(l,t+\frac{\Delta t}{2})$$
$$= G^*_{a,f}(l-\Delta l)(V(l-\Delta l,t+\frac{\Delta t}{2}) - V(l,t+\frac{\Delta t}{2})) + G^*_{a,b}(l+\Delta l)(V(l+\Delta l,t+\frac{\Delta t}{2}) - V(l,t+\frac{\Delta t}{2}))$$
$$+G^*_{a,f}(l-\Delta l)(V_e(l-\Delta l,t+\frac{\Delta t}{2}) - V_e(l,t+\frac{\Delta t}{2})) + G^*_{a,b}(l+\Delta l)(V_e(l+\Delta l,t+\frac{\Delta t}{2}) - V_e(l,t+\frac{\Delta t}{2})) \tag{3.13}$$

Where the generalised discretised equation (eq. (3.13)) is obtained, by writing down conservation of current as in equation (3.10).

We can now rewrite equation (3.7), or its generalisation, in a matrix system that determines $\bar{V}(t + \frac{\Delta t}{2})$:

$$\overline{\overline{A_1}}\bar{V}(t+\frac{\Delta t}{2}) + \bar{I}_s(\bar{V}(t+\frac{\Delta t}{2}), t+\frac{\Delta t}{2}) = \overline{\overline{B}}\bar{V}(t) + \overline{\overline{C_E}}\bar{E}_l(t+\frac{\Delta t}{2}) \tag{3.14}$$

And analogously for equation (3.13):

$$\overline{\overline{A_1}}\bar{V}(t+\frac{\Delta t}{2}) + \bar{I}_s(\bar{V}(t+\frac{\Delta t}{2}), t+\frac{\Delta t}{2}) = \overline{\overline{B}}\bar{V}(t) + \overline{\overline{C_V}}\bar{V}_e(t+\frac{\Delta t}{2}) \tag{3.15}$$

We see that $\overline{\overline{A_1}}$, $\overline{\overline{C_E}}$ and $\overline{\overline{C_V}}$ are (non-constant) tridiagonal-matrices, that can be defined by the *spdiags* command in Matlab. The matrix $\overline{\overline{B}}$ is diagonal. This Crank-Nicholson scheme determines $\bar{V}(t + \frac{\Delta t}{2})$ implicitly as function of $\bar{V}(t)$ and $\bar{E}_l(t + \frac{\Delta t}{2})$ or $\bar{V}_e(t + \frac{\Delta t}{2})$: these vectors determine the right-hand sides of eq. (3.14) and eq. (3.15) and are supposed to be known. The Crank-Nicholson matrices depend on the neuronal parameters and on the applied boundary conditions. They will be determined explicitly for some types of boundary conditions in section 3.2.

The $\bar{I}_s(\bar{V}(t + \frac{\Delta t}{2}), t + \frac{\Delta t}{2})$-vector depends on the gate-parameters at time $t + \frac{\Delta t}{2}$; its expression depends on the used model. For the Hodgkin-Huxley model, the CRRSS-model and the passive model, the discretised equation for the membranevoltage V can be written down completely as a matrix-equation. We have:

$$I_s^{HH} = \pi d\Delta l(G_{Na}m^3h(V - V_{Na}) + G_K n^4(V - V_K) + G_L(V - V_L)) \tag{3.16}$$
$$I_s^{CRRSS} = \pi d\Delta l(G_{Na}m^2h(V - V_{Na}) + G_L(V - V_L)) \tag{3.17}$$
$$I_s^{P} = \pi d\Delta l(G_m(V - V_r)) \tag{3.18}$$

Where I_s^{HH}, I_s^{CRRSS} and I_s^P are the currents for the Hodgkin-Huxley, CRRSS and passive model respectively. We introduced conductances per unit area $\pi dG = g$, with d the diameter of the neuron. We note that the diameter d, and even the discretisation step Δl will in generally

[2] We only need one of the definitions for the forward and backward conductance, because of the relation: $G^*_{a,f}(l) = G^*_{a,b}(l + \Delta l)$. We maintain both notations however to make the equations more clear.

depend on the spatial parameter l. The $\bar{I}_s(\bar{V}(t+\frac{\Delta t}{2}), t+\frac{\Delta t}{2})$-vector can now be rewritten, using matrices:

$$\bar{I}_s(\bar{V}(t+\frac{\Delta t}{2}), t+\frac{\Delta t}{2}) = \overline{\overline{A_2}}\bar{V}(t+\frac{\Delta t}{2}) - \bar{V}^*(t+\frac{\Delta t}{2}) \tag{3.19}$$

We note that the matrix $\overline{\overline{A_2}}$ and the vector $\bar{V}^*$ depend on the gate-parameters for the active models at $t+\frac{\Delta t}{2}$. We finally obtain, defining $A = A_1 + A_2$:

$$\begin{aligned}\overline{\overline{A}}\bar{V}(t+\frac{\Delta t}{2}) &= \bar{b}\\ &= \overline{\overline{B}}\bar{V}(t) + \overline{\overline{C_E}}\bar{E}_l(t+\frac{\Delta t}{2}) + \bar{V}^*(t+\frac{\Delta t}{2})\\ &= \overline{\overline{B}}\bar{V}(t) + \overline{\overline{C_V}}\bar{V}_e(t+\frac{\Delta t}{2}) + \bar{V}^*(t+\frac{\Delta t}{2})\end{aligned} \tag{3.20}$$

The membrane-voltage at $t+\frac{\Delta t}{2}$ is now obtained, by calculating the solution of this equation, which can be done efficiently in Matlab.

For the FH model we have:

$$\begin{aligned}I_s^{FH} = \Delta l P_{Na} m^2 h \frac{VF^2}{RT}\frac{[Na]_0 - [Na]_i \exp\{\frac{VF}{RT}\}}{1-\exp\{\frac{VF}{RT}\}} + \Delta l P_K n^2 \frac{VF^2}{RT}\frac{[K]_0 - [K]_i \exp\{\frac{VF}{RT}\}}{1-\exp\{\frac{VF}{RT}\}}\\ + \Delta l P_p p^2 \frac{VF^2}{RT}\frac{[Na]_0 - [Na]_i \exp\{\frac{VF}{RT}\}}{1-\exp\{\frac{VF}{RT}\}} + \pi d \Delta l G_L (V - V_L)\end{aligned} \tag{3.21}$$

And analogous equations for the SE and SRB model. We see that for these models, there doesn't exist a simple matrix expression to determine $V(t+\frac{\Delta t}{2})$. The solution of equation (3.14) or (3.15) is now obtained by using an iterative solver in Matlab. When $V(t+\frac{\Delta t}{2})$ is known, we calculate $V(t+\Delta t)$ by:

$$V(t+\Delta t) = 2V(t+\frac{\Delta t}{2}) - V(t) \tag{3.22}$$

We now need to update gate-parameters at $t+\frac{3}{2}\Delta t$ to finish the leap-frog staggered in time scheme. This is easily done, for instance for the m-gate parameter, discretising equation (2.9).

$$\begin{aligned}\frac{m(t+\frac{3}{2}\Delta t) - m(t+\frac{1}{2}\Delta t)}{\Delta t} = \alpha_m(t+\Delta t)(1 - \frac{m(t+\frac{3}{2}\Delta t) + m(t+\frac{1}{2}\Delta t)}{2})\\ - \beta_m(t+\Delta t)\frac{m(t+\frac{3}{2}\Delta t) + m(t+\frac{1}{2}\Delta t)}{2}\end{aligned} \tag{3.23}$$

In Matlab the electric and geometric parameters of each compartment (soma, dendrite, ...) will first be initialised. Then each compartment will be discretised with a specific space-step Δl. The Matlab code then determines an appropriate Δt, making use the Courant limit. The equations described in this section will then be iterated and the resulting fields are stored and displayed. The different Crank-Nicholson matrices still depend on the applied type of boundary condition. In the next section, we will discuss two types of boundary conditions, for which we will obtain explicit Crank-Nicholson matrices.

3.2 Implementation of boundary conditions

In this section we will give an explicit formulation for the Crank-Nicholson matrices $\overline{\overline{A_1}}$,$\overline{\overline{A_2}}$,$\overline{\overline{B}}$, $\overline{\overline{C_E}}$ $\overline{\overline{C_V}}$ and $\bar{V}^*$, to finish the discretisation of the neuronal models. These Crank-Nicholson matrices depend on the applied boundary conditions. In this thesis we will discuss sealed-end boundary conditions and clamped-voltage boundary conditions (Koch et al., 1998 [46],p.34).

3.2.1 Sealed-end boundary conditions

The sealed-end boundary conditions are often used in literature. The boundary-condition holds for a neuron that is sealed at its ends, so that no axonal current I_a will flow at $x = 0$ and $x = L$. When discretising the neuron, the center of the first compartment is made to coincide with $x = 0$, while the center of the last compartment will coincide with $x = L$. These compartments are thus halved by the boundary conditions. The sealed-end boundary conditions are then implemented, by complementing equation (3.13) with two equations at the two ends, for instance for $x = 0$:

$$\begin{aligned}&\frac{1}{2}(\frac{2C_m(0)^*}{\Delta t}(V(0,t+\frac{\Delta t}{2})-V(0,t))+I_s(0,t+\frac{\Delta t}{2}))\\&\quad=G^*_{a,b}(\Delta l)(V(\Delta l,t+\frac{\Delta t}{2})-V(0,t+\frac{\Delta t}{2}))+G^*_{a,b}(\Delta l)(V_e(\Delta l,t+\frac{\Delta t}{2})-V_e(0,t+\frac{\Delta t}{2}))\end{aligned} \tag{3.24}$$

The factor $\frac{1}{2}$ is due to the fact that the first compartment is halved, thus halving the compartmental capacitance and membrane current. A similar relation holds for $x = L$.

Combining equation (3.13) with the sealed-end boundary conditions equations, equation (3.24), we obtain:

$$\overline{\overline{A_1}} = \begin{bmatrix} \frac{2C^*_m(0)}{\Delta t}+2G^*_{a,b}(\Delta l) & -2G^*_{a,b}(\Delta l) & 0 & ... & 0 \\ -G^*_{a,f}(0) & \frac{2C_m(\Delta l)^*}{\Delta t}+G^*_{a,m}(\Delta l) & -G^*_{a,b}(2\Delta l) & ... & 0 \\ ... & ... & ... & ... & ... \\ 0 & 0 & 0 & ... & \frac{2C^*_m(L)}{\Delta t}+2G^*_{a,f}(L-\Delta l) \end{bmatrix} \tag{3.25}$$

Here we defined the conductivity $G^*_{a,m}(x) = G^*_{a,f}(x - \Delta l) + G^*_{a,b}(x + \Delta l)$, which is used along the diagonal of $\overline{\overline{A_1}}$. The matrix $\overline{\overline{B}}$ is diagonal:

$$\overline{\overline{B}} = \begin{bmatrix} \frac{2C^*_m(0)}{\Delta t} & 0 & ... & 0 \\ 0 & \frac{2C^*_m(\Delta l)}{\Delta t} & ... & 0 \\ ... & ... & ... & ... \\ 0 & 0 & ... & \frac{2C^*_m(L)}{\Delta t} \end{bmatrix} \tag{3.26}$$

The $\overline{\overline{C_E}}$-matrix is given by:

$$\overline{\overline{C_E}} = \begin{bmatrix} -G^*_a(0)\Delta l & 0 & ... & 0 \\ G^*_a(0)\Delta l & -G^*_a(\Delta l)\Delta l & ... & 0 \\ ... & ... & ... & ... \\ 0 & 0 & ... & -G^*_a(L-\Delta l)\Delta l \\ 0 & 0 & ... & G^*_a(L-\Delta l)\Delta l \end{bmatrix} \tag{3.27}$$

We notice that a spatial mismatch is introduced, when discretising the $E_l(x)$-field. Indeed, in the discretised equation of $V(x)$ we need $E_l(x-\frac{\Delta l}{2})$ and $E_l(x+\frac{\Delta l}{2})$. If we only want to store the fields at the grid-locations $x_i = i\Delta l$ ($i = 0...S-1$; where S is the number of segments), a spatial mismatch is necessary. We made the identification $x_i + \frac{\Delta l}{2} \to x_i$, which results in an error that corresponds to shifting the electromagnetic field E_l over $\frac{\Delta l}{2}$. This error thus depends on the discretisationstep Δl, and will be small if $\Delta l \ll 1$. The E_l-vector is then a $(S-1)\times 1$-vector, unlike all other vectors (V,m,n,...) that are $S \times 1$-vectors. We notice that the corresponding matrix $\overline{\overline{C_E}}$ is a $S \times (S-1)$-matrix.

The $\overline{\overline{C_V}}$-matrix is given by:

$$\overline{\overline{C_V}} = \begin{bmatrix} -2G^*_{a,b}(\Delta l) & 2G^*_{a,b}(\Delta l) & 0 & ... & 0 \\ G^*_{a,f}(0) & -G^*_{a,m}(\Delta l) & G^*_{a,b}(2\Delta l) & ... & 0 \\ ... & ... & ... & ... & ... \\ 0 & 0 & 0 & ... & -2G^*_{a,f}(L-\Delta l) \end{bmatrix} \tag{3.28}$$

To finish the discretisation with sealed-end boundary conditions, we take a final look at the $\bar{I_s}(\bar{V}(t+\frac{\Delta t}{2}), t+\frac{\Delta t}{2})$-vector. This vector can be split into a linear component $\bar{I_s}^L$, which is only non-zero at passive, Hodgkin-Huxley and CRRSS compartments, and a non-linear component $\bar{I_s}^{NL}$, which is non-zero at the SRB, SE and FH compartments. The component $\bar{I_s}^L$ is called linear, because it can be written as:

$$\bar{I_s}^L(\bar{V}(t+\frac{\Delta t}{2}), t+\frac{\Delta t}{2}) = \overline{\overline{A_2}}\bar{V}(t+\frac{\Delta t}{2}) - \bar{V}^*(t+\frac{\Delta t}{2}) \tag{3.29}$$

Here the $\overline{\overline{A_2}}$-matrix is given by:

$$\overline{\overline{A_2}} = \begin{bmatrix} G^*_m(0) & 0 & ... & 0 \\ 0 & G^*_m(\Delta l) & ... & 0 \\ ... & ... & ... & ... \\ 0 & 0 & ... & G^*_m(L) \end{bmatrix} \tag{3.30}$$

Similarly for $\bar{V}^*(t+\frac{\Delta t}{2})$ we write: $\bar{V}^*(t+\frac{\Delta t}{2}) = [V^*(0) \quad V^*(\Delta l) \quad ... \quad V^*(L)]^T$.

The compartmental membrane-conductance $G^*_m(x_i)$ is only non-zero for passive, HH and CRRSS compartments:

$$G^*_m(x_i) = \begin{cases} \pi d \Delta l G_m & x_i \in \Omega_P \\ \pi d \Delta l (G_{Na} m^3 h + G_K n^4 + G_L) & x_i \in \Omega_{HH} \\ \pi d \Delta l (G_{Na} m^2 h + G_L) & x_i \in \Omega_{CRRSS} \\ 0 & x_i \in \Omega_{FH} \cup \Omega_{SRB} \cup \Omega_{SE} \end{cases}$$

Where the right-hand side has to be evaluated in x_i. We denoted the different neuronal model domains by Ω. For instance Ω_{HH} is the set of x_i-positions along the neuron, where a Hodgkin-Huxley model was applied. Similarly we obtain for $V^*(x_i)$:

$$V^*(x_i) = \begin{cases} \pi d\Delta l G_m V_r & x_i \in \Omega_P \\ \pi d\Delta l(G_{Na}m^3hV_{Na} + G_K V_K n^4 + G_L V_L) & x_i \in \Omega_{HH} \\ \pi d\Delta l(G_{Na}m^2hV_{Na} + G_L V_L) & x_i \in \Omega_{CRRSS} \\ 0 & x_i \in \Omega_{FH} \cup \Omega_{SRB} \cup \Omega_{SE} \end{cases}$$

Finally we obtain the equation to be solved for the membrane-voltage ($\overline{\overline{A}} = \overline{\overline{A_1}} + \overline{\overline{A_2}}$):

$$\begin{aligned} \overline{\overline{A}}\bar{V}(t + \frac{\Delta t}{2}) + \bar{I_s}^{NL}(\bar{V}(t + \frac{\Delta t}{2}), t + \frac{\Delta t}{2}) = \bar{b} & \\ = \overline{\overline{B}}\bar{V}(t) + \overline{\overline{C_E}}\bar{E}_l(t + \frac{\Delta t}{2}) + \bar{V}^*(t + \frac{\Delta t}{2}) & \\ = \overline{\overline{B}}\bar{V}(t) + \overline{\overline{C_V}}\bar{V}_e(t + \frac{\Delta t}{2}) + \bar{V}^*(t + \frac{\Delta t}{2}) & \end{aligned} \tag{3.31}$$

Equation (3.31) is the general matrix-equation that determines V over the whole neuron, that consists of different compartments, that are described by different neuronal models (passive model, HH, CRRSS, FH, SRB or SE model). This equation is solved numerically by Matlab in this thesis.

3.2.2 Clamped-voltage boundary conditions

In clamped-voltage boundary conditions, the voltage at the neuronal ends is held constant: $V(0) = V_0$ and $V(L) = V_L$. The voltage can now only vary at $S-2$ segments. The boundary conditions can easily be implemented, by using a $S-2$-dimensional vector $\bar{V}$ that holds all membrane voltages for $x_i = i\Delta l$ with $i = 1, ..., S-2$. The electromagnetic-field vector $\bar{E}_l$ is still the same $S-1$-dimensional vector. We obtain then again equation (3.31) as completely discretised equation in V. The Crank-Nicholson matrices are now $S-2 \times S-2$ matrices, except for $\overline{\overline{C_E}}$ which is a $S-2 \times S-1$ matrix:

$$\overline{\overline{A}} = \begin{bmatrix} \frac{2C_m^*(\Delta l)}{\Delta t} + 2G_{a,m}^*(\Delta l) + G_m^*(\Delta l) & -G_{a,b}^*(2\Delta l) & 0 & ... & 0 \\ -G_{a,f}^*(\Delta l) & \frac{2C_m(2\Delta l)^*}{\Delta t} + G_{a,m}^*(2\Delta l) + G_m^*(2\Delta l) & -G_{a,b}^*(3\Delta l) & ... & 0 \\ ... & ... & ... & ... & ... \\ 0 & 0 & 0 & ... & \frac{2C_m^*(L-\Delta l)}{\Delta t} + 2G_{a,m}^*(L-\Delta l) + G_m^*((L-\Delta l) \end{bmatrix} \tag{3.32}$$

For $\overline{\overline{B}}$ we obtain te diagonal matrix:

$$\overline{\overline{B}} = \begin{bmatrix} \frac{2C_m^*(\Delta l)}{\Delta t} & 0 & ... & 0 \\ 0 & \frac{2C_m^*(2\Delta l)}{\Delta t} & ... & 0 \\ ... & ... & ... & ... \\ 0 & 0 & ... & \frac{2C_m^*(L-\Delta l)}{\Delta t} \end{bmatrix} \tag{3.33}$$

Finally for the $\overline{\overline{C}}$ matrices we obtain:

$$\overline{\overline{C_E}} = \begin{bmatrix} G_a^*(0)\Delta l & -G_a^*(\Delta l)\Delta l & ... & 0 & 0 \\ ... & ... & ... & ... & ... \\ 0 & 0 & ... & G_a^*(L-2\Delta l)\Delta l & -G_a^*(L-\Delta l)\Delta l \end{bmatrix} \tag{3.34}$$

$$\overline{\overline{C_V}} = \begin{bmatrix} 2G_{a,m}^*(\Delta l) & -G_{a,b}^*(2\Delta l) & 0 & ... & 0 \\ -G_{a,f}^*(\Delta l) & G_{a,m}^*(2\Delta l) & -G_{a,b}^*(3\Delta l) & ... & 0 \\ ... & ... & ... & ... & ... \\ 0 & 0 & 0 & ... & 2G_{a,m}^*(L-\Delta l) \end{bmatrix} \tag{3.35}$$

The boundary-conditions are included in the vector $\bar{V}^*$:

$$\bar{V}^* = \begin{bmatrix} V^*(\Delta l) + G_{a,f}^*(0)V_0 \\ V^*(2\Delta l) \\ ... \\ V^*(L-\Delta l) + G_{a,b}^*(L)V_L \end{bmatrix} \tag{3.36}$$

3.3 Program verification by comparison with literature

We now would like to validate the Matlab code by comparison with literature. In Rattay (2005) [12], $p.22$, the transmembranevoltage is simulated on a single straight neuron, without bifurcations. The results obtained in Rattay [12] are shown in figure 3.1. The electromagnetic field distribution is excited by a point electrode in a completely homogeneous extracellular fluid with resistivity ρ_e. As represented in figure 3.1, the electrode is placed just above the soma (with distance $d(soma, electrode) = d_{elec} = 1mm$). The field is generated by a current pulse ($I_{elec} = 5mA$) that holds on for $T_{pulse} = 100\mu s$. In this case we don't need S4L-simulations to determine the electromagnetic field distribution, because the external potential V_e can be calculated analytically. We have, with r the distance from the point electrode:

$$V_e = \frac{\rho_e I_{elec}}{4\pi r} \tag{3.37}$$

We assume equation (3.37) to be quasistatically valid for every time t. The used neuron consists of 40 compartments. There are 10 dendrite compartments with variable diameter d and length l that are all described with a passive transmissionline model. The soma is described as one compartment with a Hodgkin-Huxley model. The initial segment is calculated by a CRRSS-model as one compartment. Then the axon is segmentated into 11 myelinated internode compartments, that are described with the passive model, implying 10 nodes of Ranvier that are described with a CRRSS-model. The other 7 compartments are described by a Hodgkin-Huxley model: 6 compartments for the unmyelinated part of the axon, with variable diameter and length, and 1 compartment for the synapse. For the exact neuronal data we refer to Rattay $p.23 - p.24$ [12].

In Rattay (2005) [12] the membranevoltage is calculated on this single, multi-compartmental neuron. The result obtain in Rattay, is shown in figure 3.1. The membranevoltage is shown as 7 full lines. Each line corresponds with a fixed time. These times are separated by time intervals of $50\mu s$, so line 1 is the spatial distribution at $t = 50\mu s$, line 2 at $t = 100\mu s$,... The dashed line (corresponding with the dashed scale) in figure 3.1 represents the activating function f, which is defined in Rattay [12], as:

$$f(l) = \frac{G^*_{a,f}(l - \Delta l)(V_e(l - \Delta l) - V_e(l)) + G^*_{a,b}(l + \Delta l)(V_e(l + \Delta l) - V_e(l))}{C^*_m(l)} \tag{3.38}$$

Here f is evaluated after the electrode is turned on, at $t = 0$. The activating function f is expressed in $\frac{V}{s}$ and it can be interpreted using equation (3.13): the activating function is the rate of change of the membranevoltage V in each compartment, when the neuron is initially at rest. Regions where the activating function f is strongly positive are potential candidates for spike initiation of an action potential, while regions with a strongly negative activating function are likely to be hyperpolarised.

Although the electrode is located just above the soma, the activating function f has no maximum, nor minimum at the soma. This indicates that the soma will not be the location of the neuron from where an actionpotential will start to propagate. The most negative value of f is reached at the first node of Ranvier, the next node of Ranvier still has a negative value of f, all other Ranvier-nodes are however likely to depolarise due to a positive peaking value of f. The strongest positive value of f is obtained at the first unmyelinated element of the axon. This

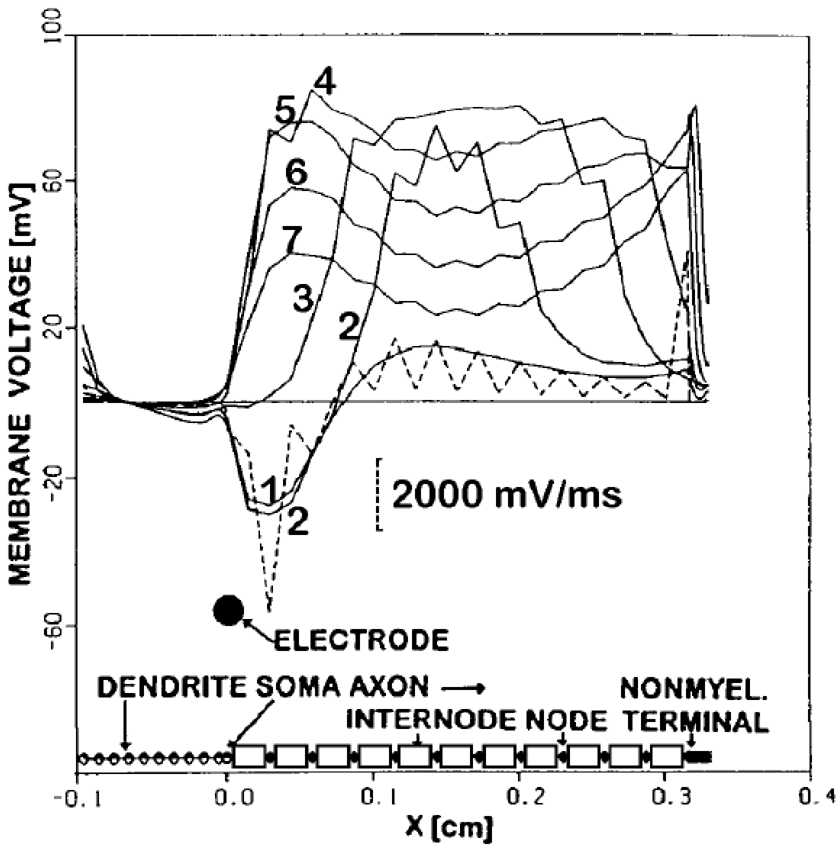

Figure 3.1: Result obtained in Rattay [12] for the simulation of the membranevoltage on a single straight neuron without bifurcations. The 7 full lines represent snapshots of the spatial distribution of the membranevoltage in intervals of $50\mu s$ (line 1 is at time $50\mu s$, line 2 at time $100\mu s, \ldots$). The dashed scale corresponds to the dashed line, which shows the spatial distribution of the activating function f. Figure reproduced from Rattay (2005) [12].

behaviour, where stimulation does not occur at the electrode, is typical for so-called anode-make stimulation (see also chapter 4). The stimulation is called "make", because the depolarisation on the neuron is caused by applying a voltage on the electrode. This is in contrast with "break" stimulation, where an action potential might occur after turning the applied voltage off. Because $I > 0$ the electrode is an anode here. Both for cathode-make and anode-make stimulation depolarisation occurs at the (virtual) cathodes (Rattay, 1987 [47]; Ranck, 1975 [48]; Roth, 1993 [15]). This means that for the simulation under consideration, it is expected that depolarisation will not occur right under the electrode (which is an anode). Instead, depolarisation will occur at the end of the axon, at the so-called "virtual"-cathode.

We now compare the results obtained in Rattay [12] with the results obtained by the Matlab code for the transmembranevoltage V in figure 3.2 and the activating function f in figure 3.3.

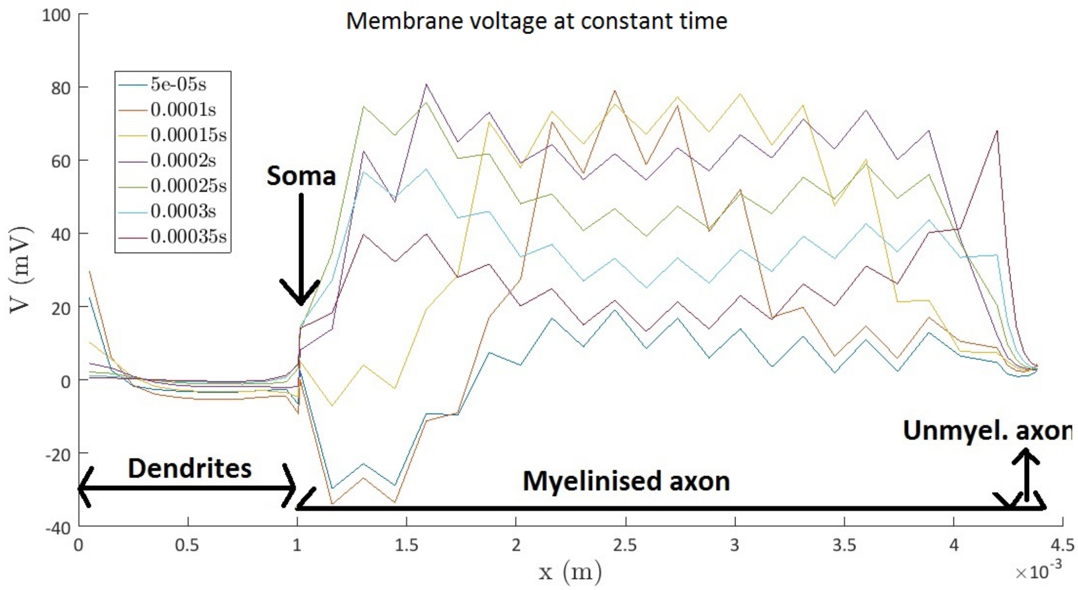

Figure 3.2: The simulation from Rattay (2005) [12] of the reduced membrane voltage along a single neuron is reproduced by the Matlab code. The spatial distribution of $\tilde{V}$ is shown at 7 subsequent times along the same neuron.

We notice that the results obtained by the Matlab-code are indeed similar to these obtained by Rattay [12]: the activating function (fig. 3.3) is in both cases strongly negative at the first node, stays negative at the second node and obtains positive stimulating values at the other nodes of Ranvier. The membranevoltage at the other hand in fig. 3.2 is initially hyperpolarised at the first two nodes of Ranvier, while depolarising activation first occurs at node $4-6$ in both cases. Because of the strong hyperpolarisation at the beginning of the axon we see that in Rattay [12], as in our case, the generated actionpotential will first reach the end of the myelinated axon, before reaching the soma. This effect is more clear when we plot the membranevoltage as a colour map, as is done in figure 3.4[3]. This is a manifestation of the fact that a hyperpolarised region can effectively "block" the propagation of an actionpotential (Fang et al.,1991 [49]; Ranck, 1975 [48]). We notice that although the actionpotential reaches node 10 before reaching the soma, it will never reach the synapse in the simulation time $T_{sim} = 350\mu s$ (it will reach the synapse though, when we extend the simulation time). This is due to the fact that propagation of the actionpotential is slowed down when entering the unmyelinated part of the axon. This corresponds with the well known fact that information propagates faster in myelinated axons, compared with unmyelinated axons (Kandel, 2000 [50]). Furthermore we notice that at the dendrite-terminals (i.e. $x = 0m$) depolarisation occurs over about $20mV$, as can be seen in figure 3.2. This is a manifestation of the fact that neuronal bendings and terminations are especially sensitive to depolarisation, as will be discussed in chapter 5.

[3] To illustrate the position on the neuron for any location on the colour map, a schematic representation of the neuron is shown along the y-axis on the right of the figure. This schematic representation of the neuron will be used in all colour maps in this thesis, and is reproduced from Rattay (2005) [12] (see also figure 3.1)

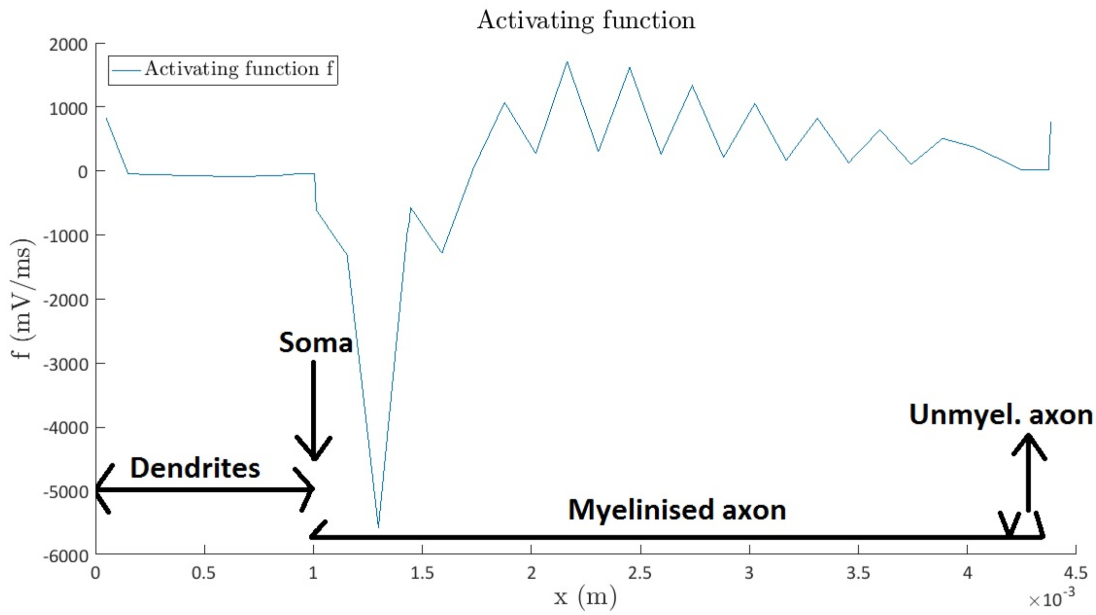

Figure 3.3: The simulation from Rattay (2005) [12] of the activation function f along a single neuron is reproduced by the Matlab code.

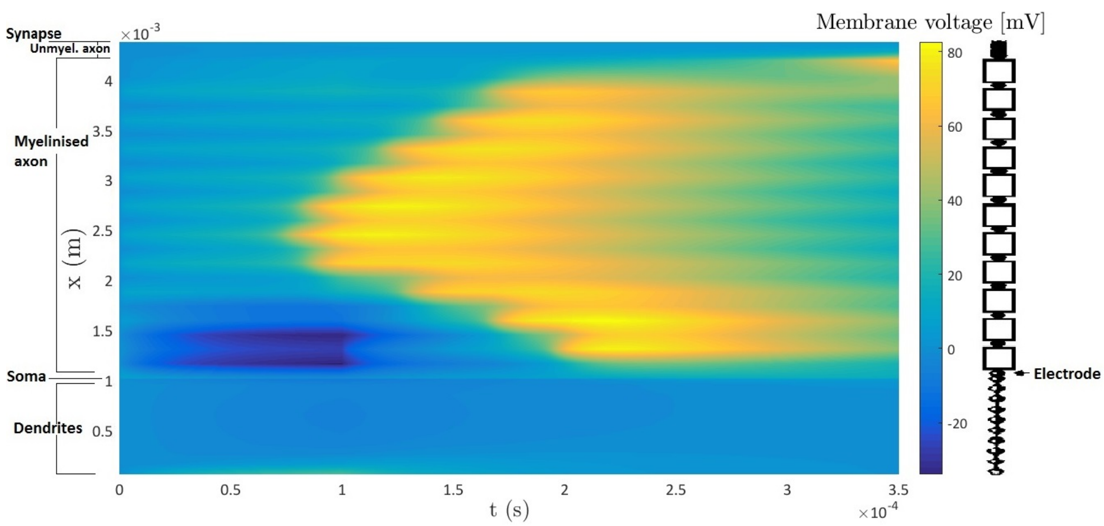

Figure 3.4: Colour map of the reduced membrane voltage in time and space. The colours represent the value of $\tilde{V}$. The map is obtained by stimulation with a spherical electrode ($10V$) at $1mm$ from the soma of a straight neuron.

We can also plot the gate-parameters, as is done for the m-gate parameters in figure 3.5. We notice that the m gate-parameter reflects the behaviour of the membrane voltage on the axon. When a strongly positive activating function f is obtained at a node of Ranvier, the sodium-gates will open and the neuronal membrane will depolarise: an actionpotential is generated that will propagate over the neuronal axon. This phenomenon of the opening of the sodium gates is described by m and h. The activation gate-parameter m contributes to the fast opening of the sodium channels and will increase when activation occurs. The inactivation gate h in contrast (Figure 3.6), contributes to the relatively slow closing of the sodium gates, and will decrease when activation occurs. Because of this, the sodium channel current will be transient. We notice that the m gate-parameter is by definition zero at the dendrites and myelinated internodes, because these compartments are described by a passive model. The m and h parameter can only be non-zero at active (in this case Hodgkin-Huxley and CRRSS) compartments.

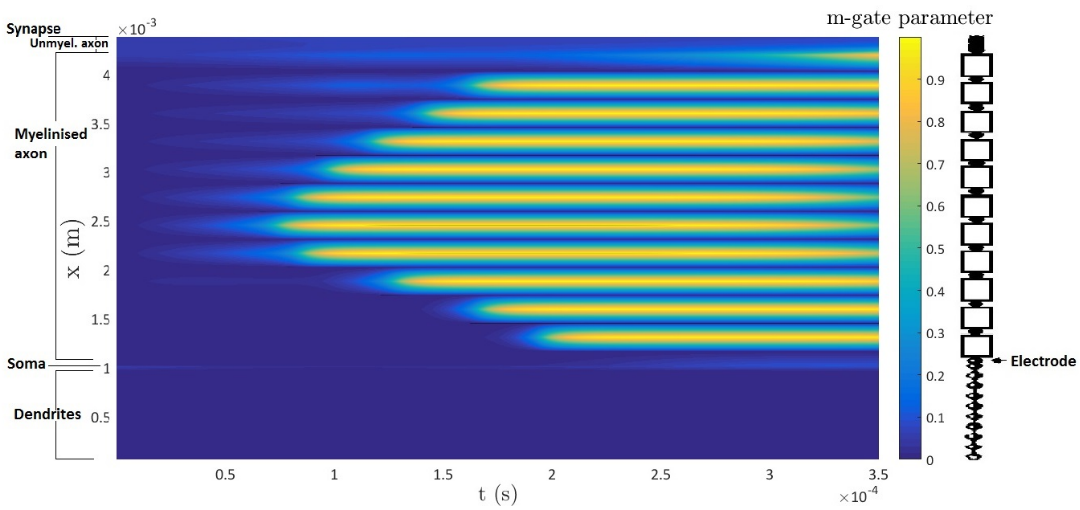

Figure 3.5: Colour map of the m-gate parameter in time and space. The colours represents the value of m. The map is obtained by stimulation with a spherical electrode ($10V$) at $1mm$ from the soma of a straight neuron.

A similar discussion holds for the gate parameter n, shown in figure 3.7. This gate parameter describes the opening of the potassium gates, and will increase by activation. However this gate-parameter is not used in the CRRSS-model, that we used for the initial segment and Ranvier nodes. Because of this the n gate parameter will be by definition zero at the passive compartments (dendrites and myelinated internodes) and at the Ranvier nodes and the initial segment. The n parameter still reflects the activation at the Hodgkin-Huxley compartments though (unmyelinated axonterminal, synapse and the soma).

We are now also able to determine if the neuron has been activated. Neuronactivation occurs if the neuronal membrane has depolarised, which can be formulated mathematically by requiring $V > V_{tresh}$, for some thresholdvoltage V_{thresh}. This depolarisation of the membrane is called

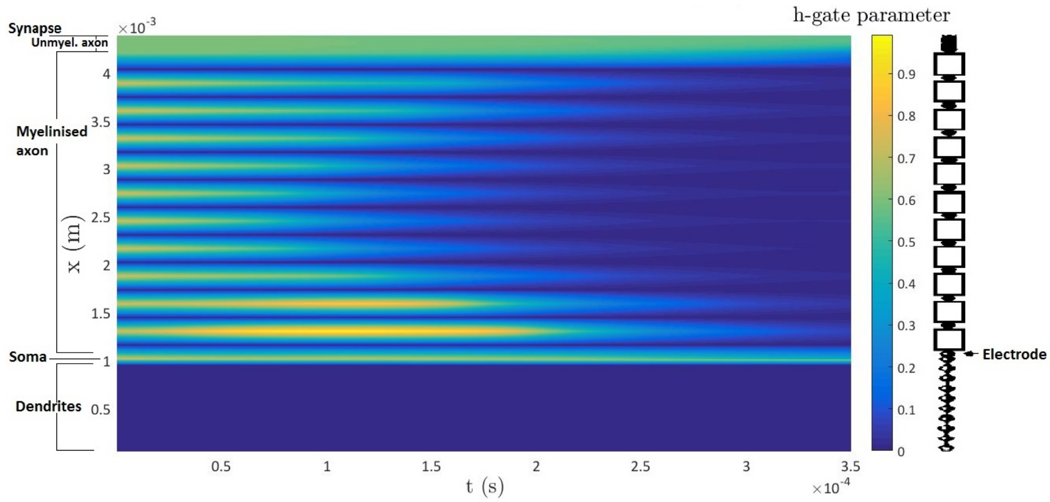

Figure 3.6: Colour map of the h-gate parameter in time and space. The colours represents the value of h. The map is obtained by stimulation with a spherical electrode $(10V)$ at $1mm$ from the soma of a straight neuron.

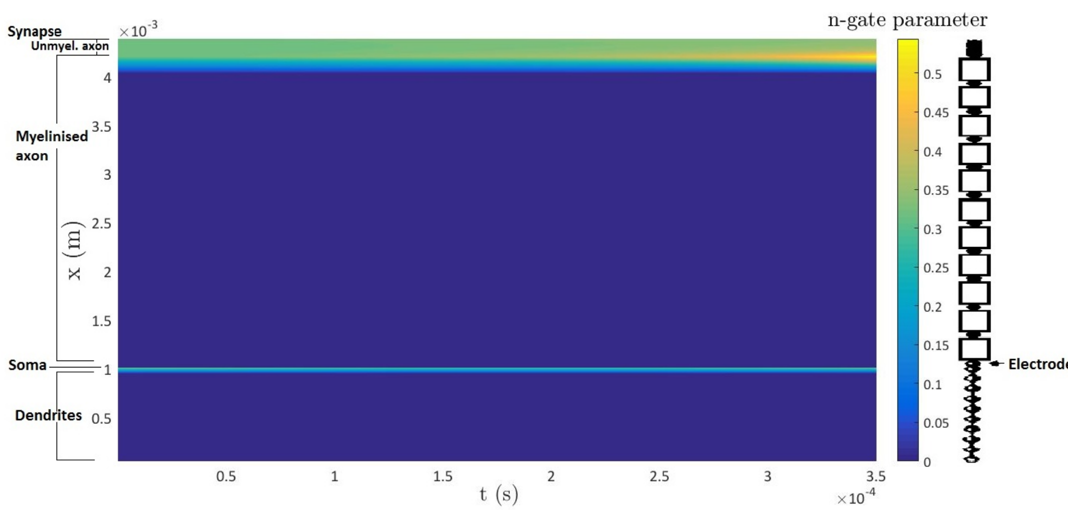

Figure 3.7: Colour map of the n-gate parameter in time and space. The colours represents the value of n. The map is obtained by stimulation with a spherical electrode $(10V)$ at $1mm$ from the soma of a straight neuron.

an actionpotential. We only consider the active compartments when we want to determine neuronactivation. Furthermore we require that the actionpotential has to propagate over the neuron. We will discuss the details of this problem of determining neuronactivation in section 4.3. The Matlab code will determine if the neuron has been activated and summarize the results in an activationtable, as represented in figure 3.1. We see that the activationtable mentions that the neuron is indeed activated at 3 locations at the same time $t = 0.1ms$ after initiation of the stimulationpulse. The locations correspond with the fourth till sixth node of Ranvier. This result can also be noted by inspecting the colour maps for V in figure 3.4 and for the m gate-parameter in figure 3.5. We notice that indeed activation initiates somewhat simultaneously at nodes $4-6$. The activationtable mentions all 3 activationpositions corresponding to node 4, 5 and 6, because the Matlab code could not find any causal relation between the actionpotentials that originated at these nodes. In this case the external source electrode caused activation on node 4, 5 and 6, which caused subsequently activation on the other nodes of Ranvier due to propagation of the signal through the myelinated internodes. The actionpotential propagates both in the direction of the soma and the direction of the synapse (antidromic and orthodromic propagation).

	Activated	Synapse activated	nr.	pos. (mm)	time (ms)	MSOAf (m/s)	MSOAb (m/s)
Rattay config	yes	no	1.	2.1635	0.1000	18.2094	7.0757
			2.	2.4505	0.1000	15.1745	9.4343
			3.	2.7375	0.1000	12.1396	11.7929

Table 3.1: Activation table summarizing neuronal activation locations, times and speeds. The table is obtained by stimulation with a spherical electrode $(10V)$ at $1mm$ from the soma of a straight neuron.

We note that the table 3.1 also mentions if the activationpulse has propagated to the synapse in the simulationtime T_{sim}. This is not the case for this simulation. However when extending the simulationtime the actionpotential will reach the synapse. The neuron will then transmit the signal to the next neuron by neurotransmission at the synapse.

The activationtable will also show the mean speeds by which the activationpotential has propagated, denoted by $MSOA_f$ and $MSOA_b$ for the forward and backward mean speed of propagation respectively. We emphasize that these speeds are ofcourse mean speeds, because the instaneous speed of propagation depends on the compartment (propagation through myelinated internodes versus propagation through nodes of Ranvier). We see from the activationtable that the mean speed in the forward direction (i.e. to the synapse), $12\frac{m}{s}$, is faster than the speed of propagation towards the soma $7\frac{m}{s}$. This is due to the initial hyperpolarisation of the first two nodes of Ranvier, preventing the actionpotential to propagate towards the soma. When considering the forward speed, notice that $MSOA_f(4) = 18\frac{m}{s} > MSOA_f(5) = 15\frac{m}{s} > MSOA_f(6) = 12\frac{m}{s}$. With $MSOA_f(i)$ the $MSOA_f$ on node i. This is due to the fact that the actionpotential starts almost simultaneously at the 4th, 5th and 6th node. When determining $MSOA_f(5)$, the Matlab-code will include the speed of propagation from node from node 5 to node 6, increasing the mean. The mean speed on the 4th node is consequently even higher. Ofcourse in this case only the $MSOA_f(6)$ is relevant. An analogous discussion is valid for the backward mean speed $MSOA_b$. We will discuss neuronal activation and the corresponding activationtables in detail in section 4.3.

Part II

Simulating single neurons

Chapter 4

Simulation of the transmembrane voltage and gate-parameters on a single neuron

In this chapter we will consider some more general simulations on single neurons. Simulations on bundles of multiple neurons will be discussed in part III of this thesis. In this chapter, we use a simple stimulation set-up of a spherical electrode in a homogeneous medium. The electric field will now be simulated by Sim4life, as discussed in section 1.1. In contrast with the simulation from section 3.3, the electrode is no longer a point-electrode, boundary conditions are now applied at the end of the simulation domain and the electric field is simulated numerically with Sim4life. This transition from an analytical solution for the electric field to a numerically simulated field distribution by S4L, is also useful to prepare us to consider Sim4life simulations of a more general Medtronic electrode in chapter 7. Although the simulations discussed in this chapter make use of some simplifications (spherical electrode, homogeneous medium, single neuron), they are still interesting because they lead to some conceptual insights about the activation and stimulation of neurons. We will first consider simulations on a neuron that is completely straight, in section 4.1. Subsequently we discuss a neuron that is bending at a certain location in section 4.2.

4.1 Simulations on a single straight neuron

In this section, we will consider five simulations on a completely straight neuron. We will make use of the neuron we defined in section 3 (see p.22-p.23 in Rattay (2005) [12]).

The first simulation in subsection 4.1.1 is similar to the configuration of the simulation in section 3.3. However instead of using an analytically calculated electric potential, the electric field distribution is now simulated by Sim4life. Furthermore, instead of turning the electrode off after $100\mu s$ as was done in subsection 4.1.1, the electrode will now stimulate the neuron for the whole simulation time ($T_{sim} = 350\mu s$). Consequentially, there will be some differences between the simulation set-up of subsection 3.3 and subsection 4.1.1. Nevertheless, we expect a similarity between the results of both simulations. This similarity can then be seen as a verification of the code necessary to couple the Matlab program with the Sim4life simulations. This coupling of electromagnetic simulations with the multi-compartmental neuronsolver will subsequently be used in all the following simulations in this thesis.

Simulations $2-4$ deal with a configuration of a spherical electrode at $2mm$ from the soma. In simulation 2, discussed in subsection 4.1.2, a constant electrode voltage of $60V$ is applied and the neuron is solved under sealed-end boundary conditions. As such, this simulation can be compared with simulation 1 (subsection 4.1.1). The influence of the boundary conditions is studied in simulation 3 (subsection 4.1.3) in which the neuron is voltage-clamped, while an electrode voltage of $60V$ is applied. In simulation 4 we test for cathode-make stimulation, by applying a negative electrode voltage of $-60V$. The neuron in simulation 4, is again solved with sealed-end boundary conditions.

Finally, in simulation 5 (section 4.1.5), we study the influence of the location of the electrode. Anode-make stimulation is used ($V_{elec} = 60V$), while the electrode is placed $2mm$ above the centre of the neuron (i.e. at the myelinated axon).

4.1.1 Simulation 1. Anode-make stimulation by spherical electrode (10 V) at 1 mm from soma

The first simulation on a single straight neuron, is similar to the simulation of section 3.3. As in section 3.3 we use a spherical electrode at $1mm$ from the soma of a straight neuron. Furthermore the simulation is again done for a completely homogeneous medium. The difference with section 3.3 is that now no longer a point electrode is used, on which a specific stimulus current is applied. Instead we use a spherical electrode with radius $0.1mm$ on which a constant voltage of $10V$ is applied. Also, the field distribution is no longer obtained analytically but by simulation with Sim4life. This means that now boundary conditions are applied at the end of the simulation domain. To subsequently calculate the neuronal response to the simulated field distribution, an interpolation step from the Sim4life grid to the Matlab grid is now necessary, as was explained briefly in chapter 1. Furthermore, instead of turning the electrode off after $100\mu s$, as was done in the simulation of subsection 3.3, the electrode will now stimulate the neuron during the whole simulation time T_{sim}. Although this simulation has some differences with the simulation of subsection 3.3, we expect similar results. As such the simulation discussed in this section makes it possible to qualitatively verify the additional code to couple the Sim4life simulations with the Matlab code, that will be used to calculate more general simulation-setups later on.

Because the applied voltage is positive and because the neuron-stimulation will occur due to the fact that the electrode is turned on, the stimulation is called anode-make stimulation. Because of this we expect, similarly as in subsection 3.3, that neuronal activation does not occur under the electrode (i.e. at the soma), but rather at the axon (at the virtual cathode). This observation that stimulation occurs at the (virtual) cathode(s), is discussed in Roth (1993) [15]. Furthermore, a region of hyperpolarisation (RoH) is expected at the (virtual) anode(s). In this case, the electrode is the anode and consequentially we expect hyperpolarisation right under the electrode.

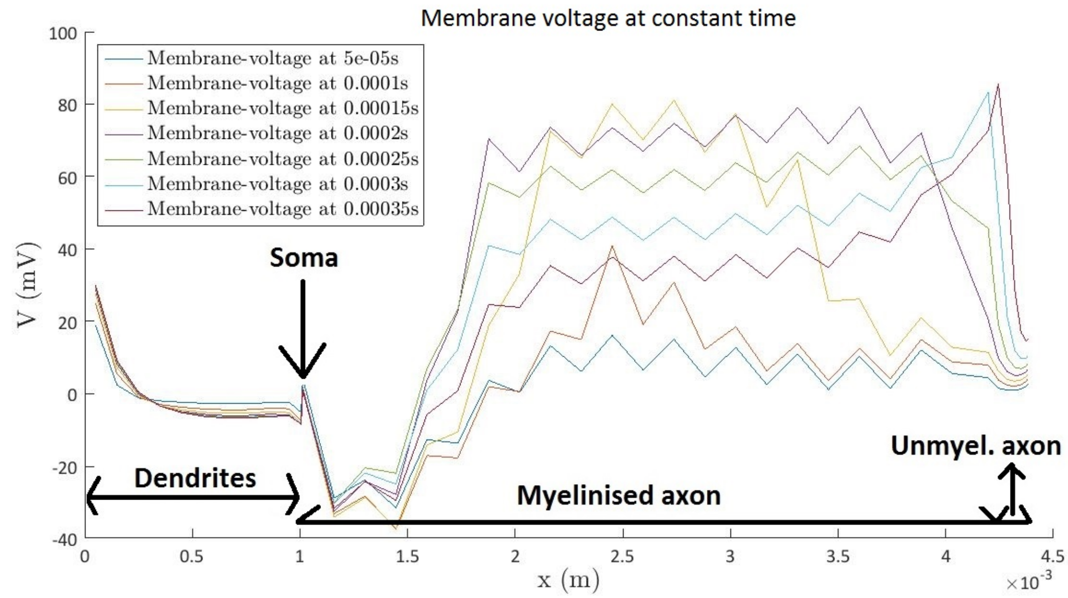

Figure 4.1: Anode-make stimulation by spherical electrode ($10V$) at $1mm$ from the soma. Spatial distribution of the reduced membrane voltage $\tilde{V}$ at 7 subsequent times is shown.

The electrode is turned on at $t = 0$, we can thus write for the electrode potential $V_{elec}(t)$,

$$V_{elec}(t) = 10V\theta(t) \tag{4.1}$$

with θ the Heaviside function. The electrode-potential is turned on for the whole simulation time T_{sim}. We assume that the electric field distribution varies quasistatically with this Heaviside pulse. This implies that the electric field can be calculated with a single Sim4life simulation at $0Hz$.

The activation function f is shown in figure 4.2. The results are seen to be qualitatively similar to those obtained in subsection 3.3. This is a result of the fact that the activation function f is evaluated just after the electrode is turned on (at $t = 0$). The longer duration of the electrode-stimulus in this simulation (compared to the simulation of subsection 3.3) has consequentially no effect on f. There are some small differences between the activation functions of both simulations though. These can be explained by the difference in electrode-shape, which is now no longer a point source, and the difference in the applied dirichlet-conditions on the electrode (dirichlet-condition on the voltage ($10V$) in S4L-simulation (this subsection) versus condition on the applied electrode current ($5mA$) in the exact solution of the electric field distribution (subsection 3.3)). Furthermore boundary conditions at the end of the simulation domain are now applied and the electric field distribution is simulated at the discretised grid locations. This is in contrast with the simulation of subsection 3.3, where an exact solution for the electric field in a homogeneous tissue was used.

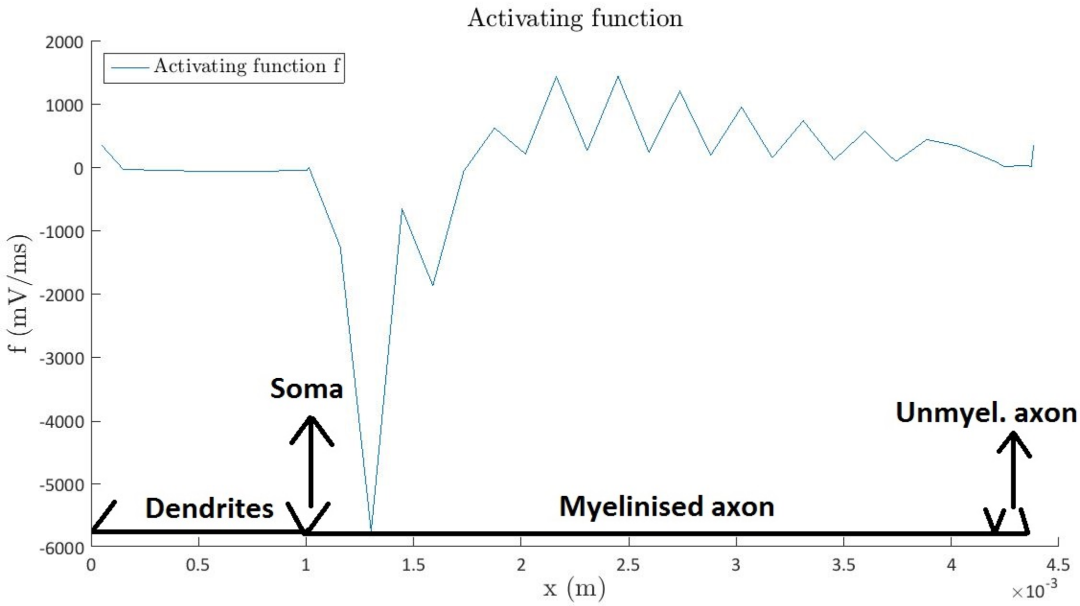

Figure 4.2: Anode-make stimulation by spherical electrode ($10V$) at $1mm$ from the soma. Spatial distribution of the activation function f is shown.

The spatial distribution of the reduced membranevoltage $\tilde{V}$ is displayed in figure 4.1. We notice the difference with the simulation of the membranevoltage in subsection 3.3 (figure 3.2). We can clearly see the effect of turning the electrode off at $100\mu s$ (as done in subsection 3.3). The region of hyperpolarisation at the electrode-position, will disappear when the electrode is turned off at $t = 100\mu s$, allowing the actionpotential to travel towards the soma. In contrast, in the simulation of this subsection, the electrode is not turned off and the RoH will persist. The actionpotential is consequentially not allowed to propagate towards the soma.

The colour maps for the reduced membranevoltage $\tilde{V}$ and gate-parameter m are shown in figures 4.3 and 4.4 respectively. We note that the results are again similar to those obtained in subsection 3.3. In these colour maps we can now clearly see that the region of hyperpolarisation at the beginning of the axon will persist, when the electrode is not turned off.

	Activated	Synapse activated	nr.	pos. (mm)	time (ms)	MSOAf (m/s)	MSOAb (m/s)
Rattay config	yes	no	1.	2.4505	0.1531	9.1974	11.9875

Table 4.1: Activation table for a straight neuron, stimulated by a spherical electrode ($10V$) at 1 mm from the soma.

The activationtable is shown in figure 4.1. The neuron is activated and activation starts at $2.45mm$ from the beginning of the neuron. This corresponds to the 5th node of Ranvier at

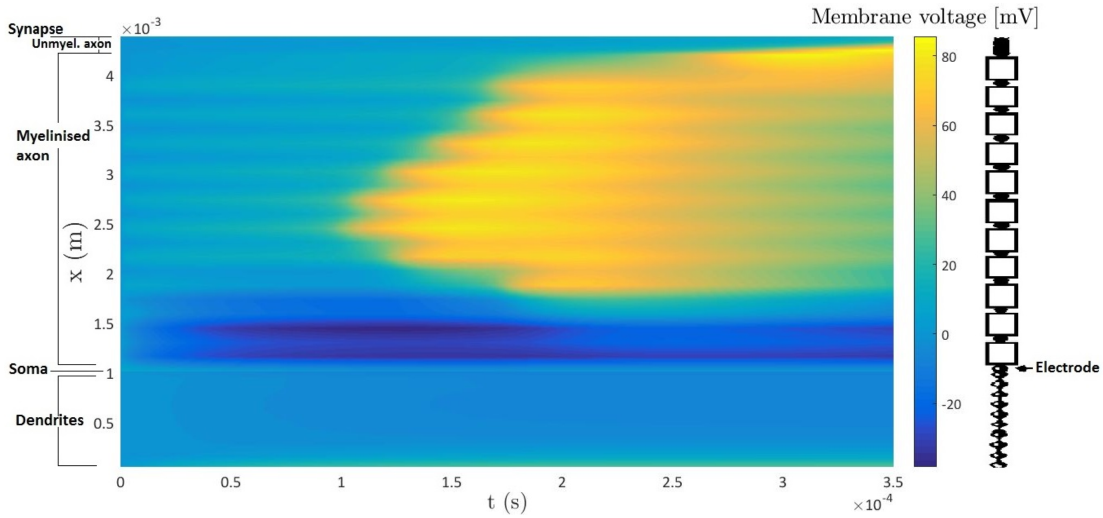

Figure 4.3: Colour map of the reduced membrane voltage in time and space. The colours represent the value of $\tilde{V}$. The map is obtained by anode-make stimulation by a spherical electrode ($10V$) at $1mm$ from the soma of a straight neuron.

the axon. This can also be seen in the figures for the membranevoltage and m-gate parameter. We note that this corresponds to our previous simulations in subsection 3.3, where stimulation was initiated simultaneously at node 4, 5 and 6. We note that neuronal activation has shifted towards later times: in this section we obtain neuronal activation $0.15ms$ after turning on the electrode. In contrast, in subsection 3.3, we obtained activation after $0.1ms$. This observation can also be made by comparing the colour maps of the voltage or gate-parameters. However, we attribute this observation to the different electrode-conditions that were used (in this subsection the electrode-potential is set to $10V$, in subsection 3.3 the electrode-current is set to $5mA$).

The colour maps for the h-gate parameter and n-gate parameter are shown in figure 4.5 and in figure 4.6 respectively. We note again the similarity with the corresponding plots in subsection 3.3. Furthermore the fact that the region of hyperpolarisation persists, can also be observed in the plot of the h-gate parameter. As in subsection 3.3 the n-gate parameter is identically zero on the axon, because no n value is used in the CRRSS-model used for the nodes of Ranvier.

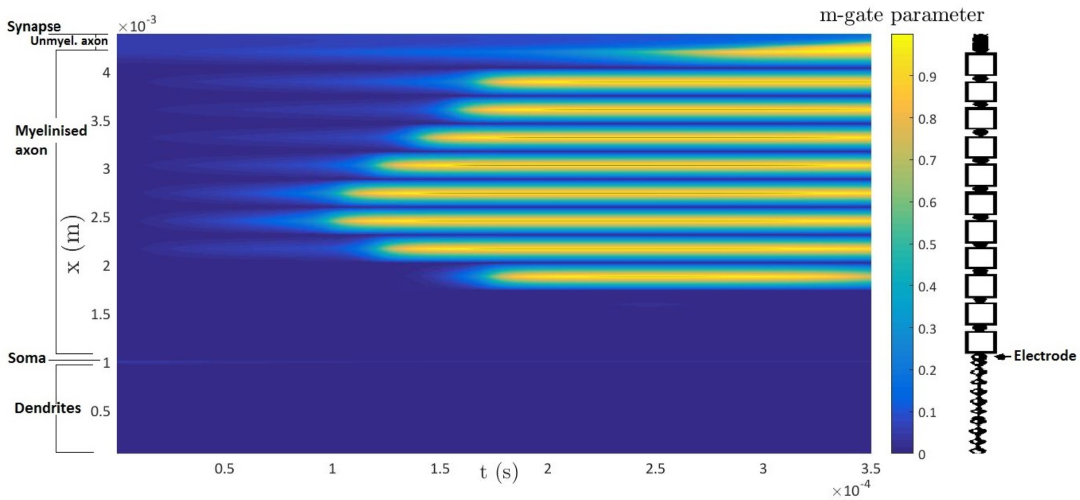

Figure 4.4: Colour map of the m-gate parameter in time and space. The colours represent the value of m. The map is obtained by anode-make stimulation by a spherical electrode ($10V$) at $1mm$ from the soma of a straight neuron.

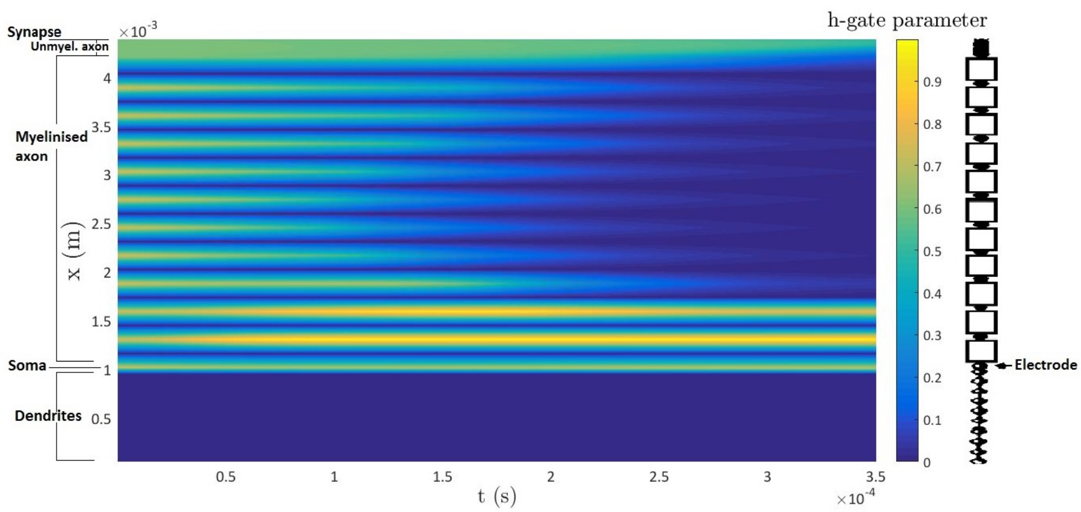

Figure 4.5: Colour map of the h-gate parameter in time and space. The colours represent the value of h. The map is obtained by anode-make stimulation by a spherical electrode ($10V$) at $1mm$ from the soma of a straight neuron.

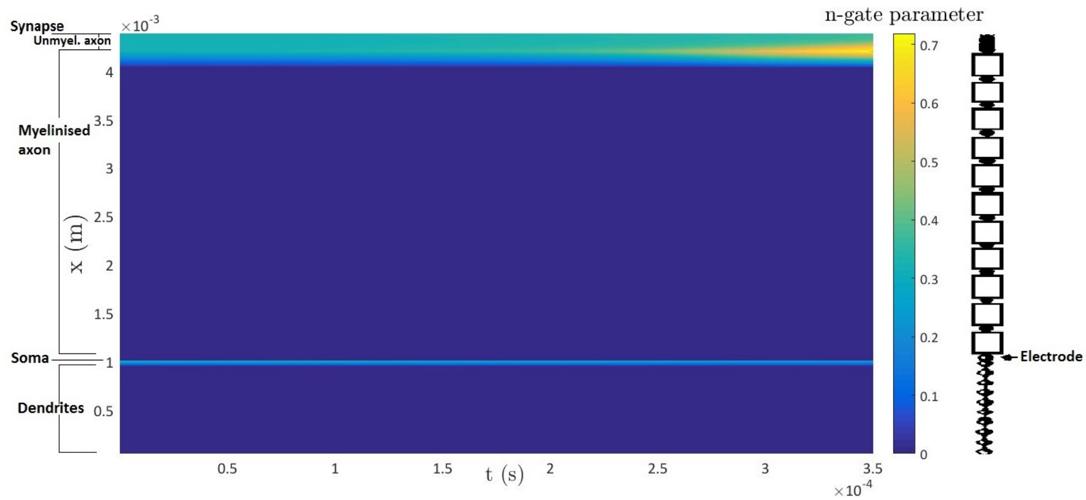

Figure 4.6: Colour map of the n-gate parameter in time and space. The colours represent the value of n. The map is obtained by anode-make stimulation by a spherical electrode ($10V$) at $1mm$ from the soma of a straight neuron.

4.1.2 Simulation 2. Anode-make stimulation by spherical electrode (60V) at 2 mm from soma.

We will now observe the effect of the distance of the electrode to the neuron. In this subsection, we increase the distance between the electrode and the soma from $1mm$ to $2mm$. Because this will result in a decrease of the electromagnetic field on the neuron, we increase the electrode-potential V_{elec} from $10V$ to $60V$. The electromagnetic field at the neuron excited by the source of $10V$ will not be strong enough to stimulate the neuron, and we would like to study activated neurons in this subsection. The simulation setup with an electrode potential of $10V$ and electrode at $2mm$ from the soma however, is treated as an appendix (section A.2). Furthermore a similar simulation with an electrode source at $2mm$ from the soma, but with electrode potential at $40V$, will also result in neuronal activation, and is treated in section A.3. To study the effect of the electrode potential on the transmembrane voltage and gate-parameters, the results from this subsection and from section A.3 can be compared.

The results for the membranevoltage and activation function f, for the configuration of a spherical electrode at $2mm$ from the soma and at $60V$, are shown in figure 4.7 and 4.8. We compare the results of this subsection, with the results of the previous subsection (subsection 4.1.1), to identify the influence of distance between the electrode and the neuron. From the activation function f we notice that the region of hyperpolarisation around the electrode-position has extended from the first two nodes of Ranvier to the first four nodes of Ranvier. The strenght of hyperpolarisation isn't significantly altered for the first node of Ranvier however. The subsequent three nodes however will now be hyperpolarised more strongly, leaving only six nodes (as compared to eight Ranviernodes in subsection 4.1.1 and section 3) where depolarisation can occur. This behaviour is also reflected in the membranevoltage in figure 4.7: the region

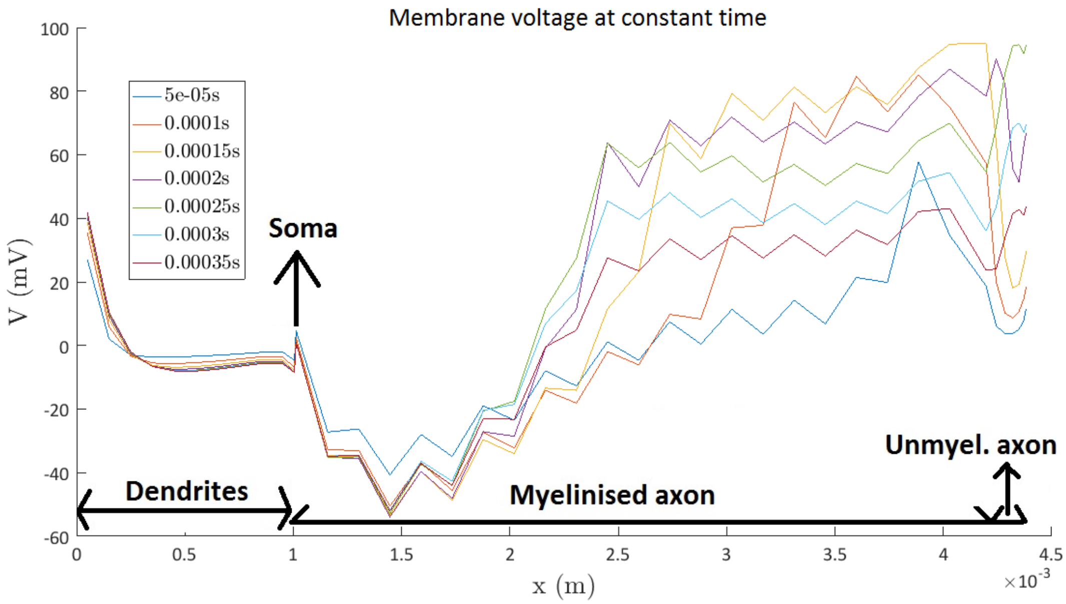

Figure 4.7: Anode-make stimulation by spherical electrode ($60V$) at $2mm$ from the soma. Spatial distribution of the reduced membrane voltage $\tilde{V}$ at 7 subsequent times is shown.

of depolarisation and neuronal activation is shifted to the end of the axon, while the first four Ranviernodes are now hyperpolarised.

The same conclusions hold for the colour maps of the reduced membranevoltage $\tilde{V}$ and gate-parameter m in figure 4.9 and 4.10 respectively. The activation of the neuron is shifted to the last sixth nodes of Ranvier, as can be seen most clearly in the plot for the m-gate parameter 4.10.

The initiation of the actionpotential is consequently also shifted towards the end of the neuron, as can be seen in the activationtable 4.2. The startpoint of the actionpotential has moved from $2.45mm$ in simulation 1 (subsection 4.1.1) to $3.6mm$ in this simulation.

From a theoretical perspective (Roth, 1993 [15]), it makes sense that increasing the distance between the electrode and the neuron will increase the length of the central region of hyperpolarisation in anode-make stimulation. Analogously, increasing the distance between electrode and neuron will increase the length of the central region of depolarisation in cathode-make stimulation. This is due to the fact that the distance between the (virtual) cathode(s) and (virtual) anode(s) will increase with d_{elec}. The electrode-potential in contrast does not alter the shape of the activation function. Indeed, from linearity we see that by scaling the electrode-potential, the activation function will scale with the same parameter. We conclude that the shape of the activation function f is dictated by the electrode-neuron distance, while altering the electrode-potential will only scale f with a constant value and will not alter the shape of f. To verify these theoretical observations, we compare the results of this subsection, with the results of

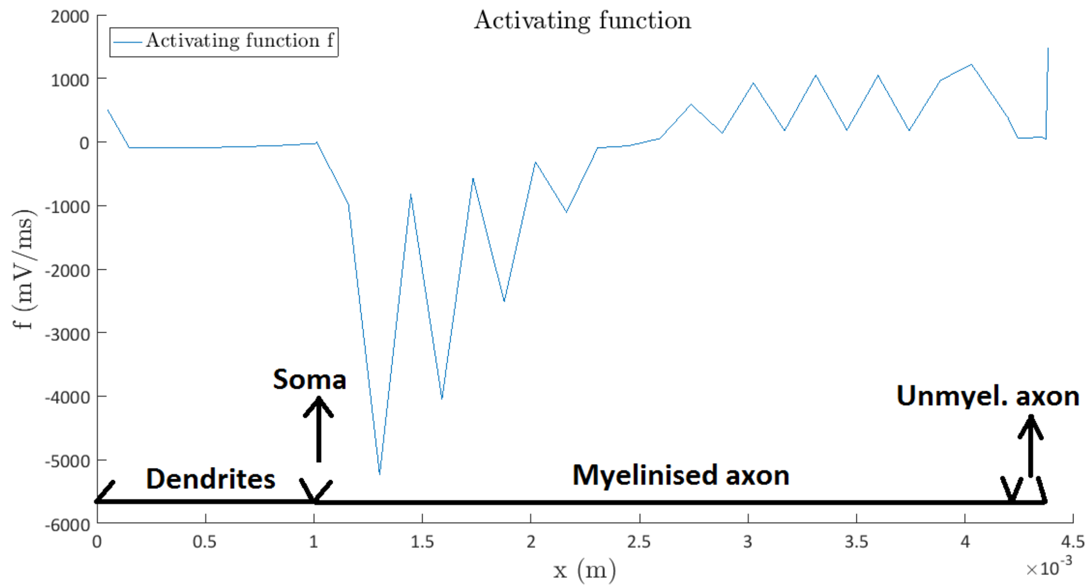

Figure 4.8: Anode-make stimulation by a spherical electrode ($60V$) at $2mm$ from the soma. Spatial distribution of the activation function f is shown.

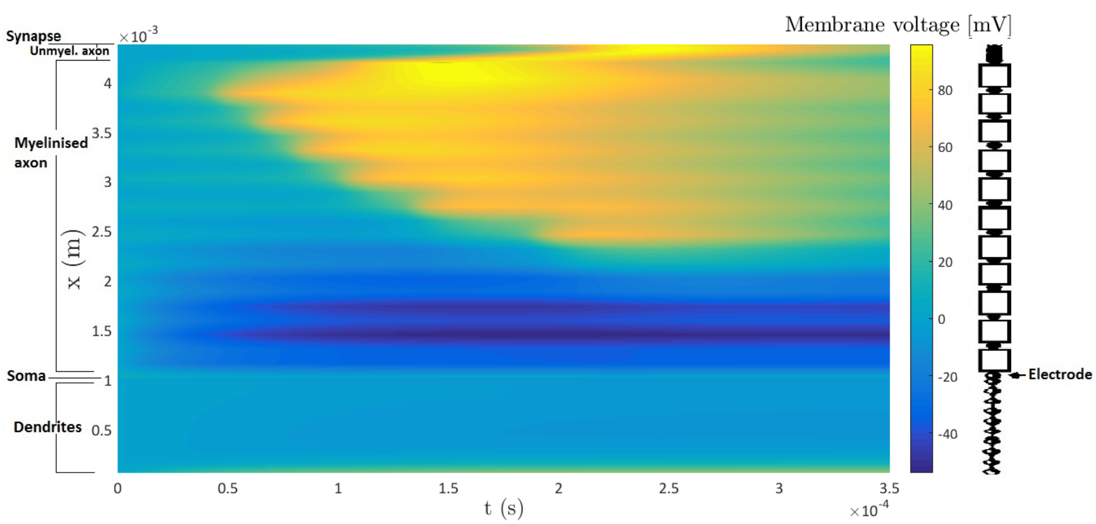

Figure 4.9: Colour map of the reduced membrane voltage in time and space. The colours represent the value of $\tilde{V}$. The map is obtained by anode-make stimulation by a spherical electrode ($60V$) at $2mm$ from the soma of a straight neuron.

section A.2 (anode-make stimulation with $10V$) and section A.3 (anode-make stimulation with $40V$). We indeed notice from the respective activation functions ($10V$ in figure A.9, $40V$ in figure A.19, $60V$ in figure 4.8) that the electrode-voltage will only introduce a scaling, and will not alter the shape of the activation function.

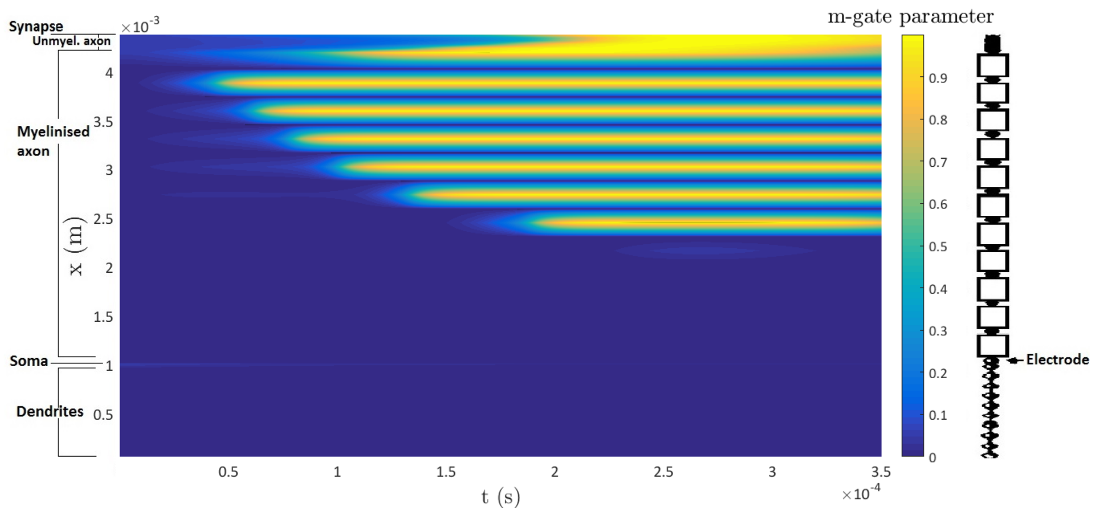

Figure 4.10: Colour map of the m-gate parameter in time and space. The colours represent the value of m. The map is obtained by anode-make stimulation by a spherical electrode ($60V$) at $2mm$ from the soma of a straight neuron.

The results for the m-gate, h-gate and n-gate parameters for anode-make stimulation ($60V$) with a spherical electrode at $2mm$ from the soma, is shown in figure 4.10, figure 4.11 and figure 4.12 respectively. These colour maps again agree with the conclusion, that with increasing electrode-neuron distance the length of the region of hyperpolarisation will increase. The action potential will start further on the axon.

We can compare the results, for the membrane voltage and gate-parameters, obtained in this subsection for anode-make stimulation at $60V$, with the results obtained in section A.3 for anode-make stimulation at $40V$[1]. Both for $60V$ and $40V$ stimulation the neuron will be activated and the distribution of the voltage and gate-parameters will be similar. This could be anticipated from the fact that the activation function has the same shape for both simulations. Furthermore by comparing the activation tables (figure 4.2 and figure A.3), we note that activation occurs at the exact same location ($3.5985mm$ from the start of the dendrites). However the neuronal activation will start on a later time for the anode-make stimulation at $40V$, i.e. at $t_{act} = 0.14ms$, than for the anode-make stimulation at $60V$ ($t_{act} = 0.11ms$). This makes sense, because for $60V$-stimulation, the activation function f will have higher values, so depolarisation

[1]For the spatial distribution of the membrane-voltage we compare figure 4.7 with figure A.17. For the colour map of the membrane voltage we compare figure 4.9 with figure A.18. For the m, n, and h parameter, compare figures 4.10, 4.12, 4.11 with figures A.20, A.22, A.21 respectively

is likely to occur faster than for $40V$-stimulation.

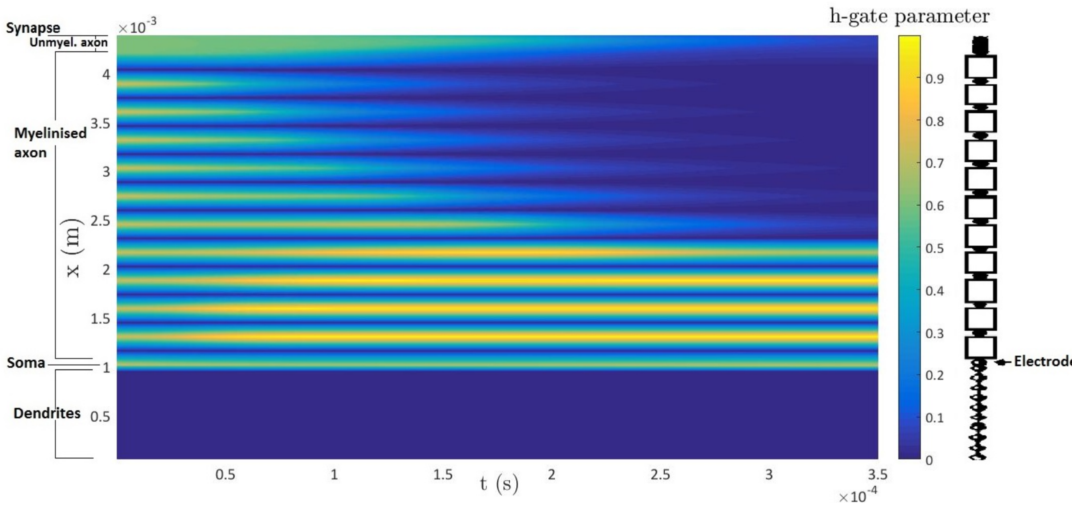

Figure 4.11: Colour map of the h-gate parameter in time and space. The colours represent the value of h. The map is obtained by anode-make stimulation by a spherical electrode ($60V$) at $2mm$ from the soma of a straight neuron.

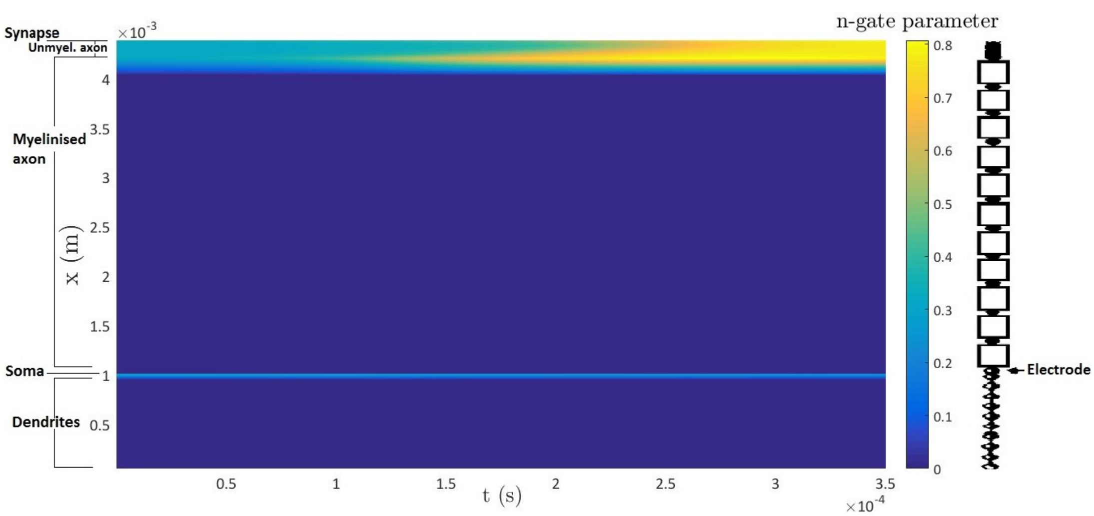

Figure 4.12: Colour map of the n-gate parameter in time and space. The colours represent the value of n. The map is obtained by anode-make stimulation by a spherical electrode ($60V$) at $2mm$ from the soma of a straight neuron.

Finally we can also compare the results from this subsection and section A.3, with the results obtained by anode-make stimulation at $10V$ in section A.2[2]. However for stimulation at $10V$ the neuron will not be activated: no action potential will propagate along the axon. Consequentially there is little similarity between the maps for the voltage and gate-parameters for stimulation at $60V$ and stimulation at $10V$.

	Activated	Synapse activated	nr.	pos. (mm)	time (ms)	MSOAf (m/s)	MSOAb (m/s)
Config 1: anode-make (60 V)	yes	yes	1.	3.5985	0.1113	5.6256	10.8438

Table 4.2: Activation table for a straight neuron, stimulated by a spherical electrode ($60V$) at 2 mm from the soma.

4.1.3 Simulation 3. Anode-make stimulation of voltage-clamped neuron by spherical electrode (60 V) at 2 mm from soma

Until now we always used "sealed-end" boundary conditions in the simulations of the membrane voltage and gate-parameters. We would like to examine the effect of the boundary conditions on distribution of the voltage, gate-parameters and activation function and the effect on neuronal activation. For this end we consider anode-make stimulation by a spherical electrode ($60V$) at $2mm$ from the soma (i.e. the simulation setup is identical to simulation 2, in subsection 4.1.2). However the difference between simulation 3 (in this subsection) and simulation 2 (in the previous subsection) is that sealed-end boundary conditions were used in simulation 2, while in this subsection voltage-clamped boundary conditions will be used. The reduced voltage will be clamped to zero at the neuronal terminations, $\tilde{V}|_{x=\pm\frac{L}{2}} = 0$. Here the neuron starts at $x = -\frac{L}{2}$ and ends at $x = \frac{L}{2}$. In other words, the non-reduced membrane voltage V is equal to the rest-voltage at the terminations of the neuron.

The spatial distribution of the reduced membrane voltage $\tilde{V}$, for the simulation with voltage-clamped boundary conditions, is shown in figure 4.13. We observe that indeed the reduced voltage is zero at the ends of the neuron. Because of this, the depolarisation over about $40V$ at the termination of the dendrites that could be observed in the simulation of the previous subsection 4.1.2, is not present anymore when applying voltage-clamped boundary conditions. Furthermore we notice that the spatial distribution of the voltage for voltage-clamp boundary conditions is very similar to the voltage distribution for sealed-end conditions. It is only close to the neuron ends, that the neuron will "feel" the boundary conditions, and the voltage will drop to zero.

The activation function for the voltage-clamped neuron is shown in figure 4.14. We observe that the activation function is identical to the activation function for sealed-end conditions, in figure 4.8. This is ofcourse the case, because the activation function does not depend on the applied boundary conditions. The neuron will be stimulated by the same activation function, leading

[2] For anode-make stimulation at $10V$ the spatial distribution of the reduced and non-reduced membrane voltage ($\tilde{V}$ and V respectively) is shown in figure A.10 and figure A.12 respectively. The colour maps of $\tilde{V}$ and V is shown in figure A.11 and figure A.13 respectively. The gate parameters are shown in figures A.14, A.16, A.15

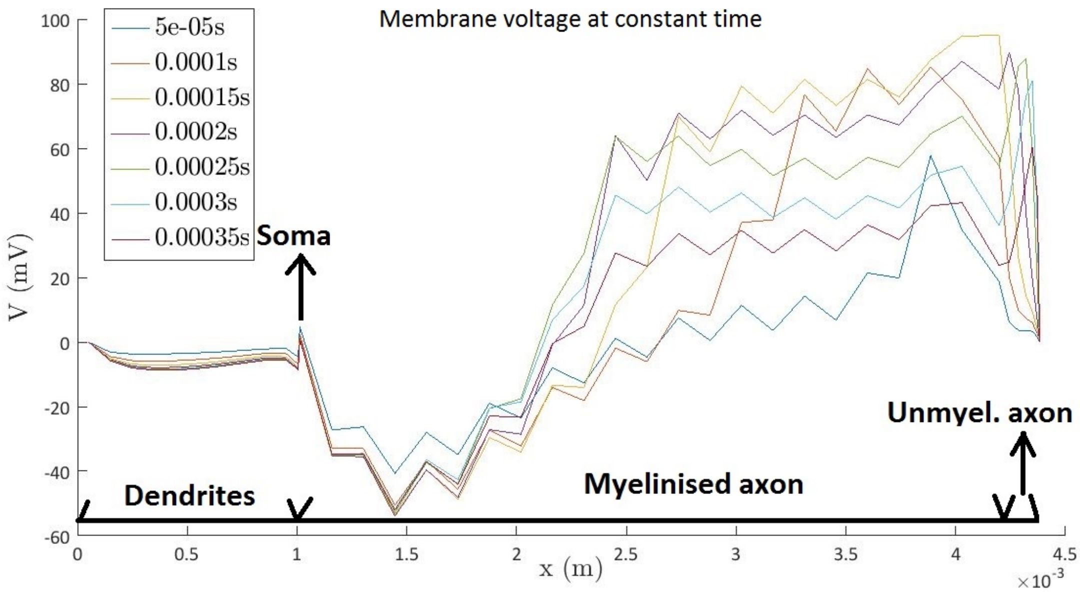

Figure 4.13: Anode-make stimulation by a spherical electrode ($60V$) at $2mm$ from the soma. Neuron is voltage clamped. Spatial distribution of the reduced membrane voltage $\tilde{V}$ is shown.

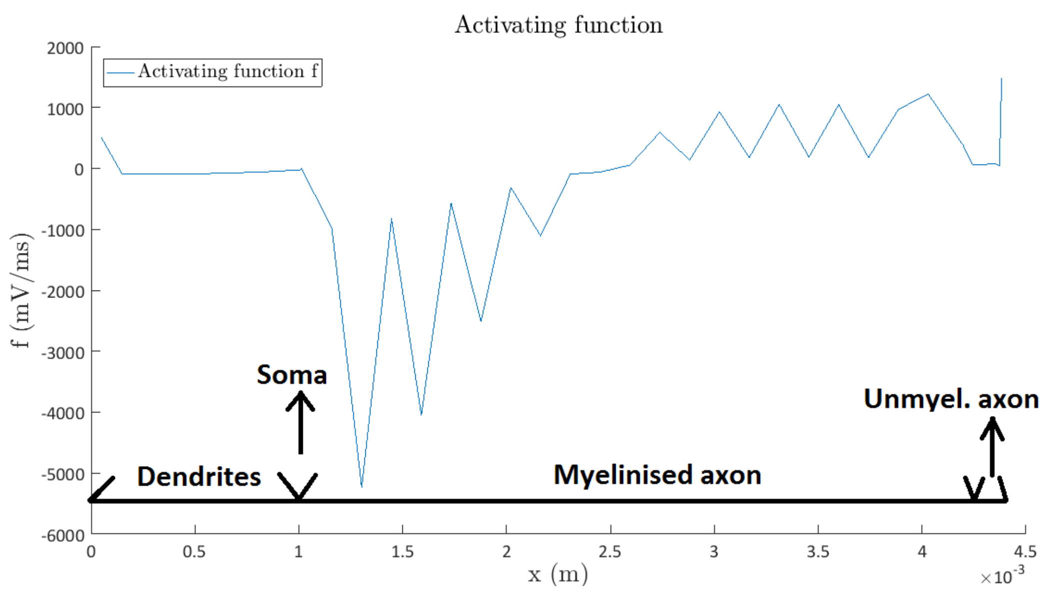

Figure 4.14: Anode-make stimulation by spherical electrode ($60V$) at $2mm$ from the soma. Neuron is voltage clamped. Spatial distribution of the activation function f is shown.

to a very similar distribution for the voltage and gate-parameters, except close to the neuron terminations where the boundary conditions are applied.

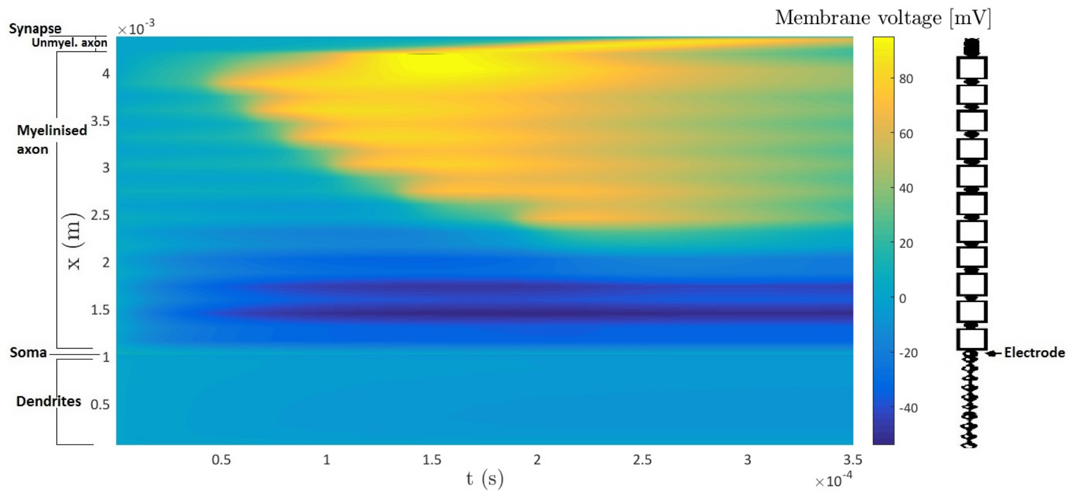

Figure 4.15: Colour map of the reduced membrane voltage in time and space. The colours represent the value of $\tilde{V}$. The map is obtained by anode-make stimulation by a spherical electrode ($60V$) at $2mm$ from the soma of a straight, voltage clamped, neuron.

Comparing the colour maps of this subsection and the previous subsection for the reduced membrane voltage $\tilde{V}$[3], we observe again that the voltage distribution is very similar. Only close to the neuron ends, the boundary conditions will influence the membrane voltage.

Also the distribution for the gate-parameters for voltage-clamped and sealed-end boundary conditions is similar[4]. At the termination of the dendrites, no gate-parameters are defined because the dendrites were modelled as a passive compartment. At the synapse, the gate-parameters are now clamped to their rest-values m_0, n_0 and h_0, and do not depend on time. This is due to the fact that the membrane voltage does not depend on time (at the synapse for voltage-clamped conditions), resulting in a stationary solution for the gate-parameters. The rest values for the gate-parameters depend on the neuronal model. We used a warm Hodgkin-Huxley model for the synapse; the rest-values for the gate-parameters in this case are:

$$m_0 = 0.0529$$

$$n_0 = 0.3177$$

$$h_0 = 0.5961$$

[3]For the reduced membrane voltage $\tilde{V}$, we compare figure 4.9 and figure 4.15.

[4]For the remainder of this chapter we will only show the m-gate parameter in the text. The n- and h-gate parameter are included in Appendix A. For the gate-parameters compare figures 4.10, 4.11, 4.12 for sealed-end conditions with figures 4.16,A.23, A.24 for voltage-clamped conditions.

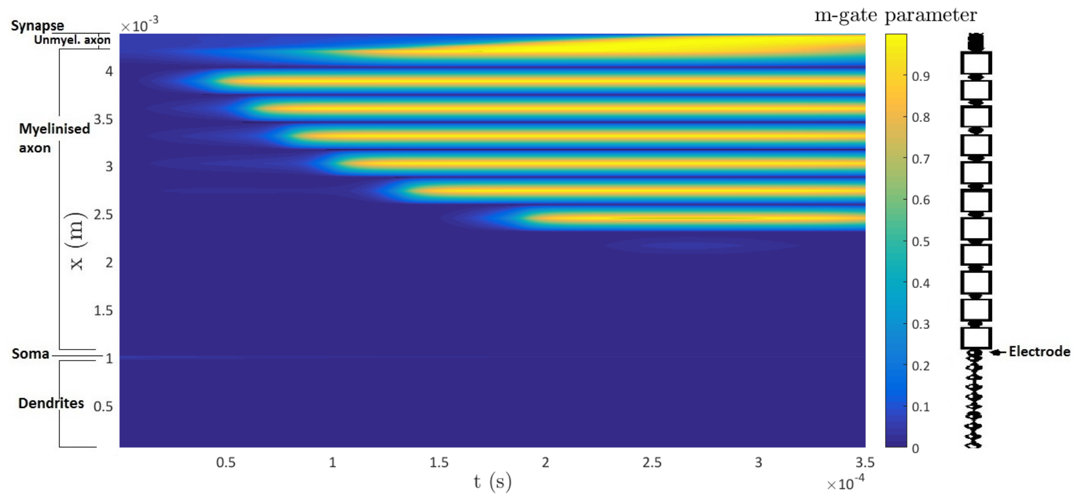

Figure 4.16: Colour map of the m-gate parameter in time and space. The colours represent the value of m. The map is obtained by anode-make stimulation by a spherical electrode ($60V$) at $2mm$ from the soma of a straight, voltage clamped, neuron.

For the simulation with voltage-clamped conditions the gate-parameters are fixed at the synapse to m_0, n_0 and h_0. The synapse can not be activated, because the membrane can't depolarize. In contrast for the sealed-end conditions, the m-gate and n-gate parameters will increase to a maximum of 0.9952 and 0.8061 respectively. The inactivation gate h will decrease to 0.0495. For sealed-end conditions, the synapse is activated.

The difference between the colour maps for the gate-parameters solved with sealed-end or clamped-voltage boundary condition, is very small. Especially for the h-gate parameter, this difference might be difficult to observe. We conclude that only very close to the synapse, the gate-parameters in the sealed-end solution differ from the gate-parameters in the clamped-voltage solution. Because the effect of the boundary conditions is very local, it is difficult to observe in a colour map. However when we plot the gate-parameters as function of time at the synapse, we conclude that at the synapse the boundary conditions have a large influence on these parameters. This is done for the m, n and h gate parameters in figures 4.17, A.26 and A.25 respectively.

	Activated	Synapse activated	nr.	pos. (mm)	time (ms)	MSOAf (m/s)	MSOAb (m/s)
Config 1: voltage clamped	yes	no	1.	3.5985	0.1113	4.2699	10.8430

Table 4.3: Activation table for a straight (voltage-clamped) neuron, stimulated by a spherical electrode ($60V$) at 2 mm from the soma.

Finally we can also compare the activationtables, table 4.3 and table 4.2. Because the effect of the boundary conditions is restricted to a small region close to the neuron terminations, the

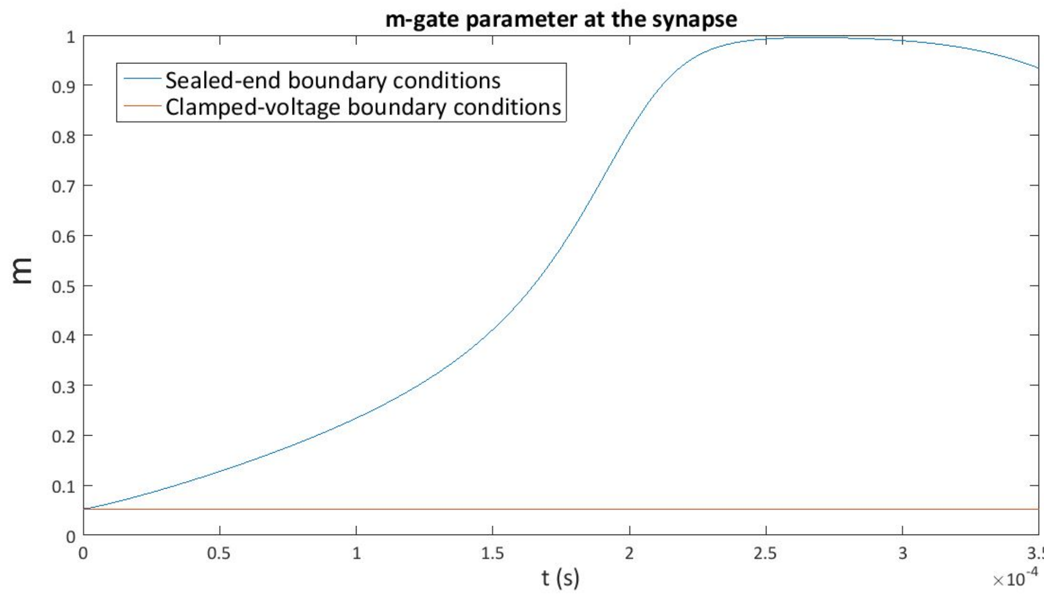

Figure 4.17: m-gate parameter as function of time at the synapse for sealed-end conditions and voltage-clamped conditions.

location and time of activation will not be affected. Ofcourse, when the voltage of the synapse is clamped at rest-voltage, the synapse will not be activated (as noted in table 4.3).

4.1.4 Simulation 4. Cathode-make stimulation by spherical electrode (-60V) at 2 mm from soma

In the previous simulations we considered anode-make stimulation. This means that the electrode-potential was positive until now: the electrode is called an anode. Anode-make stimulation results in a region of hyperpolarisation right under the electrode. A region of depolarisation is found further away from the electrode (at the virtual cathodes). We refer to Roth (1993) [15] for a theoretical explanation of the different types of electrode stimulation (cathode-make, cathode-break, anode-make and anode-break). In this subsection we would like to study a case of cathode-make stimulation, by a spherical electrode $(-60V)$ at $2mm$ from the soma of the neuron. This simulation setup can be compared with simulation 2 in subsection 4.1.2. In simulation 2 the same simulation setup is considered as in this subsection, but anode-make stimulation is applied.

From linearity it follows that the activation function for cathode-make stimulation f_{CM} is the negative of the activation function for anode-make stimulation f_{AM}: $f_{CM} = -f_{AM}$. This result is indeed obtained: the activation function for cathode-make stimulation is shown in figure 4.18 (cfr. figure 4.8 for anode-make stimulation). Because of this, we expect that for cathode-make stimulation there will now be a region of depolarisation under the electrode, where activation might potentially occur.

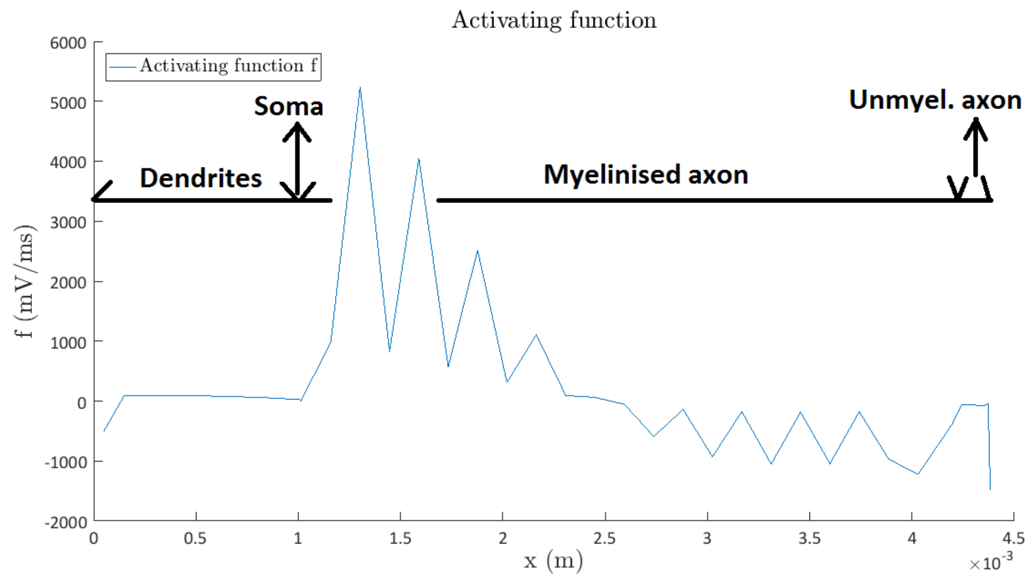

Figure 4.18: Cathode-make stimulation by spherical electrode ($-60V$) at $2mm$ from the soma. Spatial distribution of the activation function f is shown.

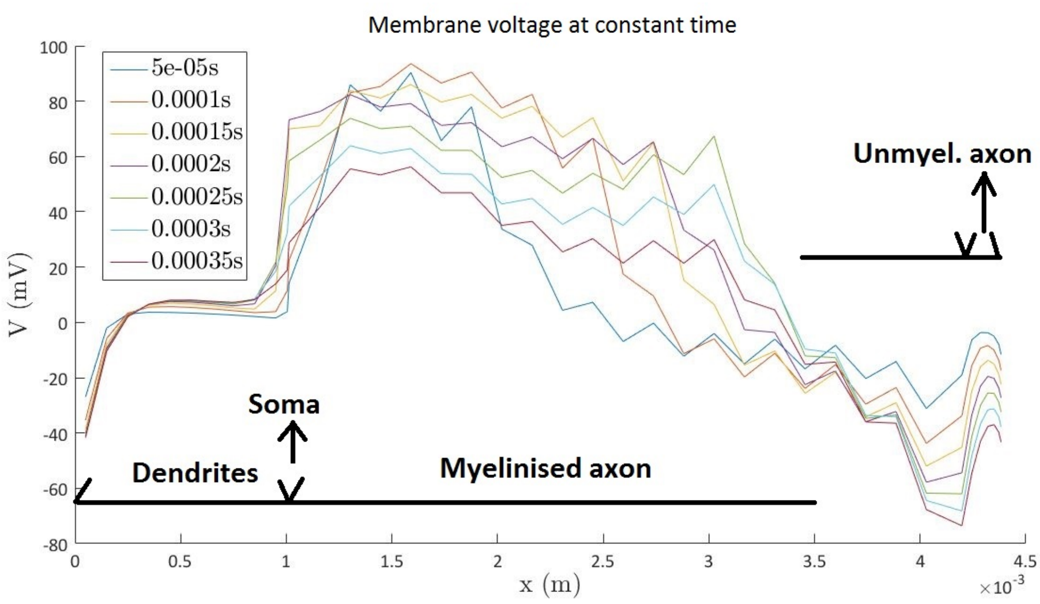

Figure 4.19: Cathode-make stimulation spherical electrode ($-60V$) at $2mm$ from the soma. Spatial distribution of the reduced membrane voltage $\tilde{V}$ at 7 subsequent times is shown.

The spatial distribution of the voltage for cathode-make stimulation is shown in figure 4.19. The colour map for the voltage and m-gate parameter for cathode-make stimulation is shown in figure 4.20 and figure 4.21 respectively. The colour maps for the other gate-parameters are included in Appendix A (see figure A.27 and figure A.28). From these plots we observe that there is indeed a region of depolarisation around the electrode. The region of hyperpolarisation is now found at the dendrite terminals and at the unmyelinated axon terminal. The activation table (table 4.4) shows that neuron activation for cathode-make stimulation starts at the beginning of the axon ($1.3025mm$ from the beginning of the neuron, this is at the first node of Ranvier). The activation pulse will however not reach the synapse. This is due to the fact that the actionpotential starts at the beginning of the axon, so the distance that the actionpotential has to travel to reach the synapse has substantially increased with respect to anode-make stimulation. Furthermore, in cathode-make stimulation, the actionpotential has to overcome a region of hyperpolarisation on its way to the synapse.

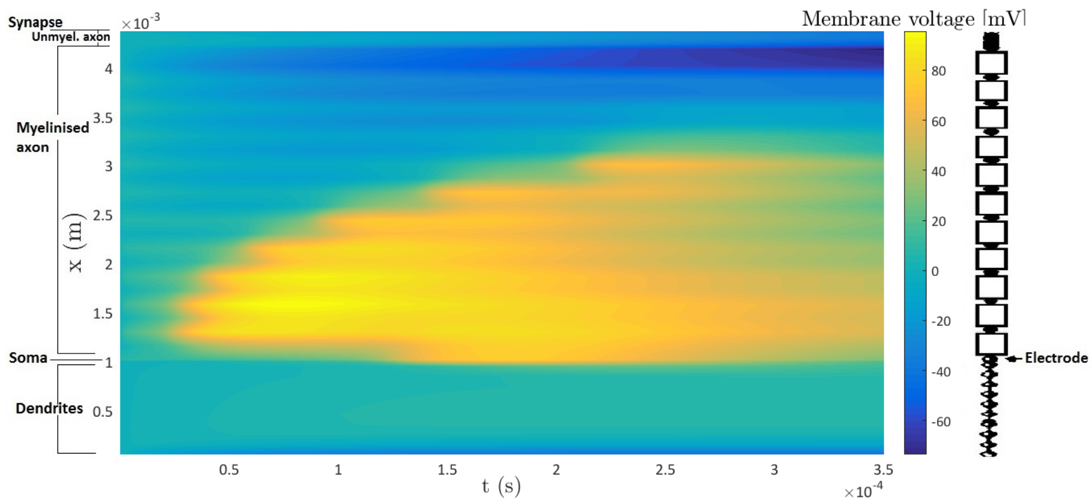

Figure 4.20: Colour map of the reduced membrane voltage in time and space. The colours represent the value of $\tilde{V}$. The map is obtained by cathode-make stimulation by a spherical electrode ($-60V$) at $2mm$ from the soma of a straight neuron.

	Activated	Synapse activated	nr.	pos. (mm)	time (ms)	MSOAf (m/s)	MSOAb (m/s)
Config 1: cathode-make	yes	no	1.	1.3025	0.0624	9.9725	2.4764

Table 4.4: Activation table for a straight neuron, stimulated by a spherical electrode ($-60V$) at 2 mm from the soma.

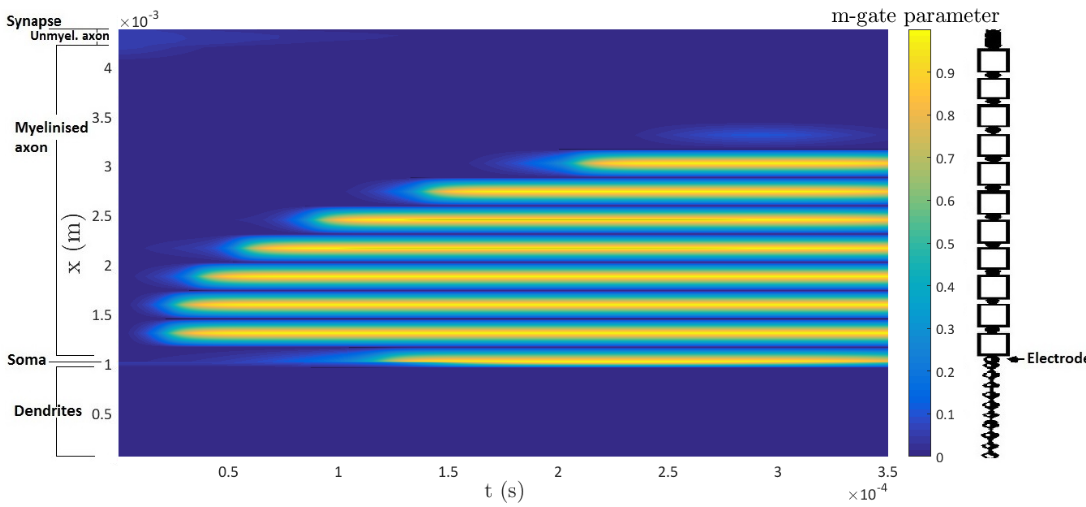

Figure 4.21: Colour map of the m-gate parameter in time and space. The colours represent the value of m. The map is obtained by cathode-make stimulation by a spherical electrode ($-60V$) at $2mm$ from the soma of a straight neuron.

4.1.5 Simulation 5. Anode-make stimulation by spherical electrode (60V) at 2 mm from centre of the neuron

We now want to observe the effects of moving the electrode parallel with the neuron. For this simulation we place the electrode at the middle of the neuron (i.e. at $2.2mm$ from the beginning of the dendrites, as the neuron has a length of $4.4mm$). The distance between the electrode and the neuron is $2mm$ and the electrode-potential is $60V$. This simulation can be compared with simulation 2 (subsection 4.1.2), which is the same simulation setup, except for the location of the electrode along the neuron. Because for anode-make stimulation the location of the electrode coincides with the region of hyperpolarisation on the neuron, we expect that now the centre of the neuron will hyperpolarise, shifting the region of neuronal activation towards the synapse.

We indeed observe from the activation function f, shown in figure 4.22, that hyperpolarisation will occur along most of the axon. The region of depolarisation has shifted to the end of the myelinated axon, making the unmyelinated axon more important for initiating the actionpotential than before.

The spatial distribution of the membrane voltage (figure 4.23) and the colour plots for the membrane voltage and gate-parameters (figures 4.24, 4.25, A.30, A.29) indeed show that neuronal activation has shifted towards the end of the neuron. The centre of the neuron, which now coincides with the location of the electrode, is hyperpolarised.

The activationtable (table 4.5) mentions that indeed the neuron is still activated, but at the unmyelinated axon terminal. The location where the actionpotential starts is determined by the Matlab code: $x_{act} = 4.197mm$. Low forward propagation velocity ($MSOA_f$) is tabulated,

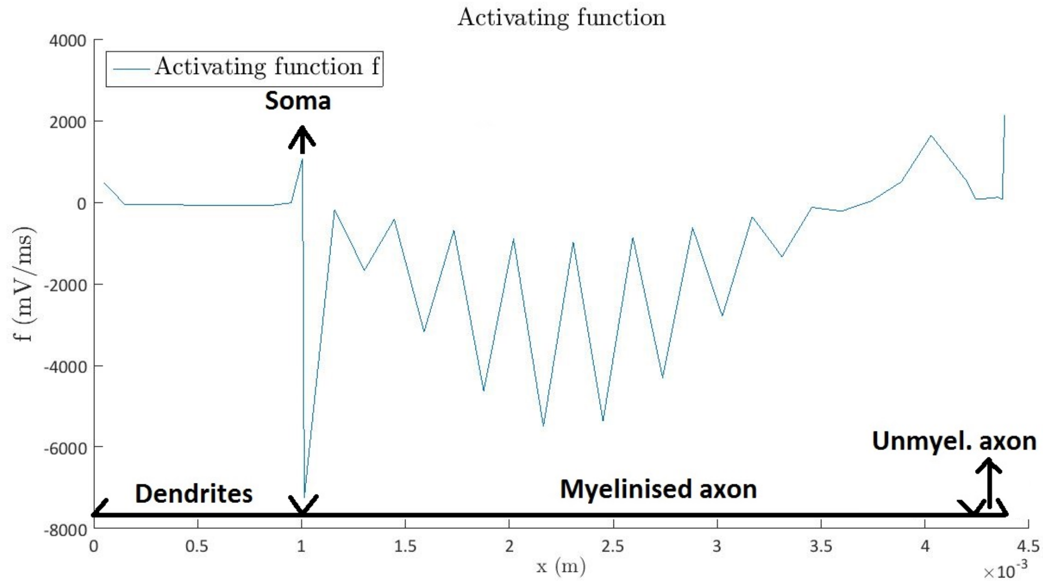

Figure 4.22: Anode-make stimulation by spherical electrode ($60V$) at $2mm$ from the centre of the neuron. Spatial distribution of the activation function f is shown.

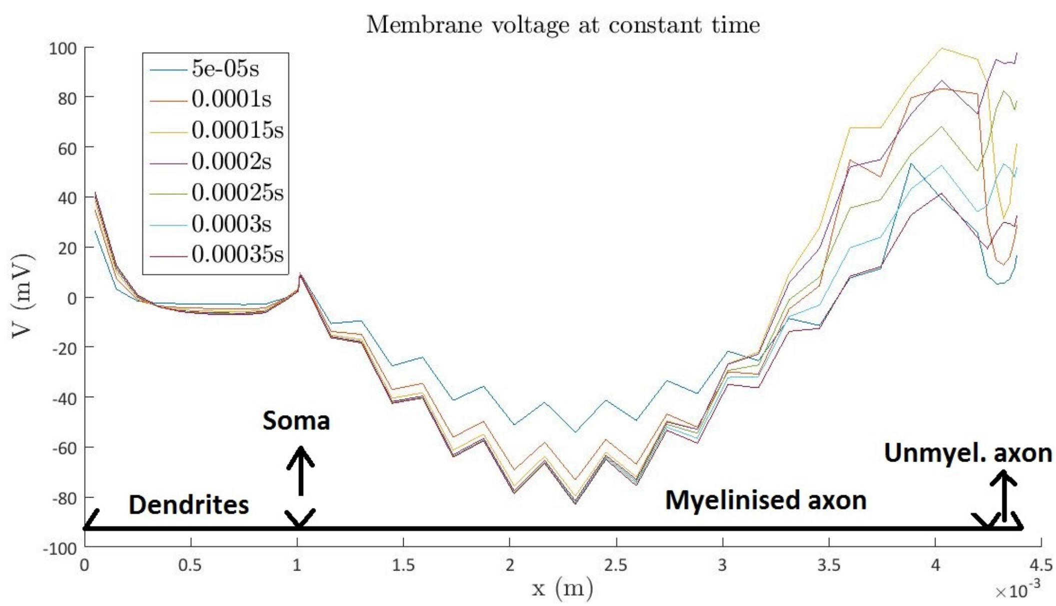

Figure 4.23: Anode-make stimulation by spherical electrode ($60V$) at $2mm$ from the centre of the neuron. Spatial distribution of the reduced membrane voltage $\tilde{V}$ at 7 subsequent times is shown.

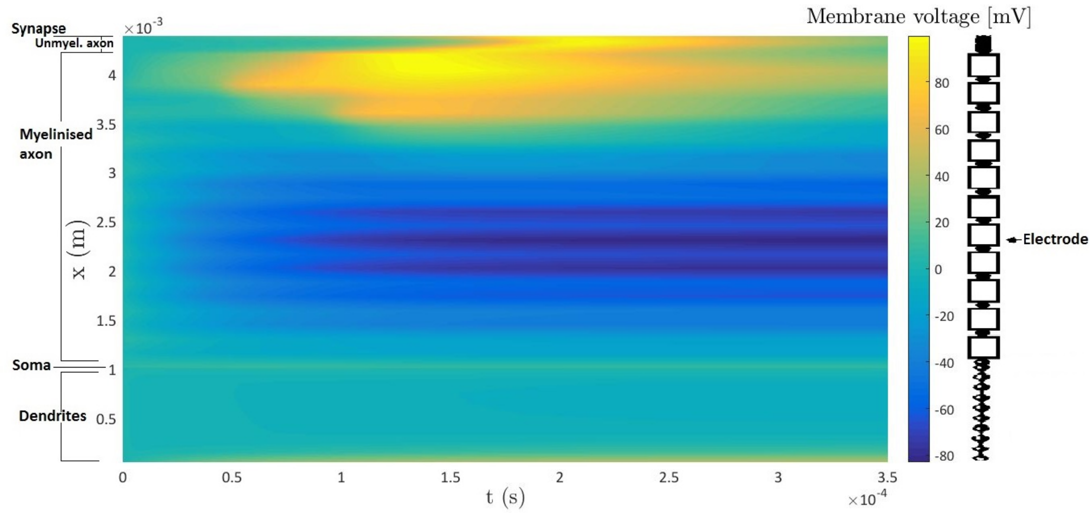

Figure 4.24: Colour map of the reduced membrane voltage in time and space. The colours represent the value of $\tilde{V}$. The map is obtained by anode-make stimulation by a spherical electrode ($60V$) at $2mm$ from the centre of a straight neuron.

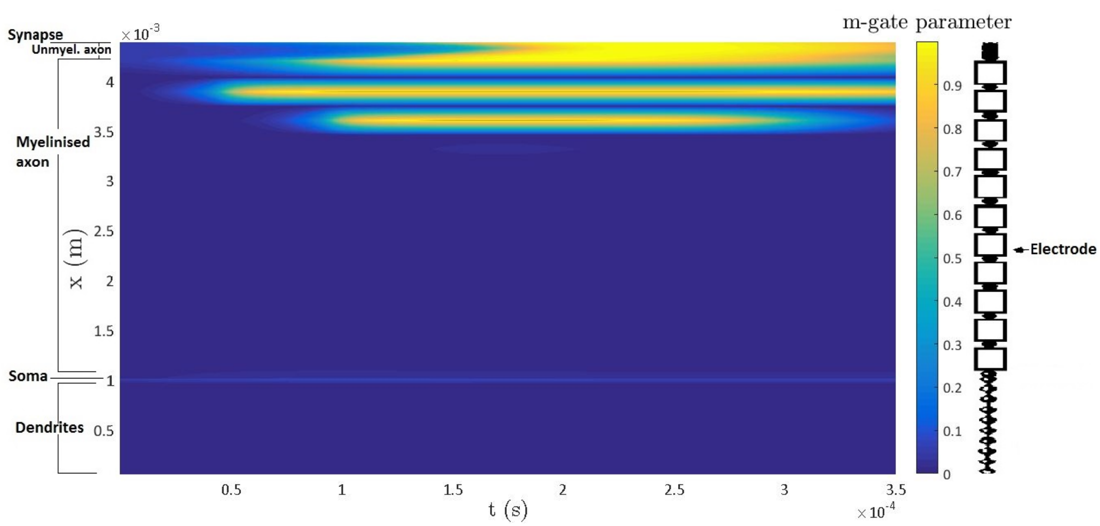

Figure 4.25: Colour map of the m-gate parameter in time and space. The colours represent the value of m. The map is obtained by anode-make stimulation by a spherical electrode ($60V$) at $2mm$ from the centre of a straight neuron.

which is due to the slow propagation of the actionpotential in the unmyelinated axon. The activation table also mentions very high backward activation speed ($MSOA_b = 94\frac{m}{s}$). However it is unlikely, for the used neuronal electric and geometric parameters, that the actionpotential did indeed propagate with this speed in the antidromic direction. Normally an actionpotential occurs at a certain location along the neuron, subsequently causing activation along the whole axon by propagation of this actionpotential. When observing the colour maps however, it seems more likely that the neuron was activated by the stimulation of the electrode at locations $x < x_{act}$, before the actionpotential could reach these locations. A similar phenomenon was observed in the activationtable of subsection 3.3. The Matlab code interprets this as propagation with very high speed, however a threshold propagation velocity can be set in Matlab to distinguish physical and unphysical speeds.

	Activated	Synapse activated	nr.	pos. (mm)	time (ms)	MSOAf (m/s)	MSOAb (m/s)
Config 2: AM (60 V) at centre	yes	yes	1.	4.1970	0.1305	1.5002	94.1562

Table 4.5: Activation table for a straight neuron, stimulated by a spherical electrode ($60V$) at 2 mm from the centre of the neuron.

4.2 Simulations on a single bending neuron

It is interesting to study simulations on neurons that bend over a specific angle. In this section we reconsider simulations on straight neurons from section 4.1, but we now add a central bending over 15°. Because the neuron is no longer straight, activation might now occur even in absence of electric field gradients, which is not possible for uniform straight neurons in a homogeneous medium. This will be discussed more theoretically in section 5. Simulation 6 (subsection 4.2.1) deals with anode-make stimulation (60 V) of a neuron, with central bending over 15°, with a spherical electrode at $2mm$ from the soma. Simulation 7 (subsection 4.2.2) will deal with the same simulation setup as in simulation 6, with the exception that the electrode location is placed at $2mm$ from the centre of the neuron.

4.2.1 Simulation 6. Anode-make stimulation of neuron with central bending (15°) by spherical electrode (60 V) at 2 mm from soma

We reconsider the simulation from subsection 4.1.2 (simulation 2), but we now introduce a bending of 15° at the centre of the neuron. The neuron bends towards the electrode. Except for this bending, the simulation in this subsection is completely the same as simulation 2, i.e. anode-make stimulation by a spherical electrode (60 V) at $2mm$ from the soma of a neuron, that is bending over 15°.

The activation function f for the neuron with a central bend, is shown in figure 4.27. When we compare this result with the corresponding simulation on a straight neuron (figure 4.8), we observe that the activation function f now has a positive peak at the bending. In other words, the neuronal bending promotes the depolarization of the membrane. The influence of bendings on neuronal activation, will be studied in more depth from a theoretical perspective in chapter 5. In literature it is observed that neuronal activation indeed tends to occur at bendings and terminations of the neuron.

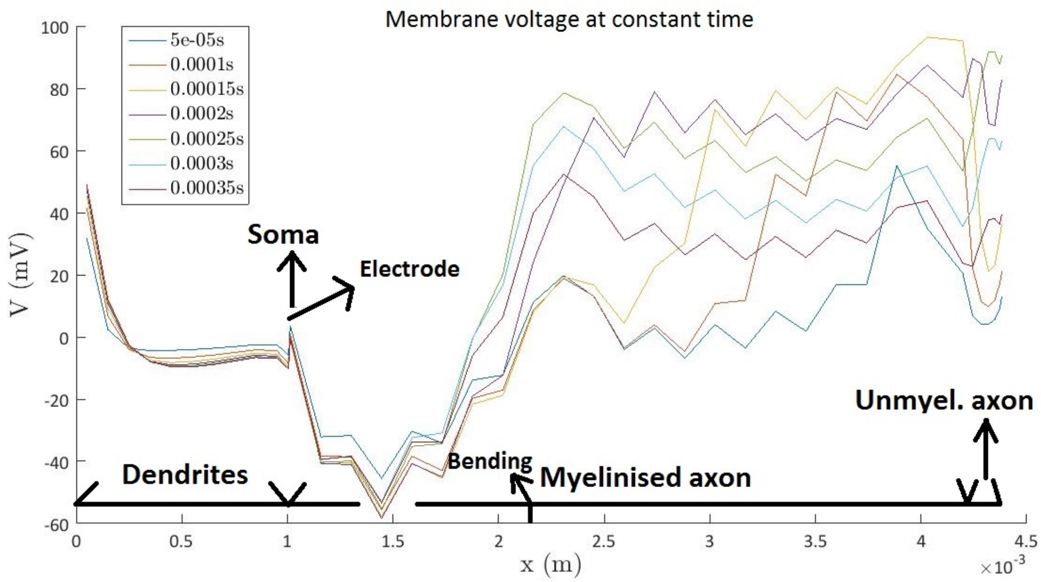

Figure 4.26: Anode-make stimulation by spherical electrode ($60V$) at $2mm$ from the soma. A bending over 15° is introduced in the centre of the neuron. Spatial distribution of the reduced membrane voltage $\tilde{V}$ at 7 subsequent times is shown.

The spatial distribution of $\tilde{V}$ for AM-stimulation of a neuron with central bending, by an electrode at the soma, is shown in figure 4.26. The colour map for the reduced voltage is shown in figure 4.28, and the gate-parameters are shown in figures 4.29, A.32, A.31. The activationtable is shown in figure 4.6. We compare these results, with the results of the corresponding simulation of a straight neuron[5]. We conclude that when a bending is introduced, the membrane will depolarize at the bending. Furthermore the width of the region of hyperpolarization that was observed for the straight neuron, is reduced in the results of this subsection.

	Activated	Synapse activated	nr.	pos. (mm)	time (ms)	MSOAf (m/s)	MSOAb (m/s)
165° bent neuron conf 1 (60V)	yes	yes	1.	3.5985	0.1236	6.8186	12.1276

Table 4.6: Activation table for a bending neuron, stimulated by a spherical electrode ($60V$) at 2 mm from the soma.

[5]For the spatial distribution of the membrane voltage, compare figure 4.28 with 4.9. For the colour maps compare figures 4.29, A.32, A.31, 4.28 with figures 4.10,4.12, 4.11, 4.9

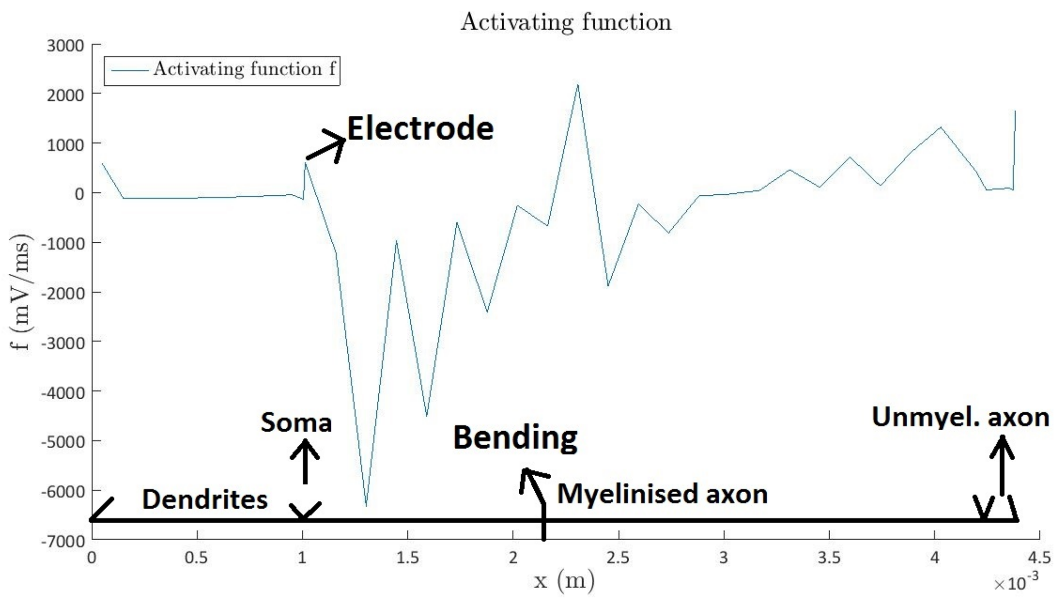

Figure 4.27: Anode-make stimulation by spherical electrode ($60V$) at $2mm$ from the soma. A bending over $15°$ is introduced in the centre of the neuron. Spatial distribution of the activation function f is shown.

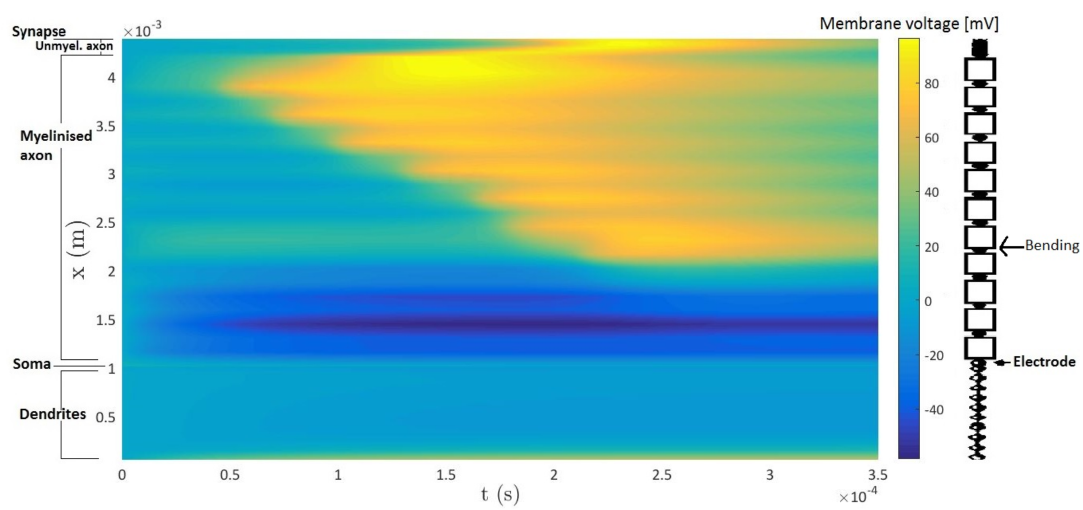

Figure 4.28: Colour map of the reduced membrane voltage in time and space. The colours represent the value of $\tilde{V}$. The map is obtained by anode-make stimulation by a spherical electrode ($60V$) at $2mm$ from the soma of a bent ($15°$) neuron.

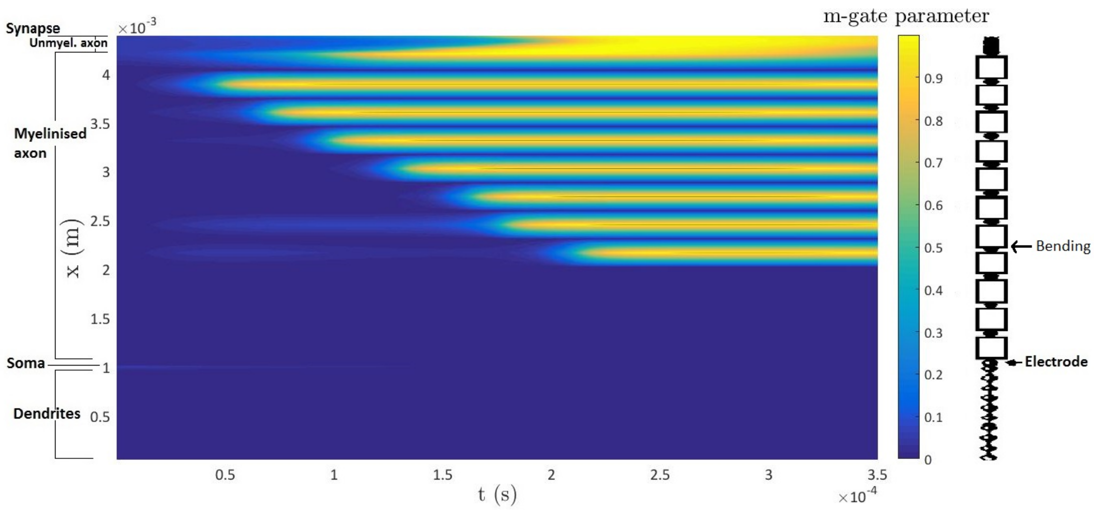

Figure 4.29: Colour map of the m-gate parameter in time and space. The colours represent the value of m. The map is obtained by anode-make stimulation by a spherical electrode ($60V$) at $2mm$ from the soma of a bent ($15°$) neuron.

4.2.2 Simulation 7. Anode-make stimulation of neuron with central bending ($15°$) by spherical electrode at 2 mm from the centre

In this last subsection, we consider another simulation on a neuron with a central bending over 15°. This simulation is similar to simulation 6 of previous subsection, except that the electrode-position is now located at the centre of the neuron and not at the soma. The corresponding simulation for a straight neuron is simulation 5 (subsection 4.1.5).

The activation function for this simulation is shown in figure 4.30. The difference with the corresponding simulation of a straight neuron is clear (compare with figure 4.22): at the bending the activation function f now has a positive peak, that was not present for the straight neuron. Consequentially the neuron will tend to depolarize at the bending.

This effect can be observed in the plots for the reduced membrane voltage (figure 4.31 and figure 4.32). In simulation 5 a large region of hyperpolarization (RoH) was observed, at the position of the electrode. Because the bending of the neuron coincides with the position of the electrode, we see that the RoH is now “interrupted” by the bending. At the bending, no net depolarization is observed, but the neuron has hyperpolarized less than it would have been, if the neuron were straight.

The colour maps for the gate-parameters are shown in figures 4.33, A.33 and A.34. The activation table is shown in table 4.7. The bending has no significant effect on the activation of the neuron: both with and without bending, neuronal activation occurs at the termination of the axon, far away from the central bending. Nevertheless there are some slight differences when comparing the actionpotential of simulation 5 with the actionpotential of simulation 7. For instance, when comparing the colour maps of simulation 5 with these of simulation 7, we notice that the “interruption” of the region of hyperpolarization, that was caused by the bending, has

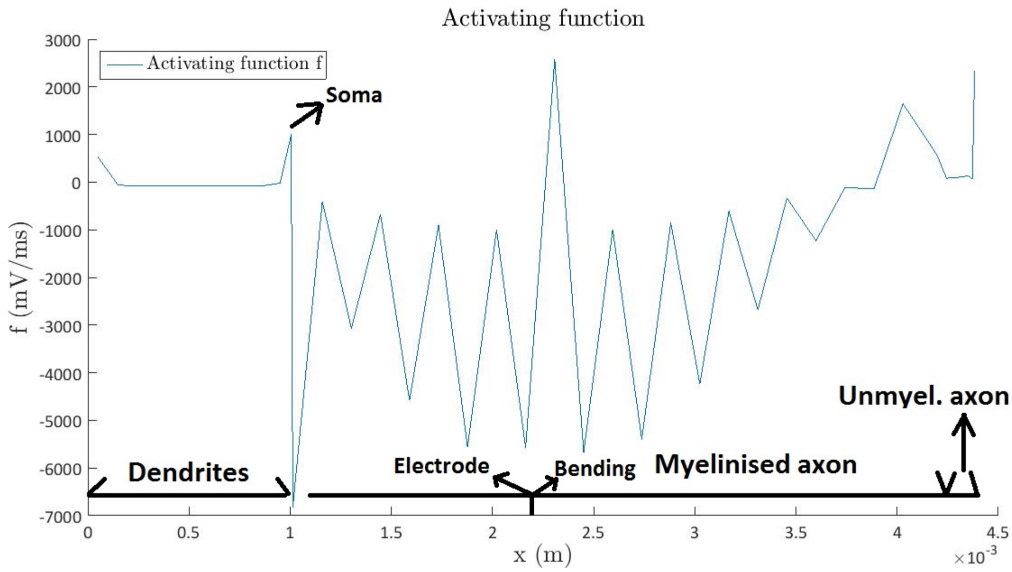

Figure 4.30: Anode-make stimulation by spherical electrode ($60V$) at $2mm$ from the centre of the neuron. A bending over 15° is introduced in the centre of the neuron. Spatial distribution of the activation function f is shown.

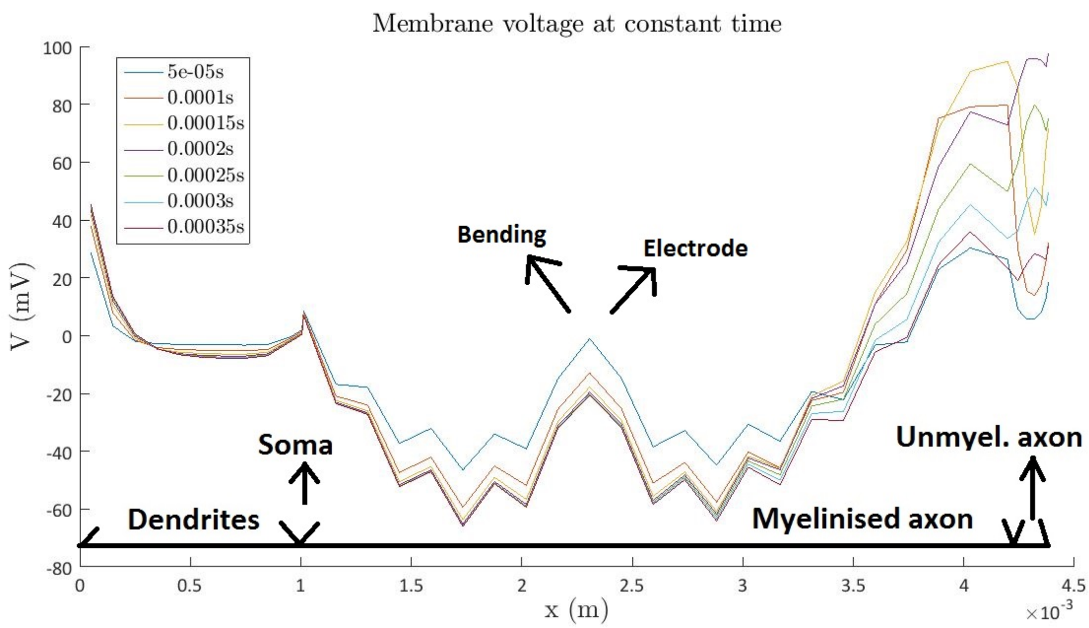

Figure 4.31: Anode-make stimulation by spherical electrode ($60V$) at $2mm$ from the centre of the neuron. A bending over 15° is introduced in the centre of the neuron. Spatial distribution of the reduced membrane voltage $\tilde{V}$ at 7 subsequent times is shown.

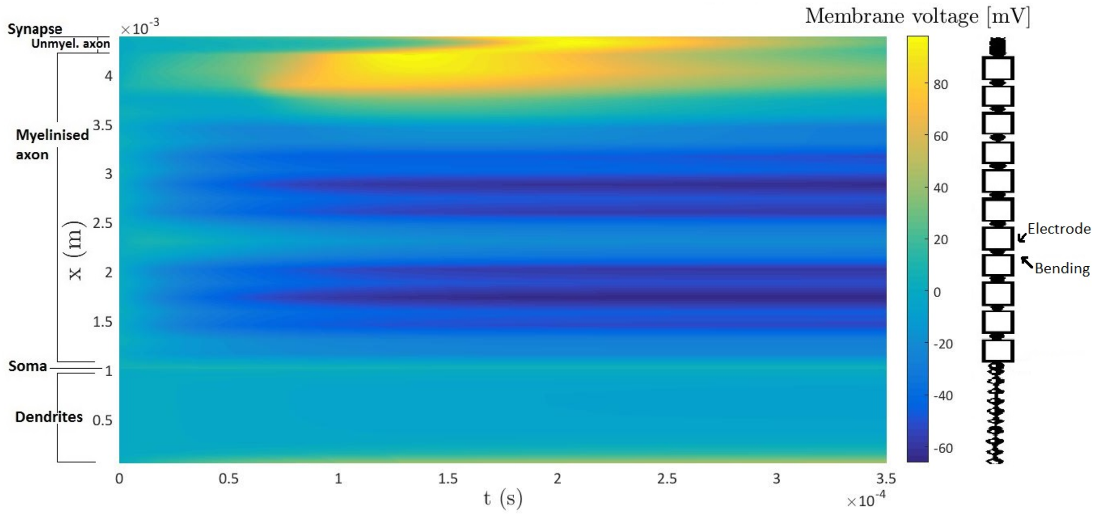

Figure 4.32: Colour map of the reduced membrane voltage in time and space. The colours represent the value of $\tilde{V}$. The map is obtained by anode-make stimulation by a spherical electrode ($60V$) at $2mm$ from the centre of a bent ($15°$) neuron.

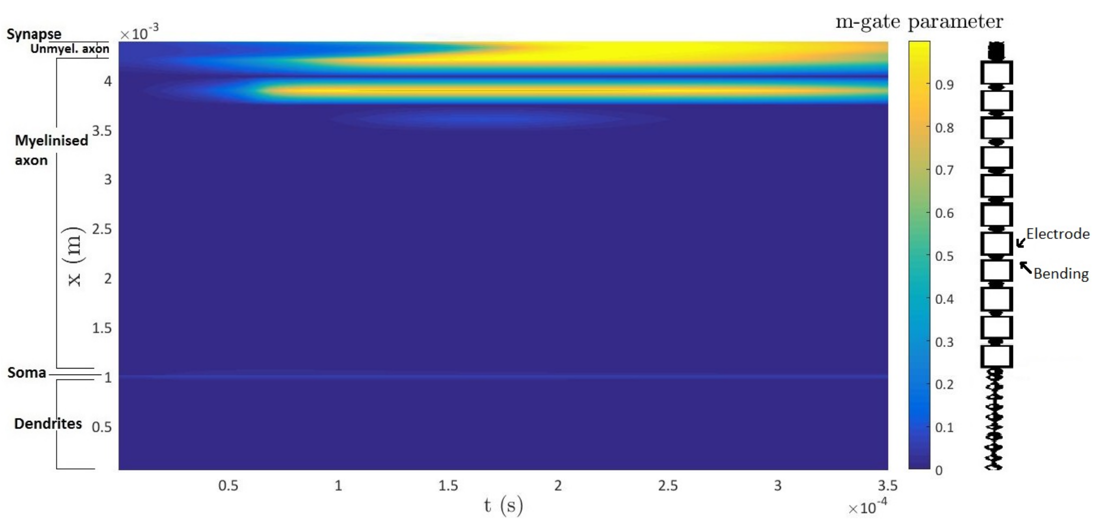

Figure 4.33: Colour map of the m-gate parameter in time and space. The colours represent the value of m. The map is obtained by anode-make stimulation by a spherical electrode ($60V$) at $2mm$ from the centre of a bent ($15°$) neuron.

pushed the now two separated parts of the RoH further up and further down the neuron.

	Activated	Synapse activated	nr.	pos. (mm)	time (ms)	MSOAf (m/s)	MSOAb (m/s)
165° bent neuron conf 2 (60V)	yes	yes	1.	3.8855	0.1128	4.5645	No backward...

Table 4.7: Activation table for a bending neuron, stimulated by a spherical electrode ($60V$) at 2 mm from the centre of the neuron.

4.3 Determination of neuronal activation

The Matlab code programmed for this thesis will first calculate the transmembranevoltage and gate-parameters on the neuron. Then it will calculate if the neuron has been activated, using the now known membranevoltage $V(x,t)$. Subsequently Matlab will determine the mean speed by which the activationpulse propagates in forward and backward direction on the axon, and will mention these speeds in the activationtable if the neuron has been activated. The resulting activationtables for simulations on a single neuron were already shown in the previous sections. However we did not yet discuss how neuronal activation is determined by the Matlab code. In this section we will examine how neuronal activation is determined by Matlab (i.e. which conditions are satisfied, if the activationtable mentions that the neuron has been activated).

We will say that neuronactivation has occurred ("the neuron has been activated"), if two conditions are satisfied:

1. An actionpotential is locally generated.
2. The actionpotential propagates over the neuron.

The first condition implies that the neuron will "feel" the electrode-stimulus. The neuronal membrane responds to the presence of the electrode by depolarisation. However, local depolarization of the membrane at a certain location on the neuron is not enough. To be able to speak of neuronactivation, the "information" should propagate along the neuron. This idea is summarized in the second condition.

A program was implemented in Matlab that checks the membrane voltage $V(x,t)$ for these two conditions. In this way, an activationtable can be generated automatically. This is for instance useful when considering a bundle with a high number of neurons. Instead of checking the neurons one by one for activation, the Matlab code will automatically calculate the percentage of activated neurons. In this section we will briefly discuss the ideas behind the implementation of the code, that will check if neuronactivation has occurred.

It is easy to quantify the first condition. For the initiation of an actionpotential somewhere on the neuron, an all-or-nothing principle applies. A higher stimulus will not result in a stronger depolarisation of the membrane. We can thus say that an actionpotential is locally generated at the position x, if the membranevoltage has increased sufficiently:

$$\tilde{V} \geq V_{thresh} \tag{4.2}$$

We will use a tresholdvoltage of $50mV$: $V_{thresh} = 50mV$. This value can be modified in Matlab however.

We will denote $\mathbb{S}$ as the set of points $P = (x, t)$[6] on the neuron, that satisfy the condition in equation (4.2). Obviously, if $\mathbb{S}$ is empty, no neuronactivation has occurred. The opposite however is not true. If the set $\mathbb{S}$ is not empty, it does not follow that the neuron is activated. Indeed, if the set $\mathbb{S}$ is not empty the second condition has yet to be satisfied: the actionpotential should have propagated over the neuron. It is not straightforward to determine from $\mathbb{S}$ if this is the case.

The set $\mathbb{S}$ is in general a continuum of points in the xt-plane. It would be easier to check if the actionpotential has propagated, with a finite set of points $\tilde{\mathbb{S}}$. We define this subset $\tilde{\mathbb{S}}$ as the set of points that satisfy the conditions:

1. $V(P) \geq V_{thresh}$
2. $\frac{\partial V}{\partial t}(P) = 0$
3. x is located at an active compartment of the neuron

The first condition corresponds to equation (4.2), ensuring that $\tilde{\mathbb{S}} \subset \mathbb{S}$. The second condition means that we identify the points where an actionpotential is locally generated, with local maxima in time of the transmembranevoltage. This condition will restrict the continuum of points of the set $\mathbb{S}$ to a discrete set of points. The third condition implies activation can only occur at active compartments, where the kalium- and natriumgates can open.

The Matlab code will determine the set $\tilde{\mathbb{S}}$, and store its information in a structured way. For this end, we define three Matlab-items:

1. A vector *xAct* containing the locations of the active compartments
2. A cell *timescell* containing the times t in $\tilde{\mathbb{S}}$
3. A cell *pkscell* containing the membrane-voltages at the points $P \in \tilde{\mathbb{S}}$

We denote the number of active compartments by AS. First, the location of the ith active compartment is stored in $xAct(i)$. Secondly, the cells *timescell* and *pkscell* are determined. A cell is a Matlab-structure, that can be seen as a matrix of matrices.
To define *timescell* and *pkscell*, we first consider the subset $\tilde{\mathbb{S}}_i := \{P = (x, t) \in \tilde{\mathbb{S}} : x = x_i\}$[7]. In words, $\tilde{\mathbb{S}}_i$ contains all points P at the ith active compartment, at which an actionpotential is locally generated (see the three conditions in the definition of $\tilde{\mathbb{S}}$). So we have defined a partition of $\tilde{\mathbb{S}}$: $\cup_{i=1}^{AS} \tilde{\mathbb{S}}_i = \tilde{\mathbb{S}}$. The time-components of the points $P \in \tilde{\mathbb{S}}_i$ are now stored as a rowvector in *timescell*$\{i\}$. So, *timescell* just holds all the times of points for which an actionpotential is locally generated. Furthermore *timescell* holds these times in a structured way: *timescell*$\{i\}$ refers to the ith active compartment. The corresponding cell *pkscell* has the same structure, but holds the corresponding membrane-voltages (pks = peaks, referring to the second condition in the definition of $\tilde{\mathbb{S}}$)[8]. It is not difficult to obtain these cells in Matlab:

[6] x denotes the spatial coordinate on the neuron, t is the time.
[7] Here $x_i = xAct(i)$ is the location of the ith active compartment.
[8] So mathematically we have that $pkscell\{i\}(j) = V(xAct(i), timescell\{i\}(j))$.

```
for i = 1:AS
[pks, locs] = findpeaks(Vactive(i,:));
times = timeflow(locs(pks>Vtres)); pks = pks(pks>Vtres);
pkscell{i} = pks; timescell{i} = times;
end
```

The for-loop runs over all active compartments. First $findpeaks$ will determine the local maxima in time at the ith active compartment (see the second condition in the definition of $\tilde{\mathbb{S}}$). The voltage at these peaks is stored in the vector pks and the corresponding times in the vector $locs$. In the third line it is then verified if the condition in equation (4.2) is satisfied. The resulting values for the times and voltages are subsequently stored in the cells $pkscell$ and $timescell$.

However as mentioned earlier, to state that the neuron has been activated at a point P_{act}, it is not enough that an actionpotential has locally been generated, as is the case for the points stored in the Matlab-cells. The actionpotential should have propagated over some amount of active compartments. However, thanks to the cells, it is easy to determine over how many active compartments an actionpotential initiated at P_{act} has propagated, in the antidromic and orthodromic direction[9]. The Matlab code will list the neuron as activated, if $\#AC_f$ and $\#AC_b$ exceed certain thresholds.

We will now briefly discuss how the values $\#AC_f$ and $\#AC_b$ are determined. First we consider two points $P_1 = (x_i, t_j), P_2 = (x_{i+1}, t_k) \in \tilde{\mathbb{S}}$, at neighbouring active compartments. By using the cells, the Matlab code determines if the actionpotential initiated at P_1 has propagated to P_2 (we denote $P_1 \to P_2$). This is done by calculating the (potential) propagation velocity of the actionpotential $v_{prop} = \frac{x_{i+1}-x_i}{t_k-t_i}$. The times necessary to determine v_{prop} are obtained from $timescell$, while the distances are obtained from $xAct$. We then have for neigbouring points:

$$P_1 \to P_2 \iff 0 \leq v_{prop} \leq v_{thresh} \tag{4.3}$$

Here v_{thresh} is a certain threshold velocity: velocities above the thresholdvelocity are assumed to be unlikely. The velocity v_{prop} has to be positive, to ensure that the actionpotential propagates from P_1 to P_2, and not the other way around. If the condition in equation (4.3) is satisfied, then we have $P_1 \to P_2$ and v_{prop} is indeed the propagation velocity of the actionpotential, while it is propagating between these two points. Furthermore the actionpotential initiated at P_1 has already propagated over at least one compartment in the forward direction. This reasoning is repeated to finally obtain $\#AC_f$ and $\#AC_b$.

[9]We denote the amount of compartments over which an actionpotential, initiated at P_{act}, has propagated by $\#AC_f$ (number of active compartments in forward direction) and by $\#AC_b$ (number of active compartments in backward direction), for the orthodromic and antidromic direction respectively.

Chapter 5

Discussion of mechanisms of neuronal activation

5.1 Introduction

From the results of the previous chapters we already observed that neuronal bendings and terminations seem to promote depolarisation of the membrane, potentially leading to an actionpotential. However also on straight uniform neurons in a homogeneous medium neuronal activation can occur. The underlying mechanism of neuronal stimulation in this case, is the excited electric field distribution that will directly alter the axonal current I_a, flowing inside the neuron. From equation (2.3) we identify the activation mechanism for a uniform straight neuron as the spatial derivate of the electric field component along the neuron, multiplied with $-\lambda^2$:

$$A_1 = -\lambda^2 \frac{\partial E_l}{\partial l} \tag{5.1}$$

Here $\lambda = \sqrt{\frac{r_m}{r_a}}$ is the square root of the membrane-resistance r_m per unit length divided by the axonal resistance r_a per unit length. The activation mechanism A_1 for straight uniform fibers is expressed in volt V. The meaning of this first activation mechanism is for instance explained in Roth (1993) [15], i.e. that for steady-state stimulation with an electric field distributed in space over distances larger than a length constant λ, the total depolarisation of the neuronal membrane will be equal to A_1. This follows from equation (2.3), because the first terms in both sides of the equation will then be negligible. However the depolarisation of the membrane voltage can be significantly different from A_1, when the applied electric field distribution varies strongly over lengths shorter than λ.

The activation mechanism A_1 is valid for straight uniform neurons in a homogeneous medium. However neuronal fibers may be short, curve, change in diameter, terminate and branch. Also the electric properties of the medium might be discontinuous. In these cases neuronal activation might occur, even in absence of electric field gradients.

At neuronal bends and at terminations, a second activation mechanism proportional to the electromagnetic field is observed (Roth, 1993 [15]). This effect was indeed observed in experiments: Maccabee et al. (1993) [13] shows that the activationtreshold is reduced for bent neurons or for stimulation at the neuronal terminals. Furthermore Nagarajan et al. (1993) [14] suggests that excitation of short axons occurs at neuronal terminations, rather than at the regions of high spatial derivative of the electric field.

At neuronal bends activation can occur, without external electric field gradient. However this can be explained, by the fact that in equation (5.1), the electric field component along the neuron is used. In other words, a constant electric field distribution does not imply that the source-term in equation (5.1) vanishes at the neuronal bend. Even if the electric field $\mathbf{E}$ is constant throughout space, the component E_l of the electric field along the neuron will have a nonzero spatial derivative along the neuronal coordinate l. For a constant electric field this spatial derivative will be proportional to a Dirac-delta distribution, centered at the bending. This delta distribution appearing in the right-hand side of equation (2.3) will result in depolarisation at the neuronal bending, even in a constant electric field distribution. This depolarisation will be proportional to λE, as will be derived in section 5.2.

Also at neuronal termination activation can occur, even while the electric field distribution is constant in space, meaning that there is no source in equation (2.3). However in this case, the electric field distribution is reintroduced in the equations, via the sealed-end boundary conditions. This will result in depolarisation at the neuronal bendings proportional to $\lambda E_n = \lambda \mathbf{E} \cdot \mathbf{u}_n$[1]. This activation mechanism at neuronal terminations will be reviewed in section 5.3.

Finally also a fourth activation mechanism proportional to $-\lambda \frac{\Delta E}{2}$ (Miranda et al., 2007 [51]) will occur at discontinuities of the electric parameters in the medium surrounding the neuron, for instance at the GM-WM interface[2]. This activation mechanisms is often negligible, compared to the former two mechanisms (De Geeter, 2014 [34]). All three mechanisms have have been computed by Silva et al. (2008) [52] in a cortical sulcus and were tested by Salvador et al. (2011) [53] on synthetic neuronal fibres.

[1] Here $\mathbf{u}_n$ is the vector at the sealed-termination, pointing outwards with respect to the neuron

[2] Gray matter - White matter interface

5.2 Activation at a neuronal bend

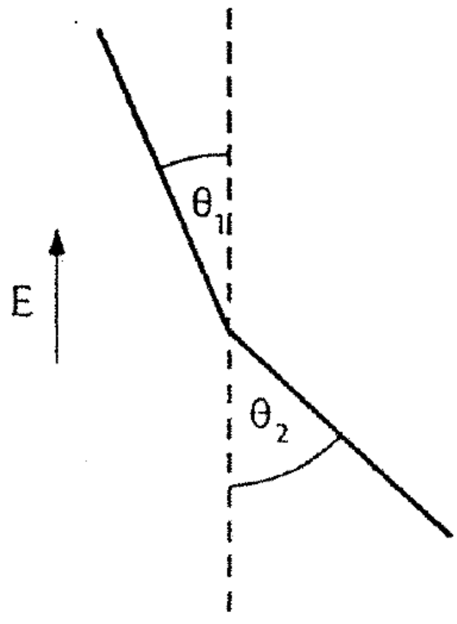

Figure 5.1: Neuron bending from an angle θ_2 with the electric field, to an angle θ_1. Figure reproduced from Roth (1993) [15].

In this section we will study the effect of a neuronal bend on the membrane potential. As noted in Maccabee et al. (1993) [13], Tranchina et al. (1986) [54], Amassian et al. (1992) [55] a bend in the neuron will cause polarisation, even in the absence of electric field gradients. This is due to the fact that even if E is constant, the projection of the electric field E_l will change in the bend, because the direction of projection $\mathbf{u_l}$ changes. This activation mechanism is proportional with the electric field λE, meaning that the depolarisation of the membrane will be proportional to λE.

We consider a (homogeneous) neuron bending from an angle θ_1 with the constant field $\mathbf{E}$ to an angle θ_2, as in Roth (1993) [15], see figure 5.1. The electric field is seen to be:

$$E_l(l) = \begin{cases} E\cos(\theta_2) & l < 0 \\ E\cos(\theta_1) & l > 0 \end{cases} \tag{5.2}$$

The spatial derivative of the electric field E_l then becomes:

$$-\lambda^2 \frac{\partial E_l}{\partial l} = -\lambda^2 (E\cos\theta_1 - E\cos\theta_2)\delta(l) \tag{5.3}$$

When applying the transmissionline equation (eq. (2.3)) and assuming steady-state ($\frac{\partial V}{\partial t} = 0$), we obtain:

$$\tilde{V} - \lambda^2 \frac{\partial^2 \tilde{V}}{\partial l^2} = -\lambda^2 (E\cos\theta_1 - E\cos\theta_2)\delta(l) \tag{5.4}$$

Again $\tilde{V}$ refers to the reduced membrane voltage: $\tilde{V} = V - V_r = V_i - V_e - V_r$. Because of the dirac delta in this equation, the spatial derivative of the membrane-voltage $\tilde{V}$ will satisfy the jump-condition:

$$\frac{\partial \tilde{V}}{\partial l}(dl) - \frac{\partial \tilde{V}}{\partial l}(-dl) = E(\cos\theta_1 - \cos\theta_2) = -2E\sin\left(\frac{\theta_1+\theta_2}{2}\right)\sin\left(\frac{\theta_1-\theta_2}{2}\right) \tag{5.5}$$

For the first equality we integrated equation (5.4) between $l = -dl$ and $l = dl$, applying continuity for $\tilde{V}$.

We can solve equation (5.4) for $l > 0$ and $l < 0$:

$$\tilde{V} = \begin{cases} A_2 \exp\left(\frac{l}{\lambda}\right) & l < 0 \\ A_2 \exp\left(-\frac{l}{\lambda}\right) & l > 0 \end{cases} \tag{5.6}$$

Here we used as boundary conditions at infinity: $\tilde{V}(\infty) = 0$ and $\tilde{V}(-\infty) = 0$, and we applied continuity of $\tilde{V}$ in $l = 0$. The coefficient A_2 can then be determined, using the jumpcondition in equation (5.5). We find:

$$A_2 = E\lambda \sin\left(\frac{\theta_1 + \theta_2}{2}\right) \sin\left(\frac{\theta_1 - \theta_2}{2}\right) \tag{5.7}$$

This result can also be verified directly by rewriting equation (5.6) as:

$$\tilde{V} = A_2 \exp\left(\frac{l}{\lambda}\right)\theta(-l) + A_2 \exp\left(-\frac{l}{\lambda}\right)\theta(l) \tag{5.8}$$

Here θ is the heaviside-function, the derivative of $\tilde{V}$ is then:

$$\frac{\partial \tilde{V}}{\partial l} = \frac{A_2}{\lambda} \exp\left(\frac{l}{\lambda}\right)\theta(-l) - \frac{A_2}{\lambda} \exp\left(-\frac{l}{\lambda}\right)\theta(l) \tag{5.9}$$

We see that indeed the jumpcondition is satisfied:

$$\frac{\partial \tilde{V}}{\partial l}(dl) - \frac{\partial \tilde{V}}{\partial l}(-dl) = -\frac{2A_2}{\lambda} \tag{5.10}$$

By calculating the second derivative of $\tilde{V}$ we can also verify equation (5.4) directly. From equation (5.10) we also see that the polarisation of the membrane-voltage at the bend $l = 0$ is given by $A_2 = E\lambda \sin\left(\frac{\theta_1+\theta_2}{2}\right) \sin\left(\frac{\theta_1-\theta_2}{2}\right)$ and is indeed proportional to λE. This second activation mechanism A_2 for neuronal bendings, was also obtained by Roth (1993) [15]. We see that if the neuron is bent toward the electric field the membrane will hyperpolarise, if the neuron is bent away from the electric field the membrane will depolarise (Roth, 1993 [15]).

We note that in the case of electric stimulation (ES)[3], the electric field is conservative and can be expressed in terms of the external voltage V_e^{ES}, which can be determined by integrating $\mathbf{E} = -\nabla V_e^{ES}$:

$$V_e^{ES} = \begin{cases} -El\cos(\theta_1) & l < 0 \\ -El\cos(\theta_2) & l > 0 \end{cases} \tag{5.11}$$

In this case the internal voltage $\tilde{V}_i^{ES} = \tilde{V}^{ES} + V_e^{ES}$ is:

$$\tilde{V}_i^{ES} = \begin{cases} A_2 \exp\left(\frac{l}{\lambda}\right) - El\cos(\theta_1) & l < 0 \\ A_2 \exp\left(-\frac{l}{\lambda}\right) - El\cos(\theta_2) & l > 0 \end{cases} \tag{5.12}$$

By calculating the derivative of equation (5.12), we note that the spatial derivative of the internal potential V_i^{ES} does not exhibit a jump, and is consequentially continuous. This can be explained

[3] This thesis focuses on deep brain stimulation, which is a type of electric stimulation.

physically. First we observe that for electric stimulation the electric field is conservative, meaning that we have for the axonal current: $I_a = -\frac{1}{r_a}\frac{\partial V_i^{ES}}{\partial l}$. Secondly, in steady-state the axonal current has to be continuous at the bending, which implies that the spatial derivative of V_i^{ES} has to be continuous to. We conclude that the jump in the spatial derivative of V^{ES}, can be completely attributed to the contribution of the external potential V_e^{ES}.

5.3 Stimulation at neuronal terminations

In a constant electric field a straight neuron can still be stimulated due to neuronal terminations. The stimulation mechanism will be proportional to $\lambda E_n = \lambda \mathbf{E}\cdot\mathbf{u}_n$ at the neuronal terminations, with $\mathbf{u}_n$ the outward unitvector. An inward electric field will result in hyperpolarisation of the membranevoltage with λE_n, while an outward electric field will result in depolarisation of V over λE_n (Plonsey et al., 1988 [56]; Rubinstein, 1993 [57]; Altman et al., 1990 [58]; Nagarajan, 1992 [59]; Nagarajan, 1993 [14]). Much of the work done by Reilly assumes that stimulation at the endpoints of the neuron is the dominant activation mechanism (Reilly, 1985 [60]; Reilly, 1989 [61]). We discuss a possible way to derive this result.

This mechanism of activation, proportional to E_n, occurs due to applying Neumann-boundary conditions on the edges when solving the transmissionline equation, eq. (2.3). If we consider a straight, but finite, neuron in a homogeneous constant electric field $\mathbf{E} = E\mathbf{u}_x$, and assume steady-state we obtain:

$$\tilde{V} - \lambda^2 \frac{\partial^2 \tilde{V}}{\partial l^2} = 0 \tag{5.13}$$

Because the electric field is constant the activation mechanism in the right hand side of the transmissionline equation, proportional to the spatial derivative of E_l, drops out. If the neuron would be infinite there would be no stimulation ($\tilde{V} = 0$), because there is no electric field gradient. However for a finite neuron, applying Neumann-boundary conditions reintroduces the electric field $\mathbf{E}$, leading to a non-zero solution. If we assume the ends are sealed, then there is no axonal current at the neuronal terminations. If the neuron is assumed to start at $x = -L$ and end at $x = L$, we can write this condition as:

$$I_a(\pm L) = 0 \rightarrow \frac{\partial \tilde{V}}{\partial l}(\pm L) = E_l(\pm L) \tag{5.14}$$

Indeed: For electric stimulation (as in the case of DBS) the electric field is conservative, so $I_a = -\frac{1}{r_a}\frac{\partial \tilde{V}_i}{\partial l} = 0$. Using $\tilde{V}_i = \tilde{V} + V_e$ and $E_l = -\frac{\partial V_e}{\partial l}$, we obtain equation (5.14).[4]

We find that the solution of equation (5.13) and equation (5.14) is given by:

[4] Note that equation (5.14) is also valid for magnetic stimulation (f.i. transcranial magnetic stimulation (TMS)). In this case the electric field is non-conservative, due to the time-dependent magnetic field. Because of the high conductivity of the tissue, the conservative part of the external electric field is negligible w.r.t. the non-conservative part: $V_e \approx 0$ (De Geeter, 2014 [34]). The axonal current can be written as the sum of the current due to the conservative part of the electric field, $I_a^{cons} = -\frac{1}{r_a}\frac{\partial \tilde{V}}{\partial l} = -\frac{1}{r_a}\frac{\partial \tilde{V}_i}{\partial l}$, with the current due to the non-conservative part of the electric field $I_a^{non-cons} = \frac{1}{r_a}E_l$. Then at the neuronal terminations we have $I_a = I_a^{cons} + I_a^{non-cons} = 0$, which indeed yields equation (5.14).

$$\tilde{V} = E\lambda \frac{\sinh \frac{x}{\lambda}}{\cosh \frac{L}{\lambda}} \tag{5.15}$$

For very small neurons $L \ll \lambda$, we have $\tilde{V} \approx Ex$. The maximum polarisation of the neuronal membrane is $\tilde{V}_{max} = EL$, increasing linearly with L. This linear relation between the maximum polarisation and L levels off to $E\lambda$, when $L \gg \lambda$. This follows from $\frac{\sinh \frac{\pm L}{\lambda}}{\cosh \frac{L}{\lambda}} \xrightarrow[L \gg \lambda]{} \pm 1$. So for $L \gg \lambda$ we obtain $\tilde{V}(\pm L) = \pm E\lambda = A_3$, which was predicted in section 5.1.

Part III

Bundles of multiple neurons

Chapter 6

Bundles of multiple neurons

In this chapter we will discuss the simulation of bundles of multiple neurons. For this end the Matlab-program was altered, to make simulation of multiple neurons at once possible. Because the membrane-voltage V and the gate-parameters m, n, h and p can be calculated for all neurons at the same time (in parallel), the time-complexity of the program will not scale linearly with the amount of neurons. The time-complexity will be considered in section 6.1. In section 6.2 we will discuss a simulation on a neuronbundle consisting of 19 neurons and the percentage of activated neurons $\%AN$ in the bundle will be determined. Finally in section 6.3 the influence of the distance from the electrode to centre of the bundle d_{elec} on the $\%AN$ will be determined.

6.1 Time-complexity

The total calculation time needed on the used computer for a single neuron is about $t_{tot}^{single} = 2.5min$. This time is defined as the total time Matlab needs to determine the membrane-voltage V and gate-parameters on the neuron. The total calculation time includes initialisation of recorders [1], itialisation of the Crank-Nicolson matrices and the iteration over time of the discretised equations. It does not include loading of the electromagnetic field and plotting the recorders.

When considering a neuron bundle, we will denote the amount of neurons in the bundle as AN. If the voltages and gate-parameters on each neuron of the bundle would be determined sequentially, the total calculation time would become $t_{tot,seq}^{bundle} = AN * 2.5min$. The time-complexity in a sequential calculation process would thus be linear, which is a disadvantageous. The main advantages of a sequential calculation process however is that the implementation in Matlab is straightforward and that the necessary RAM-memory will not scale with AN.

To limit the time-complexity a parallel calculation process was implemented in Matlab, by which the membrane-voltages and gate-parameters for all neurons in the bundle will be determined at

[1] In the Matlab code recorders are defined for the membrane voltage and gate-parameters. These recorders are vectors that store ("record") the voltage and gate-parameter values. When the program has finished, the colour maps and spatial distribution plots are obtained by plotting the recorders.

once without additional for-loop[2]. To do this the Matlab-code was altered, leading to a slower total calculation time for a single neuron of $8.5min$ for the parallel implementation as compared to $2.5min$ for the sequential implementation on the used computer. The influence of this parallel process on the time-complexity was measured in Matlab, by running the (parallel) program for several bundles with different amount of neurons AN. These simulations were done twice, to put the potential influence of the external factors (programs running in the background on the computer, ...) in perspective. The total calculation time as function of AN is shown in figure 6.1. We indeed notice that the time-complexity is sub-linear: the time needed by Matlab to calculate all fields with the parallel method doubles from $8.5min$ to $17min$ when the amount of neurons in the bundle is increased from 1 neuron to 20 neurons. We recognize that when more than 5 neurons are considered in the bundle, the program using a parallel calculation process will be considerably faster, than the program that makes use of sequential calculation.

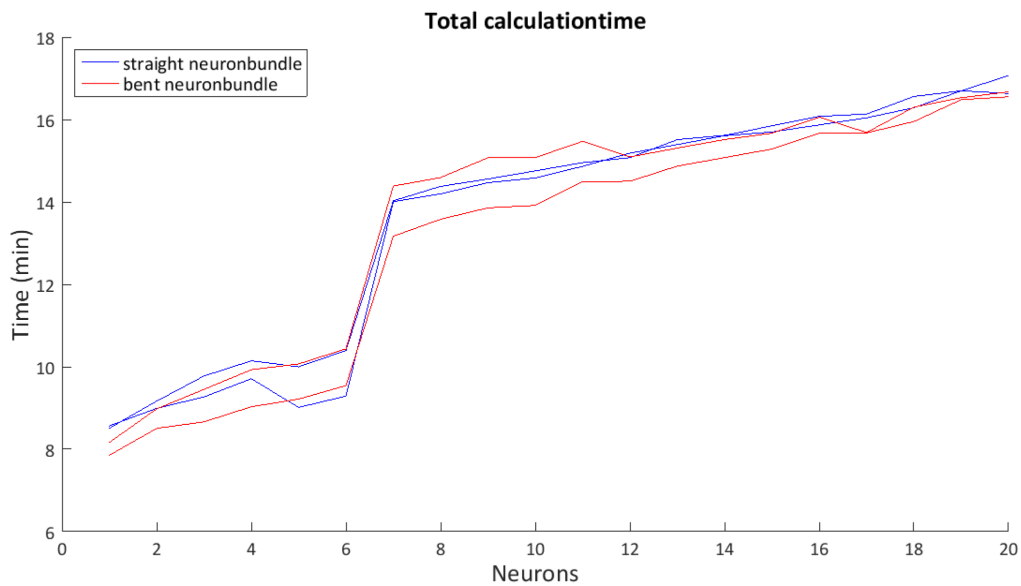

Figure 6.1: Total calculation time as function of the number of neurons in the bundle. This calculation time was determined by using the parallel calculation method. The calculation time was measured twice on the same computer. The calculationtime was determined for a straight and bent neuron bundle.

We notice that in figure 6.1 the calculationtime suddenly increases from 6 to 7 neurons. Because the calculationtime increases uniformly over the whole code, we hypothesize that the sudden increase might be explained by memory-speed considerations. The main disadvantage of a parallel

[2]For this end we define $V(x,t,n)$ for the voltage and for instance $m(x,t,n)$ for the m-gate parameter (other gate-parameters are analogous). Here as usual x is the spatial parameter along the neuron and t is the time. We now have an additional discrete parameter n, that refers to the nth neuron in the bundle. We see that the voltages and gate-parameters can be stored as three-dimensional matrices. Furthermore it is possible to iterate all neurons at once, without for-loop, by matrix operations on $S \times 1 \times AN$-matrices (S is the number of (spatial) segments, and AN the number of neurons in the bundle; one time-snapshot is considered per iteration).

calculation method to determine the voltages and gate-parameters on all neurons is that the necessary RAM-memory will increase with AN. To solve this problem the implemented Matlab-code makes use of a combination of parallel and sequential calculations. The total amount of neurons is distributed over several bundles. All neurons in each bundle will be considered in parallel, while a sequential approach is chosen for the bundles themselves. Computers with high RAM-memory will benefit from high number of neurons per bundle. Furthermore this approach enables us to use different discretisation steps and times for different types of neuronbundles[3].

6.2 Bundle of straight neurons

In this section we will consider a simulation on a bundle consisting of 19 straight neurons. The geometry is shown in figure 6.2. The black lines represent straight neurons, while the blue sphere represents the spherical electrode. The electrode is placed at $3mm$ from the centre of the bundle. A voltage of $40V$ is imposed as Dirichlet-condition on the electrode.

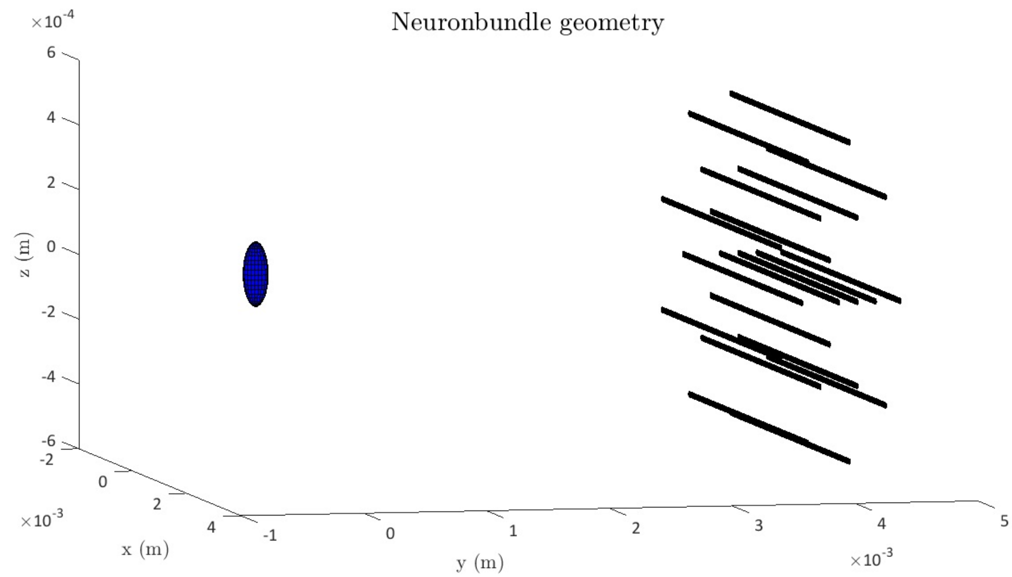

Figure 6.2: The geometry of a neuron bundle consisting of 19 straight neurons. The black lines represent the straight neuron geometry. The blue sphere is a schematical representation of the electrode.

As before Matlab will generate an activationtable mentioning for every neuron if activation occurred. The result is shown in figure 6.1. The activationtable will also mention the total

[3]For this "hybrid" method (combining sequential and parallel calculation) for instance the membrane voltage is stored in a $1 \times BDLs$ cell. Here $BDLs$ is the amount of considered neuronbundles. The $iBDL$th neuronbundle consists of $AN(iBDL)$ neurons. So $V\{iBDL\}(x,t,n)$ refers to the the nth neuron of the $iBDL$th neuronbundle at location x and time t. In the program a for-loop over the bundle-parameter $iBDL$ will be used to process the neuronbundles sequentially, while the voltage on all neurons in the same bundle (distinguished by n) is calculated in parallel (without for-loop).

percentage of activated neurons during the simulation time of $350\mu s$: $\%AN = 36.8\%$.

	Activated	Synapse activated	nr.	pos. (mm)	time (ms)
Neuron1	no	no	-	-	-
Neuron2	no	no	-	-	-
Neuron3	yes	no	1.	4.1970	0.2876
Neuron4	yes	no	1.	4.1970	0.2876
Neuron5	no	no	-	-	-
Neuron6	no	no	-	-	-
Neuron7	yes	no	1.	4.1970	0.2761
Neuron8	yes	no	1.	3.8855	0.2506
Neuron9	yes	no	1.	4.1970	0.2761
Neuron10	no	no	-	-	-
Neuron11	no	no	-	-	-
Neuron12	no	no	-	-	-
Neuron13	no	no	-	-	-
Neuron14	no	no	-	-	-
Neuron15	yes	yes	1.	3.5985	0.2198
Neuron16	yes	yes	1.	3.5985	0.2198
Neuron17	no	no	-	-	-
Neuron18	no	no	-	-	-
Neuron19	no	no	-	-	-
%AN	36.8421				

Table 6.1: Activation table of a bundle of 19 straight neurons, excited by a spherical electrode at $3mm$ from the centre of the bundle.

We can also plot the gate-parameters and membrane-voltage on each neuron as function of time and space along the neuron. As an example the membrane-voltage for two neurons (neuron 11 and 15 respectively) is shown in figures 6.3 and 6.4. The activationtable mentions that activation has occurred for neuron 15, as can be recognised by considering figure 6.4. The plot of the membranevoltage of neuron 11 in figure 6.3 shows no activation during the simulationtime, as mentioned in the activationtable (although activation might start on the end of the simulation-domain). Activation of neurons mentioned in the activationtable will always refer to activation during the simulationtime that is used.

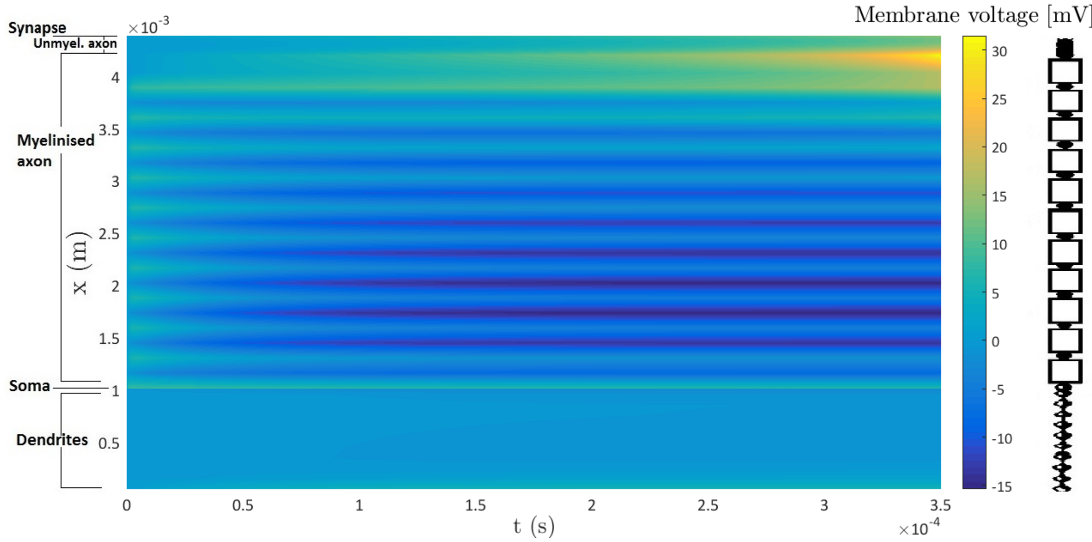

Figure 6.3: Membrane-voltage as function of space and time for neuron 11 in the bundle.

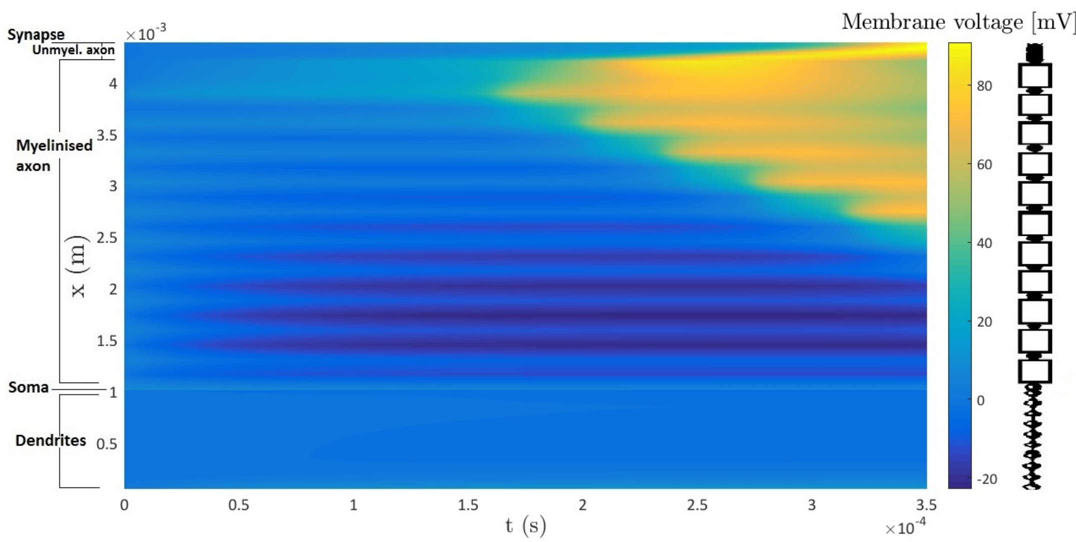

Figure 6.4: Membrane-voltage as function of space and time for neuron 15 in the bundle

6.3 Dependency of percentage of activated neurons on electrode distance

In this section we will determine the influence of the distance from the centre of the neuronbundle to the electrode d_{elec} on the percentage of activated neurons $\%AN$. We obtain this relation by moving the neuronbundle sequentially over $\Delta x = 0.1mm$. The procedure is schematically shown in figure 6.5. Every colour represents a single location of the neuronbundle, consisting of 19 neurons. In total 10 locations, corresponding to 10 colors, are considered. The total range for d_{elec} will thus be from $2.6mm$ to $3.5mm$. For electrode distances greater than $3.5mm$ the percentage of activated neurons will be zero, while for d_{elec} lower than $2.6mm$ the $\%AN$ will be 100%. We notice that due to graphical constraints not all 190 neurons are shown in figure 6.5.

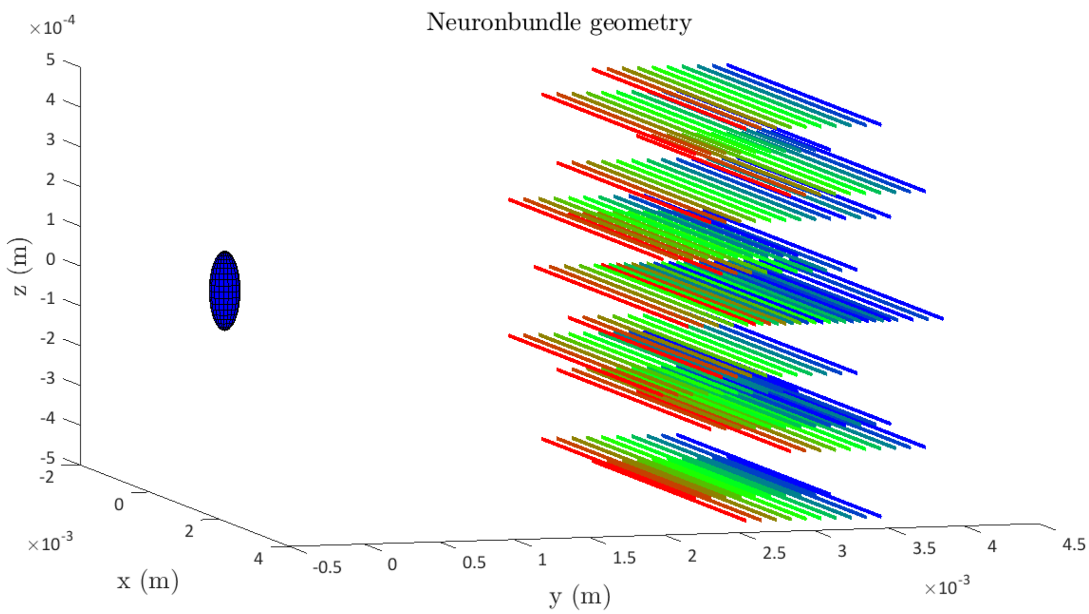

Figure 6.5: Schematical representation of all the bundles considered when determining the dependency of $\%AN$ on d_{elec}

The percentage of activated neurons is plotted as function of d_{elec} in figure 6.6 for a neuron bundle consisting of straight neurons. We notice that $\%AN$ declines monotonically from 100% to 0% when increasing d_{elec}, as expected. We expect that for a high spatial resolution, i.e. $\Delta x \to 0$, the $\%AN(d_{elec})$ function should become a staircase function. The height of the different stairs will become smaller with higher number of neurons AN, so for very high neuronnumbers, the function $\%AN(d_{elec})$ should become more continuous again. Similarly the dependency of the $\%AN$ on the distance d_{elec} for a bundle consisting of neurons, that bend over 15° is shown in figure 6.7.

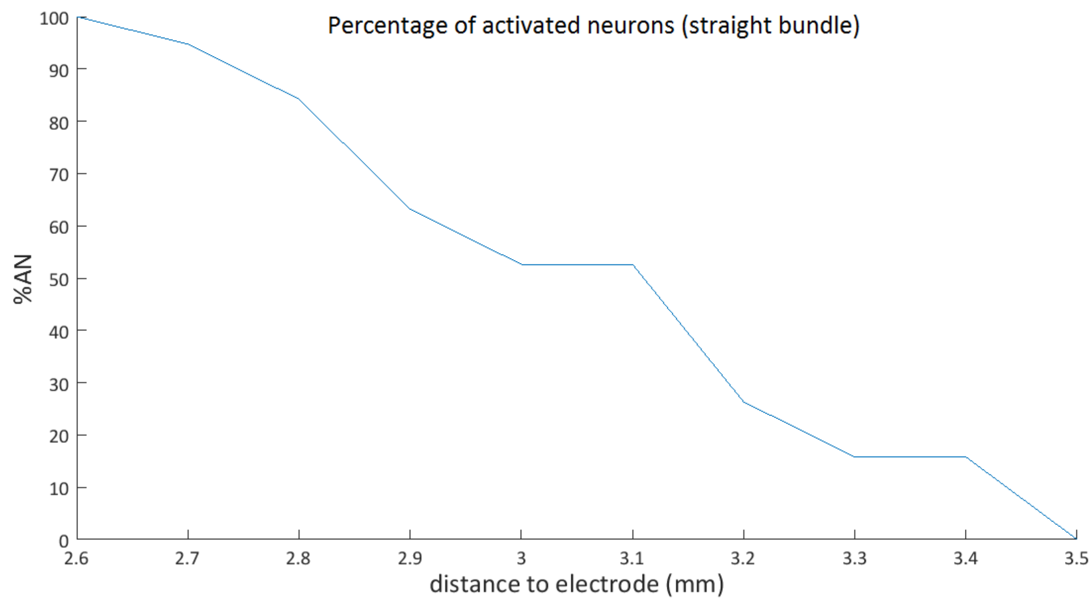

Figure 6.6: Dependency of the $\%AN$ on the distance of the electrode to the centre of the bundle d_{elec} for a bundle of straight neurons.

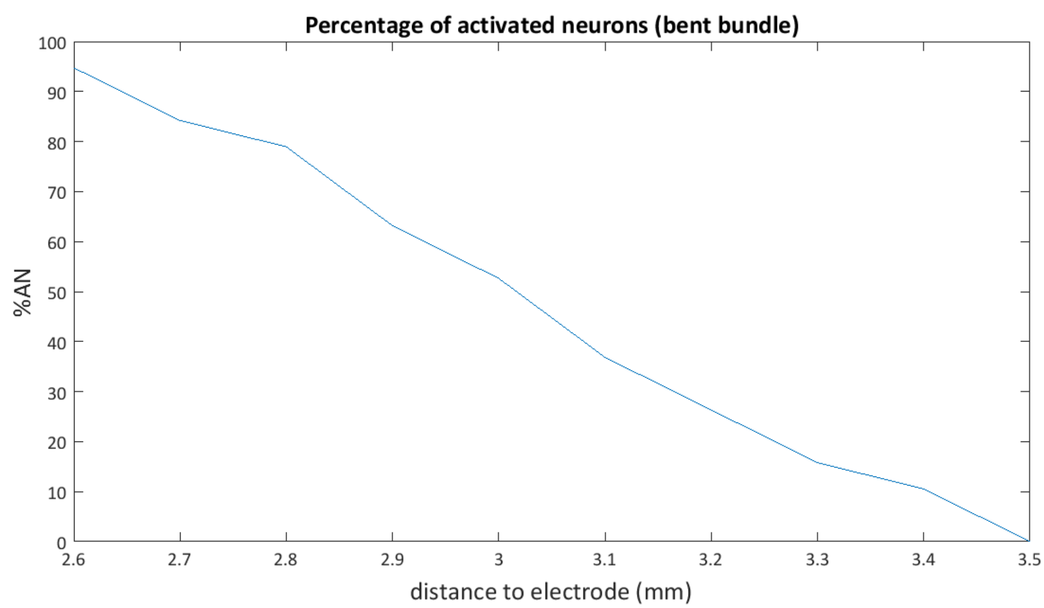

Figure 6.7: Dependency of the $\%AN$ on the distance of the electrode to the centre of the bundle d_{elec} for a bundle of neurons bending over 15°.

Chapter 7

Deep brain stimulation in MIDA-head phantom

In this chapter we describe a simulation of deep brain stimulation by a Medtronic-lead in the MIDA-head phantom. The MIDA-phantom (Iacono et al.,2015 [11]) is a high-resolution head and neck phantom, featuring a high amount of structures relevant for deep brain stimulation. The DBS lead was modelled in Sim4life based on the geometry of the Medtronic 3889 lead (Medtronic Inc., Minneapolis, MN, USA). The lead was placed at the subthalamic nucleus (STN) in the MIDA-brain. The STN is often mentioned in literature as an effective stimulation-location for Parkinson's disease (Kumar et al.;1998 [62], Kleiner et al.; 2006 [63]). The azimuthal and polar angles of the DBS-lead were set to 7° and 20° respectively, as was also done in Schmidt et al. [17]. The DBS-lead with the thalamus and globus pallidus of the MIDA-phantom is shown in figure 7.1.

As stimulus applied to the DBS-electrodes, a typical biphasic square-wave with duration of $60\mu s$ and frequency of $65Hz$ was used. The electromagnetic field was determined at $65Hz$ in Sim4life for $01xx$ and $10xx$ stimulation, to determine the frequency-response. The approximation of a frequency independent field distribution, discussed in chapter 1, was made.

Stimulation of two types of neuronal tracts are often mentioned to be therapeutic in deep brain stimulation for Parkinson's disease. Projection neurons from the STN to the globus pallidus internus (GPi) and lenticular fasciculus fibers from the GPi to the thalamus (Th). The response of these neuronal tracts on an applied square wave signal was calculated in Matlab. For this end the neuronal tracts were approximated by straight neurons. The starting and endpoints of the neurons in the thalamus, globus pallidus and STN were approximated by spheres of radius $4mm$, as shown in figure 7.2. Subsequently 100 random neurons were generated connecting the spheres representing the STN and GPi and 100 other random neurons were generated to represent the lenticular fasciculus. The neurons of the first neuronal tract (STN-GPi) were checked for intersection with the DBS-lead, and neurons intersecting the lead were removed. Finally the membrane-voltage, gate-parameters and activation table on the remaining 197 neurons was calculated in Matlab.

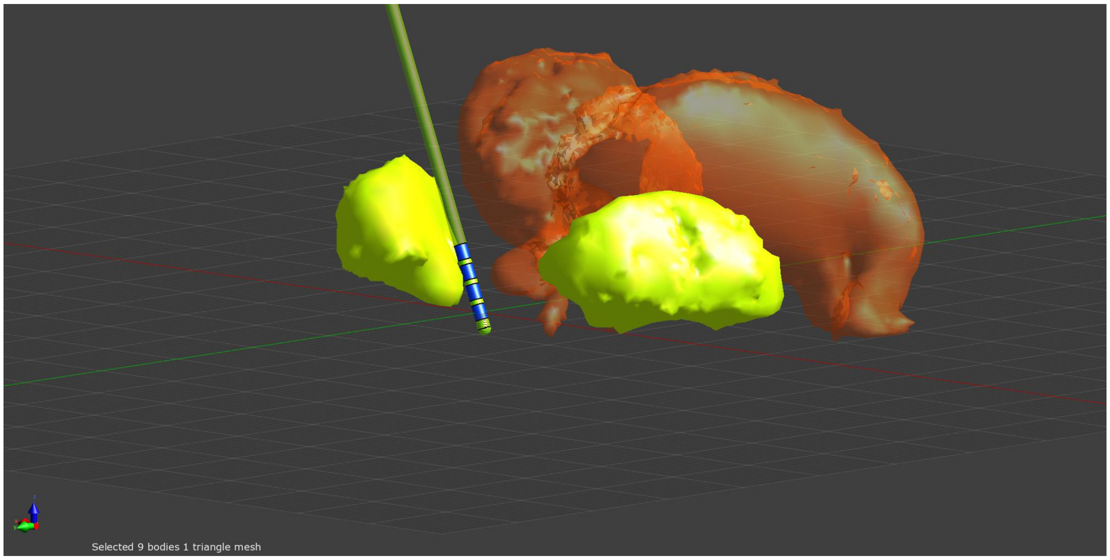

Figure 7.1: Medtronic-lead at the subthalamic nucleus in the MIDA-phantom. The thalamus (orange) and globus pallidus (yellow) are shown.

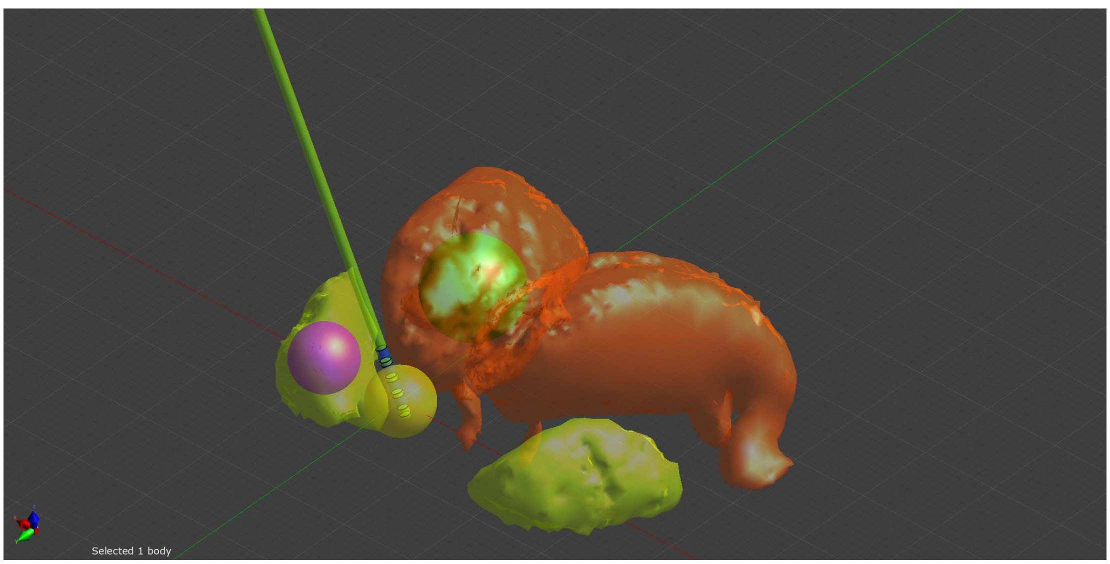

Figure 7.2: Spheres are drawn, to represent the neuronal starting- and endpoints in the thalamus, GPi and STN.

The generated neuronal tracts between the spheres that represent the thalamus, GPi and STN are shown in figure 7.3. The resulting model of the thalamus and GPi with the neuronal tracts are shown in figure 7.4 and 7.5.

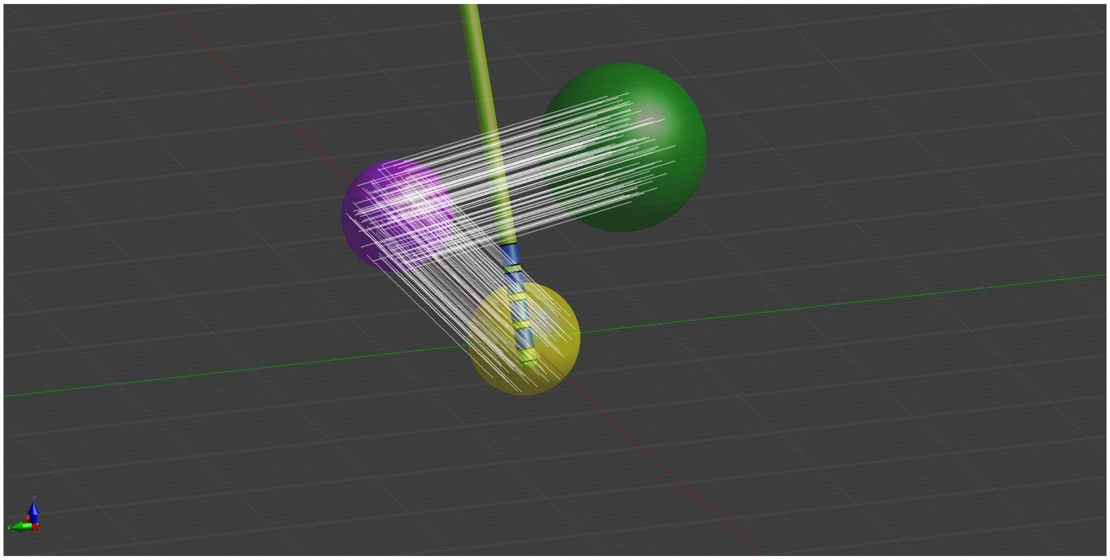

Figure 7.3: Representation of the considered neuronal tracts between the spheres that represent the Th, GPi and STN.

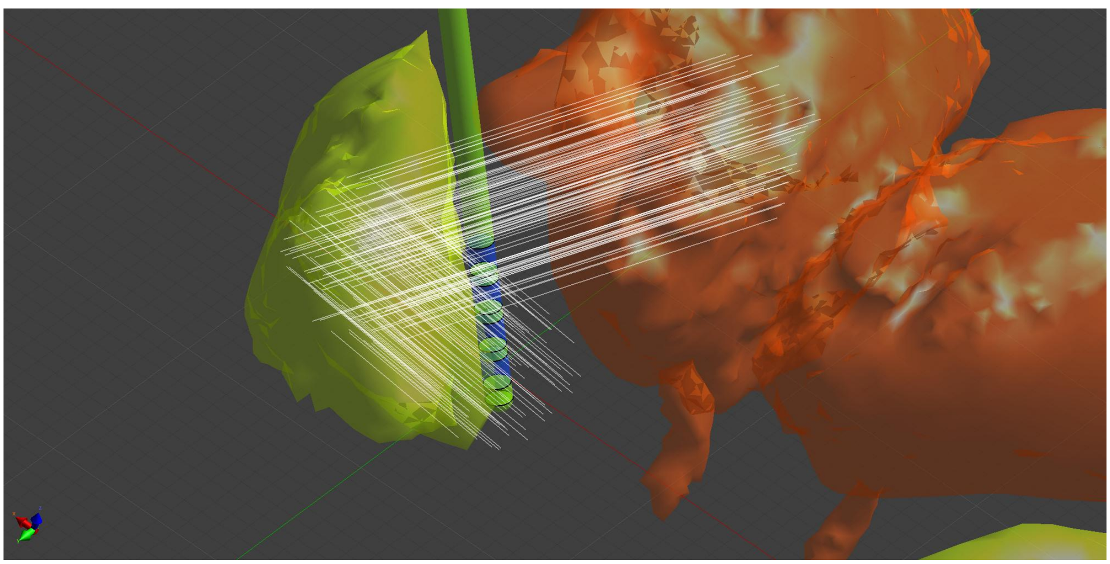

Figure 7.4: Representation of the considered neuronal tracts between the Th, GPi and STN. Surrounding brain structures are made transparent.

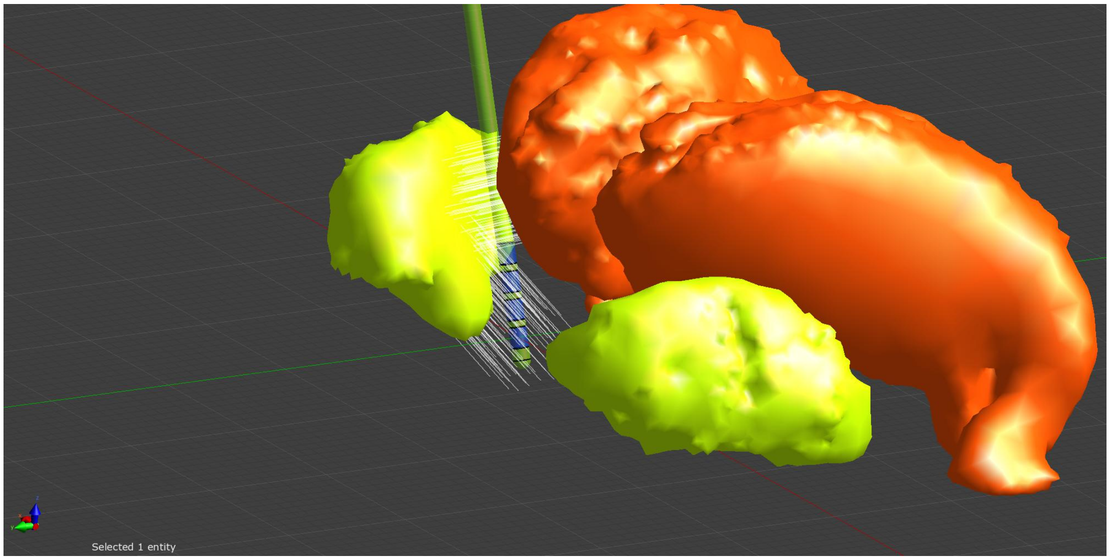

Figure 7.5: Representation of the considered neuronal tracts between the Th, GPi and STN. Surrounding brain structures are made non-transparent.

The results of these simulations are summarized in table 7.1. The table summarizes for both neuronal pathways (GPi-Th or lenticular fasciculus (LF) and STN-GPi or macaca fascicularis (MF)) and for both stimulation set-ups ($01xx$- and $10xx$-stimulation) the total percentage of activated neurons in the bundle ($\%AN$). The table also mentions the percentage of neurons in the neuronal pathway, where the synapse is activated ($\%AS$).

	$01xx$-stimulation		$10xx$-stimulation	
	Lenticular fasciculus (GPi-Th)	Macaca fascicularis (STN-GPi)	Lenticular fasciculus (GPi-Th)	Macaca fascicularis (STN-GPi)
$\%AN$	10	19.6	6	14.4
$\%AS$	6	14.4	4	9.28

Table 7.1: $\%AN$ and $\%AS$ in the lenticular fasciculus (GPi-Th) and macaca fascicularis (STN-GPi) for $01xx$- and $10xx$-stimulation.

From table 7.1 we notice that the percentage of activated neurons is higher for stimulation by a square-wave of amplitude $1V$, when the first electrode is used, rather than zeroth electrode. This is true both for the neurons of the lenticular fasciculus as for the macaca fascicularis. This can be explained for both neuronbundles by noticing that the distance between the first electrode and the axon of a typical neuron of the bundle is smaller than the distance between the zeroth electrode and the axon of a typical neuron. Furthermore neuron activation typically occurs at the axon (see f.i. chapter 4).

We note the distinction between the percentage of neurons where an activation pulse starts ($\%AN$) and the percentage of neurons where the synapse is activated ($\%AS$). The latter might be more important when considering the effect of deep brain stimulation on neuronal activation. The difference between activation of the neuron and activation at the synapse is clarified by considering some colour maps of the membrane-voltage for specific neurons in the bundle.

An example of a neuron which is not activated is shown in figure 7.6. Indeed, there is no considerable depolarisation and no action potential starts on the axon. The neuron is not at rest however: the influence of the biphasic square-wave can still be seen in the plot. Nevertheless we note that even for a neuron at rest the reduced membrane potential shown in the plots won't be zero everywhere. We refer to the appendix (appendix A.1) for a discussion of a neuron at rest.

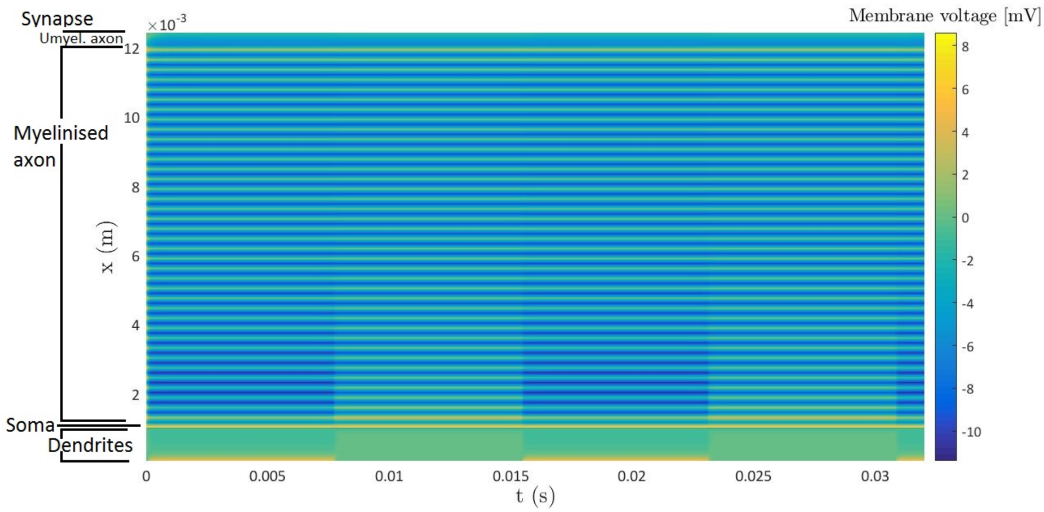

Figure 7.6: Neuron 1 in the macaca fascicularis in 01xx-stimulation. This is a representation of a neuron that is not activated by the DBS-lead. The simulation time extends over two periods of the biphasic square-wave stimulus.

Two examples of a neuron activated at the synapse are shown in figure 7.7 and figure 7.8. The activation pulse starts at the axon and travels toward the synapse and the soma. It is interesting to note that the location of the region of hyperpolarisation is not the same for both neurons. In contrast, an example of a neuron on which depolarisation has occurred, but on which no synapse activation is observed is shown in figure 7.9. In this case the propagation of the action potential is hindered by a region of hyperpolarisation. We conclude that the location of the region of hyperpolarisation, that is mostly determined by the location of the electrode with respect to the neuron (see chapter 4), plays a significant role in whether or not the actionpotential will reach the synapse.

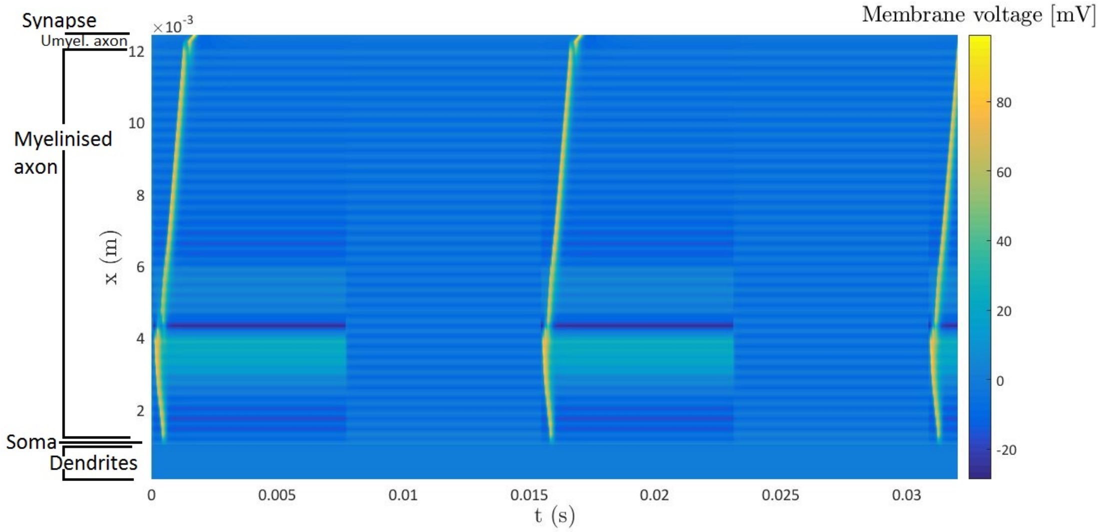

Figure 7.7: Neuron 3 in the macaca fascicularis in $01xx$-stimulation. This is a representation of a neuron on which an actionpotential is initiated. Furthermore the actionpotential has reached the synapse. The simulation time extends over two periods of the biphasic square-wave stimulus.

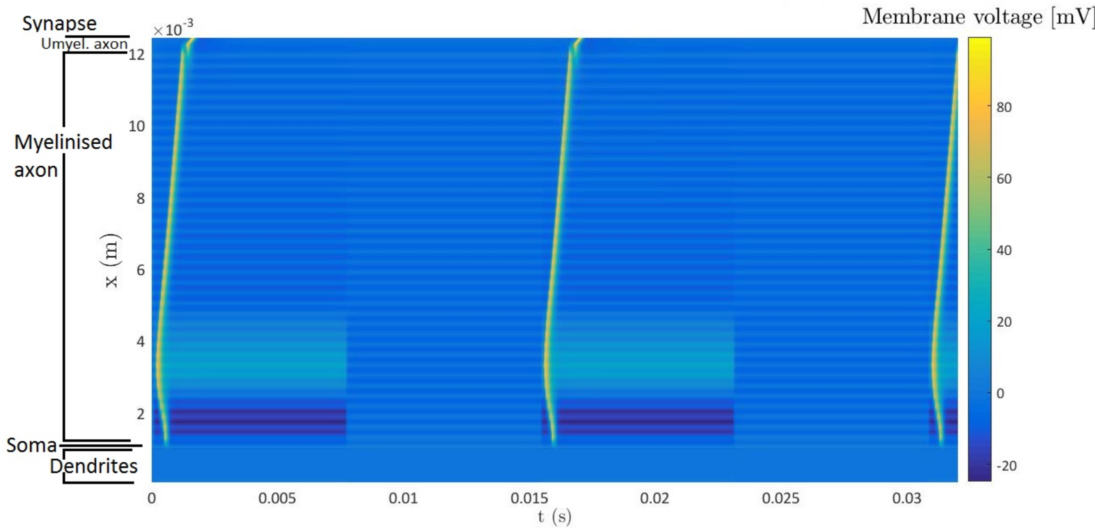

Figure 7.8: Neuron 79 in the macaca fascicularis in $01xx$-stimulation. This is a representation of a neuron on which an actionpotential is initiated. Furthermore the actionpotential has reached the synapse. The simulation time extends over two periods of the biphasic square-wave stimulus.

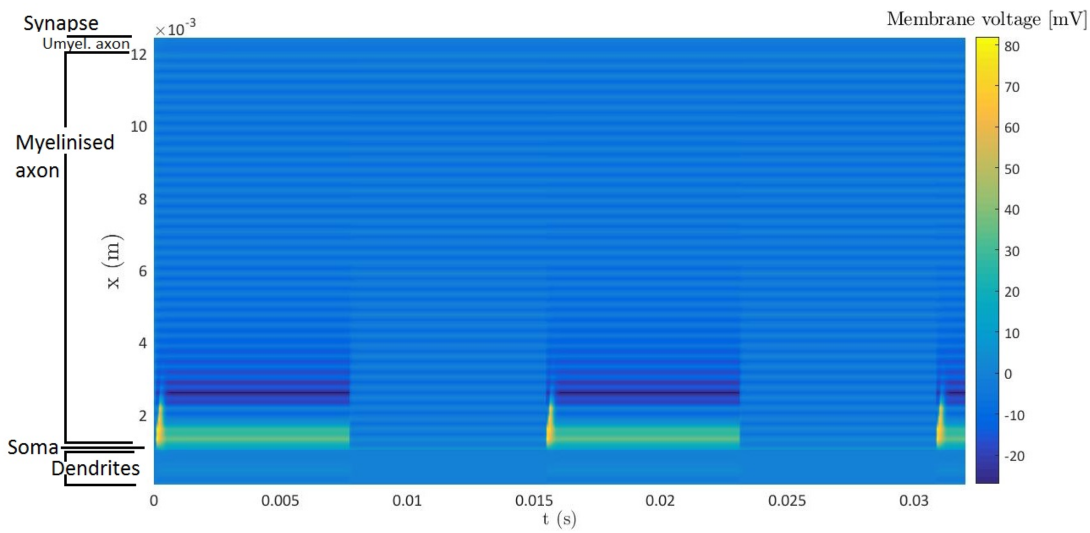

Figure 7.9: Neuron 76 in the macaca fascicularis in 01xx-stimulation. This is a representation of a neuron on which an actionpotential is initiated. Nevertheless the actionpotential has not reached the synapse. The simulation time extends over two periods of the biphasic square-wave stimulus.

Conclusions

The electric field distribution excited by a Medtronic DBS-lead (Mo. 3389, Medtronic Inc., Minneapolis, MN, USA) was simulated in the MIDA-head phantom in Sim4life (Sim4life, ZMT Zurich MedTech AG) for two types of electrode stimulation ($01xx$- and $10xx$-stimulation). For a typical biphasic square-wave with pulse width of $60\mu s$ and frequency of $65Hz$ a relevant frequency range for the simulations was determined by calculation of the fourierspectrum. This frequency range is from $10Hz$ to $100kHz$ for deep brain stimulation, as can be seen in figure 1.5. A total number of 82 FEM simulations were done in this frequency range and the electric field distribution was recognized to be roughly independent of frequency (figure 1.8 and figure 1.9). An approximation of the electric field distribution in the MIDA-head excited by a biphasic square-wave can thus be obtained by calculating the frequency response at a single frequency.

The obtained electric field distribution was subsequently used to determine the neuronal response. For this end a multi-compartmental neuron model was programmed in Matlab (MATLAB 8.6, The MathWorks Inc., Natick, MA, 2000): the neuron is segmentated into compartments described by specialised neuronal models, discussed in section 2, and the corresponding differential equations are discretised and iterated.

The Matlab code was first validated by comparison of results with literature (section 3.3). Subsequently some simple single neuron simulations were done, in which the electric field was excited by a spherical electrode in a homogeneous medium. Both anode-make and cathode-make stimulation were studied and it was observed that stimulation occurs at the (virtual) cathode(s), corresponding with literature (Roth et al.; 1993 [15]). Furthermore comparing the stimulation of straight neurons and bent neurons shows that neuronal bendings play an important role in stimulation. The activation mechanisms at neuronal bendings and terminations were discussed in section 5. The Matlab code was furthermore programmed to determine if neuronal activation has occurred and to calculate the mean speed of propagation ($MSOA$) of the activation pulse.

Finally stimulation of bundles of multiple neurons was studied. In section 6 the influence of the electrode-bundle distance on the $\%AN$ was simulated for a straight bundle consisting of 19 neurons. Subsequently in section 7 a more realistic simulation was done. Neuronal activation was simulated for a deep brain stimulation configuration. A medtronic DBS-lead was modelled in Sim4life in the MIDA-head phantom (Iacono et al.;2015) [11]. A biphasic square-wave potential was applied on the zeroth and first electrode of the DBS-lead resulting in two stimulation configurations ($01xx$ and $10xx$ stimulation). The neuronal activation and synapse activation in two types of bundles often targeted in deep brain stimulation (the lenticular fasciculus and macaca fascicularis) was studied. For this end both types of neuron bundles were approximated by randomly distributed straight neurons. We concluded that the neuronal activation is influenced by the DBS-lead stimulation configuration. Furthermore not all activated neurons will experience activation at the synapse. We observed that a region of hyperpolarisation on the neuron might impede the propagation of the action potential towards the synapse.

Part IV

Appendices

Appendix A

Additional simulation results on a single neuron

In this appendix some additional simulations on single neurons are first presented. In section A.1 we consider the membrane-voltage and gate-parameters of a neuron at rest. Next, AM-stimulation of a single neuron by a spherical electrode at $2mm$ from the soma for an electrode-potential at $10V$ and at $40V$ is discussed in section A.2 and section A.3 respectively. The results from these two sections are to be compared with AM-stimulation at $60V$, discussed in subsection 4.1.2.

Next, we briefly present some additional results for the n-gate and h-gate parameters for simulations that were discussed in the thesis. These results are mentioned in this appendix for completeness. For the simulations on a straight neuron, sections A.4, A.5, A.6 expand the results presented in subsections 4.1.3, 4.1.4, 4.1.5 respectively. For the neuron with a bending, sections A.7 and A.8 present additional results for the subsections 4.2.1 and 4.2.2 respectively.

A.1 Single multi-compartmental neuron at rest

In this section we consider a neuron at rest, i.e. no electrode is placed in its neighbourhood. This simulation is interesting, because it will allow us to recognize neurons in a bundle on which the stimulus-electrode has little effect. First, the activation function f is shown in figure A.1. Ofcourse, because no electrode is present, the activation function is identically zero.

	Activated	Synapse activated	nr.	pos. (mm)	time (ms)	MSOAf (m/s)	MSOAb (m/s)
Neuron at rest	no	no	-	-	-	-	-

Table A.1: Activation table for a straight neuron at rest.

More interesting is the spatial distribution of the reduced membrane voltage $\tilde{V}$, in figure A.2

and in figure A.3. The distribution of the reduced membrane voltage looks remarkably discontinuous. This result might be surprising at first, but can be explained by the fact that we considered a multi-compartmental neuron. Different compartments will have a different value for the rest-voltage V_r. For instance, the nodes of Ranvier and the initial segment were described by a CRRSS-model, and have as rest-voltage: $V_r^{CRRSS} = -80V$. In contrast, the synapse, soma and unmyelinated axonterminal are described by a warm Hodgkin-Huxley model, for which we have: $V_r^{HH} = -70V$. Furthermore the rest-potential V_r is defined for a uniform neuron, consisting of one compartment, at rest. However for a general multi-compartmental neuron at rest the membrane voltage will not be equal to the rest-potential. This explains why the reduced membrane voltage is not identically zero. For this case of a multi-compartmental neuron, a distinction can thus be made between the rest-voltage distribution $V_r(x)$ and the final voltage distribution $V_f(x)$. The value $V_r(x)$ will give the rest-voltage of the compartment at x. For a uniform neuron at rest made of this compartment, the voltage will everywhere be equal to the single value $V_r(x)$. The final voltage distribution $V_f(x)$ represents the non-reduced membrane voltage (NRMV; $V = V_i - V_e$) distribution on a multi-compartmental neuron at rest.

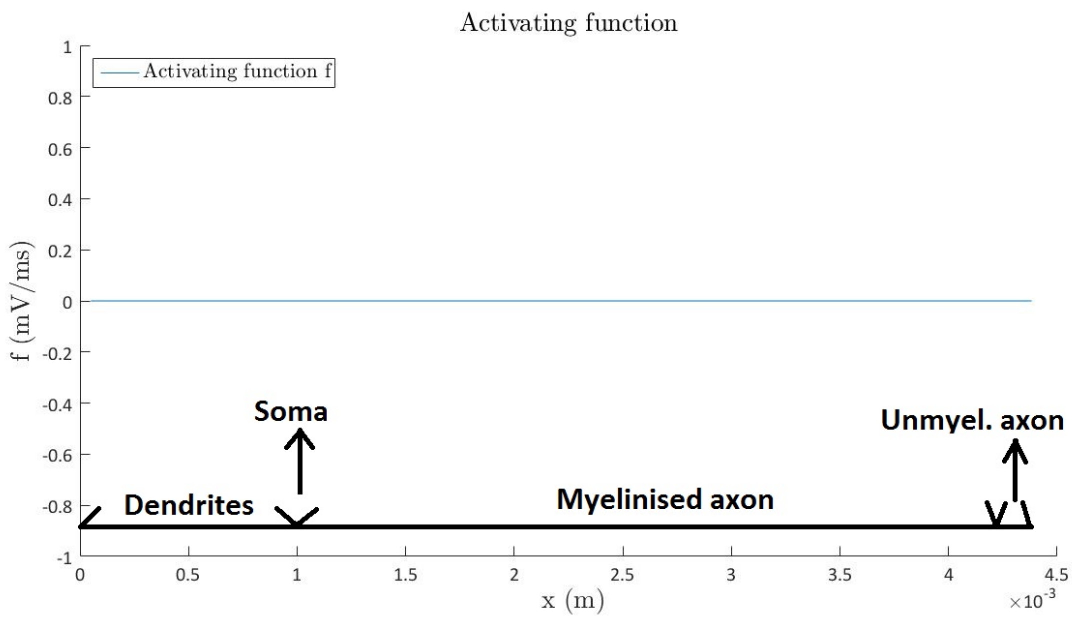

Figure A.1: Neuron at rest. Spatial distribution of the activation function f is shown.

We expect, for physical reasons, that the final voltage $V_f(x)$ will be continuous. This is indeed the case, as shown in figure A.4 and in figure A.5. We observe that at the dendrites and unmyelinated axonterminal the voltage V will be equal to $-70V$, which is the rest-voltage in the Hodgkin-Huxley and passive model. On the axon, the membrane voltage takes a value between $-70V$ and $-80V$, which is expected since the nodes of Ranvier have a rest-potential of $-80V$ and the myelinated internodes of $-70V$.

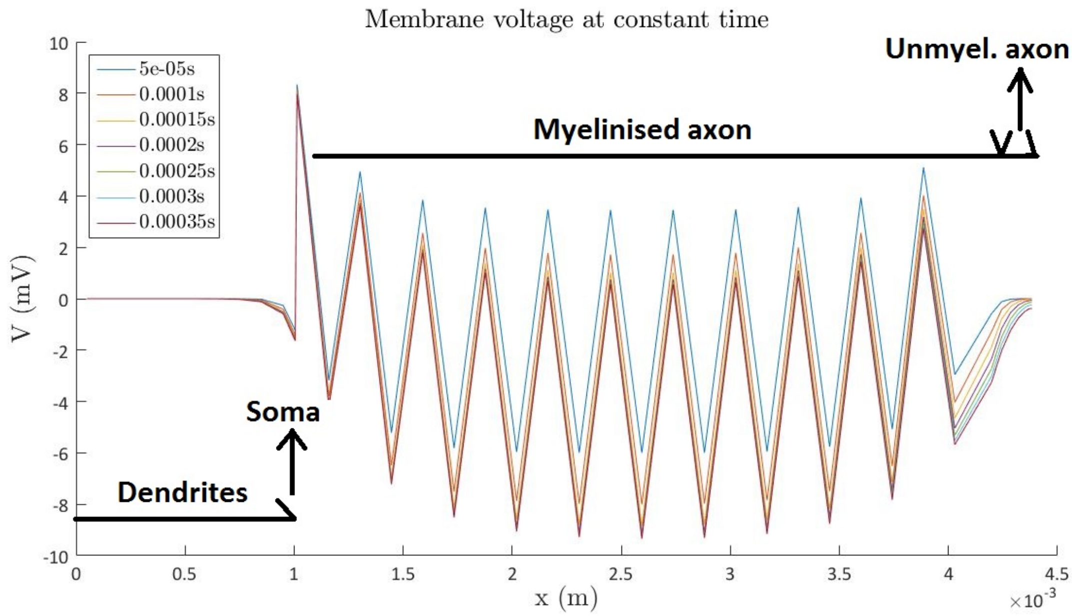

Figure A.2: Neuron at rest. Spatial distribution of the reduced membrane voltage $\tilde{V}$ at 7 subsequent times is shown.

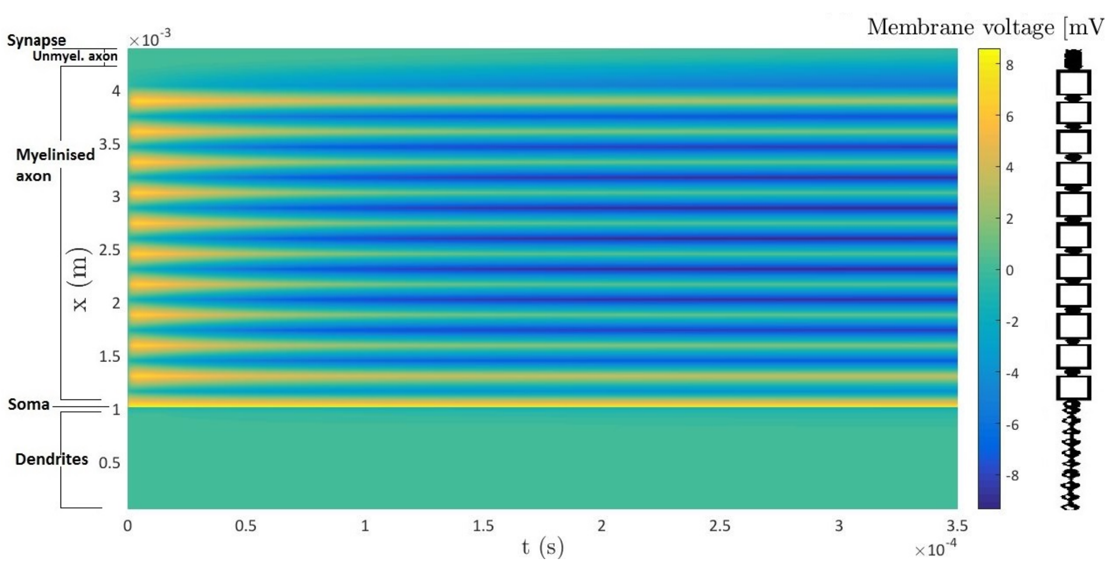

Figure A.3: Colour map of the reduced membrane voltage in time and space. The colours represent the value of $\tilde{V}$. The map is obtained for a neuron at rest.

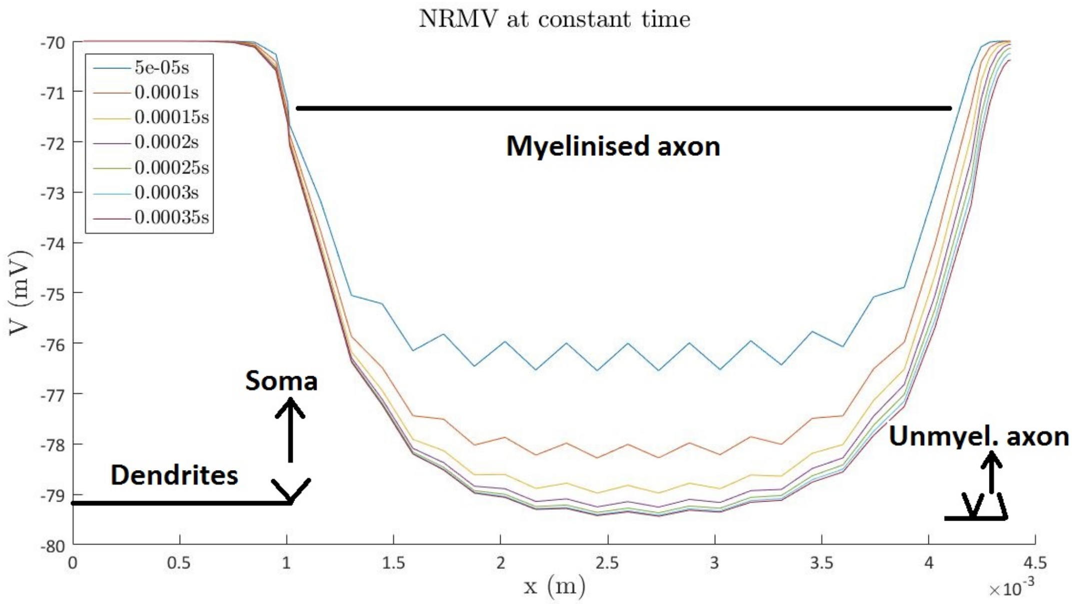

Figure A.4: Neuron at rest. Spatial distribution of the non-reduced membrane voltage (NRMV) $\tilde{V}$ at 7 subsequent times is shown.

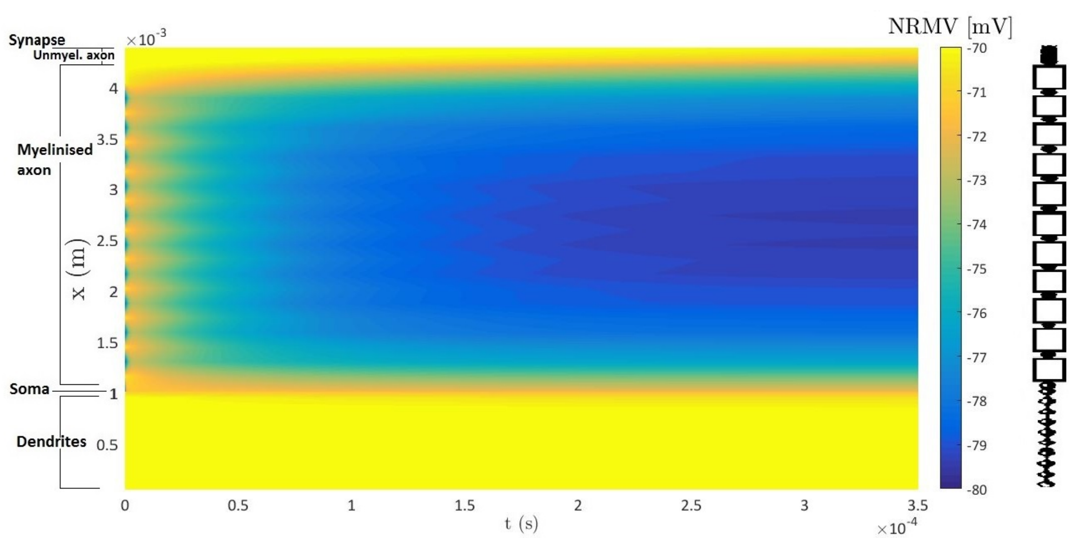

Figure A.5: Colour map of the non-reduced membrane voltage (NRMV) in time and space. The colours represent the value of V. The map is obtained for a neuron at rest.

We recognize that there is some time-dependency in the colour maps. Ofcourse, this time-dependency is unphysical, because the neuron should be at rest. The time-dependency is a consequence of the fact that Matlab needs to initialize the membrane voltage at $t = 0$. The most obvious way to do this, because the final voltage is not known, is by initialising the membrane voltage by the rest-voltage $V(x, t = 0) = V_r(x)$. However, as explained, for a multi-compartmental neuron the rest-potential will not be equal to the final membrane voltage. The plots thus show how the membrane-voltage evolves from $V(x, t = 0) = V_r(x)$ to the final voltage $V_f(x)$.

We now also understand why the reduced membrane voltage $\tilde{V}$ is discontinuous. The final voltage $V_f(x)$ is continuous, but the rest-potential distribution V_r is discontinuous, so we obtain a discontinuous reduced membrane voltage for a neuron at rest: $\tilde{V}|_{t=\infty} = V_f(x) - V_r$.

Finally the gate-parameters are shown in figures A.6, A.7 and A.8. The activation table is shown in table A.1. As expected, no action potential is initiated. The gate-parameters are close to their rest-values, for instance on the unmyelinated axon terminal a Hodgkin-Huxley model is applied. The rest-values of the gate-parameters in this model are (Rattay, 2005 [12]):

$$m_0^{HH} = 0.05$$

$$n_0^{HH} = 0.32$$

$$h_0^{HH} = 0.6$$

These theoretical values correspond well with the values obtained in the colour maps. Analogously also the rest-values for the gate-parameters in the CRRSS-model that describes the nodes of Ranvier, correspond well with the obtained results.

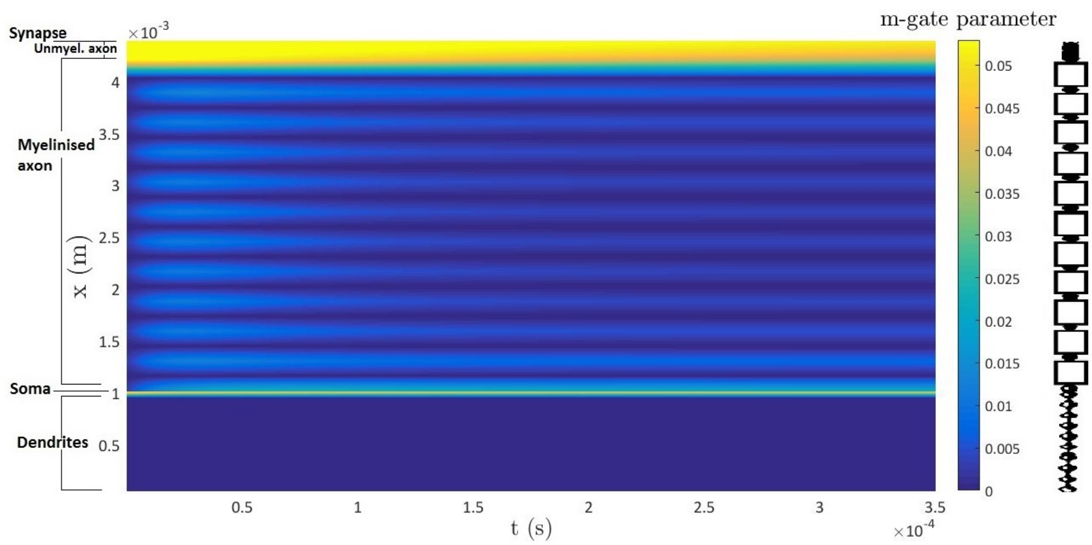

Figure A.6: Colour map of the m-gate parameter in time and space. The colours represent the value of m. The map is obtained for a neuron at rest.

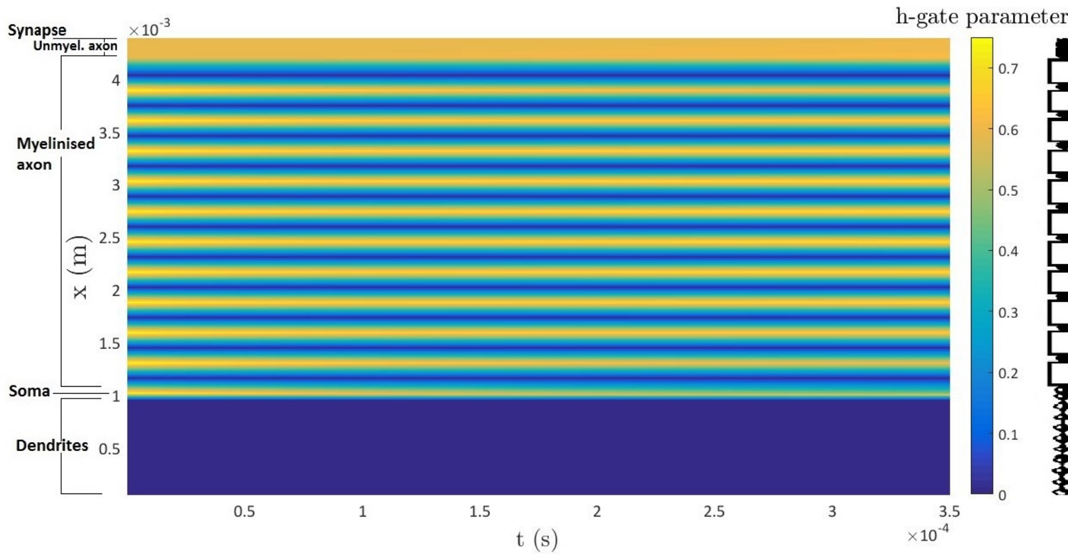

Figure A.7: Colour map of the h-gate parameter in time and space. The colours represent the value of h. The map is obtained for a neuron at rest.

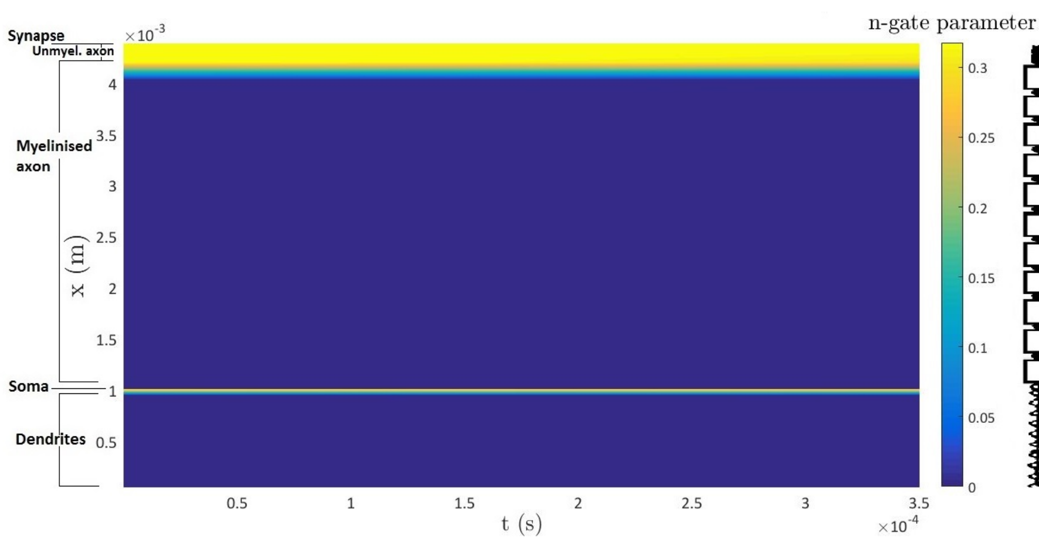

Figure A.8: Colour map of the n-gate parameter in time and space. The colours represent the value of n. The map is obtained for a neuron at rest.

A.2 Anode-make stimulation by spherical electrode (10 V) at 2 mm from soma

In this section we discuss AM-stimulation by a spherical electrode ($10V$) at $2mm$ from the soma. This simulation is to be compared with the simulation of next section (section A.3), where the electrode-potential is put at $40V$, and with the simulation of subsection 4.7, where the electrode-potential is $60V$.

	Activated	Synapse activated	nr.	pos. (mm)	time (ms)	MSOAf (m/s)	MSOAb (m/s)
Config 1: anode-make (10 V)	no	no	-	-	-	-	-

Table A.2: Activation table for a straight neuron, stimulated by a spherical electrode ($10V$) at 2 mm from the soma.

Together, the three mentioned simulations show us the influence of the electrode-potential on the membrane-voltage and gate-parameters. In this section the electrode-potential is only $10V$ and the neuron will not be activated (see table A.2). The shape of the distribution of the activation function f does not depend on the applied electrode-potential because of linearity (figure A.9). However, f scales linearly with V_{elec}, and is too low in this simulation to initiate an actionpotential.

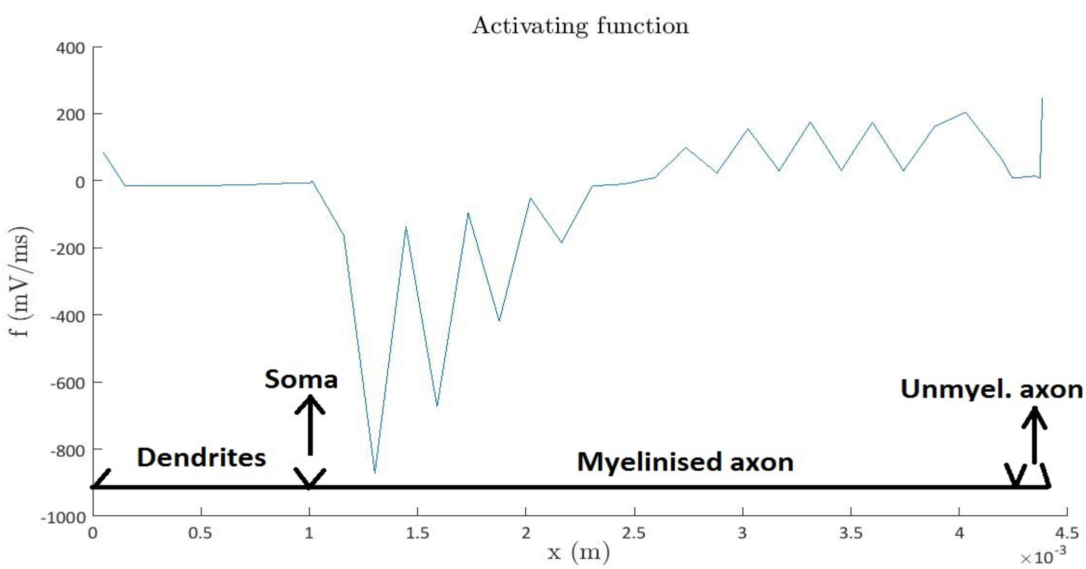

Figure A.9: Spherical electrode ($10V$) at $2mm$ from the soma. Spatial distribution of the activation function f is shown.

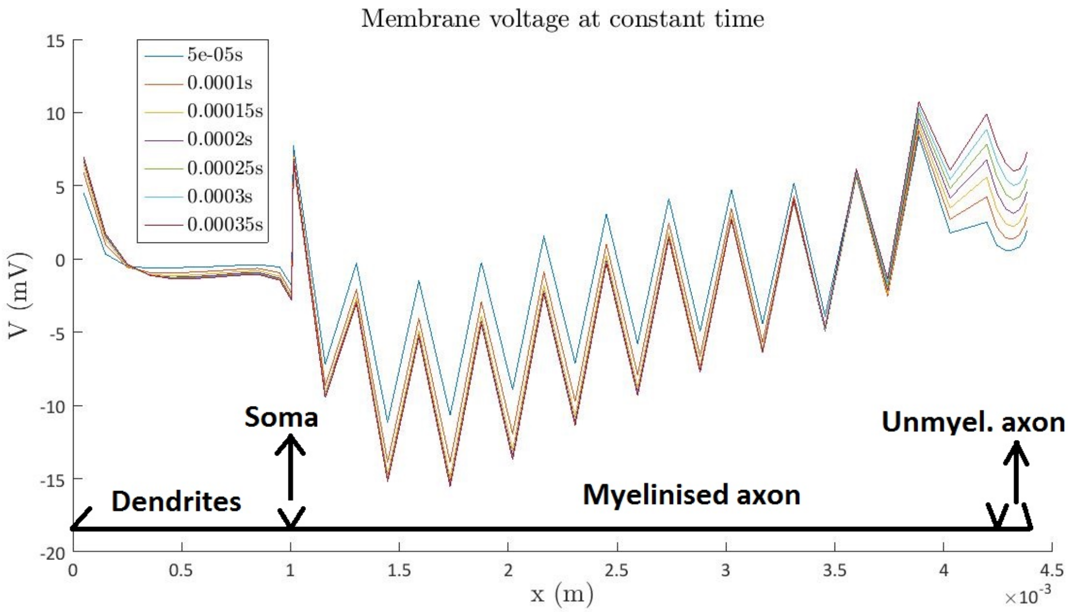

Figure A.10: Spherical electrode ($10V$) at $2mm$ from the soma. Spatial distribution of the reduced membrane voltage $\tilde{V}$ at 7 subsequent times is shown.

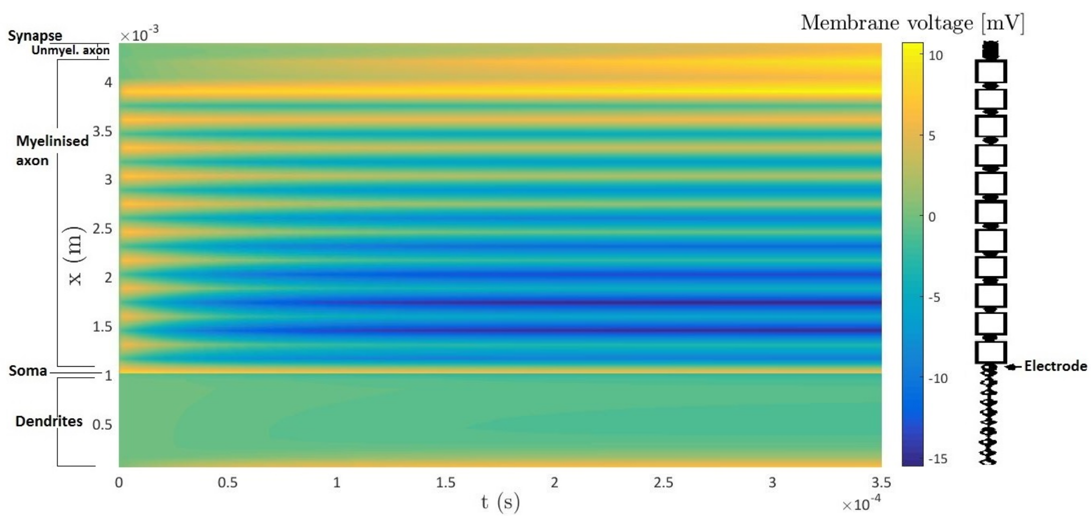

Figure A.11: Colour map of the reduced membrane voltage in time and space. The colours represent the value of $\tilde{V}$. The map is obtained by anode-make stimulation by a spherical electrode (10V) at 2mm from the soma of a straight neuron.

The reduced membrane voltage is shown in figures A.10 and A.11. As was observed in section A.1, some depolarisation and hyperpolarisation will always be present in a multi-compartmental neuron, even when the neuron is at rest. This is because a multi-compartmental neuron is not homogeneous. We see from the voltage maps that stimulation by an electrode at $10V$, will not result in the propagation of an actionpotential. Nevertheless some small polarization over about $10V$ does occur.

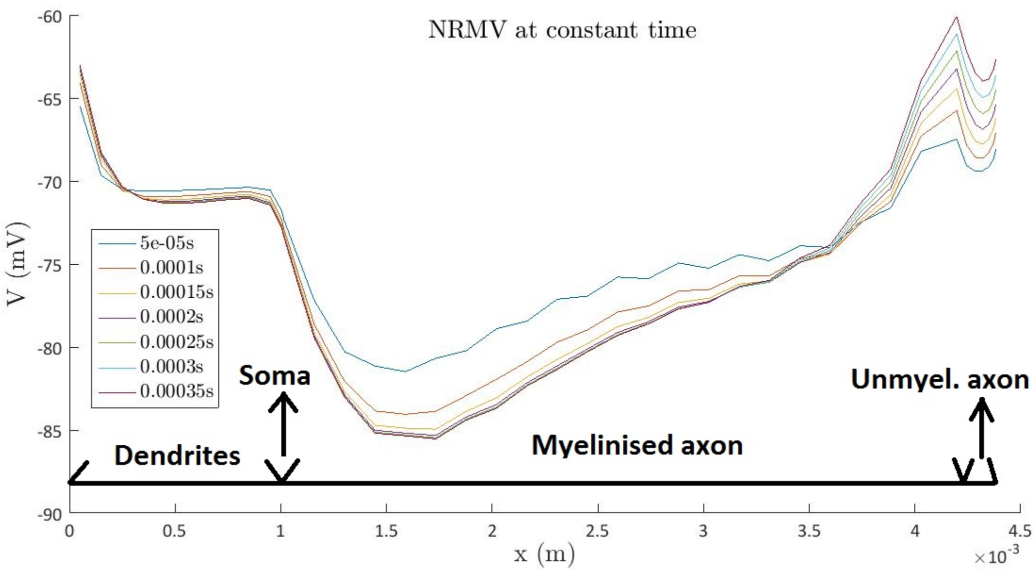

Figure A.12: Spherical electrode ($10V$) at $2mm$ from the soma. Spatial distribution of the non-reduced membrane voltage V (NRMV) at 7 subsequent times is shown.

For this (not activated) neuron, it is interesting to also consider the non-reduced membrane voltage V (figure A.12 and figure A.13). The non-reduced membrane voltage has a continuous spatial distribution, unlike the reduced membrane voltage. When we compare with the results for the neuron at rest (figure A.4 and figure A.5), we observe that the electrode has caused some small polarization, additional to the polarization that was already present in the neuron at rest.

The gate-parameters are shown in figures A.14, A.16 and A.15. There is some deviation from the rest-values of the gate-parameters. Nevertheless no actionpotential is observed in these colourplots.

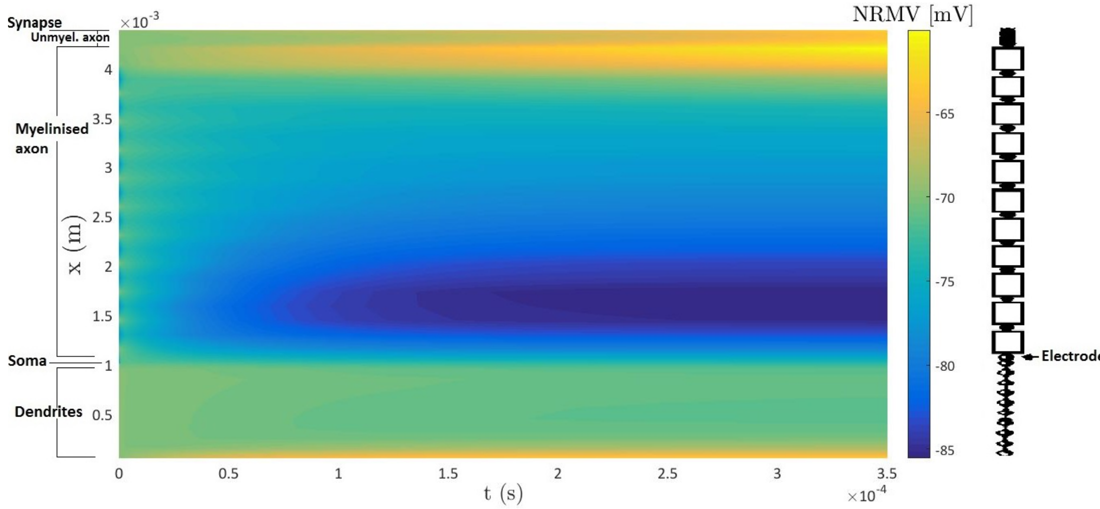

Figure A.13: Colour map of the non-reduced membrane voltage (NRMV) in time and space. The colours represent the value of V. The map is obtained by anode-make stimulation by a spherical electrode (10V) at 2mm from the soma of a straight neuron.

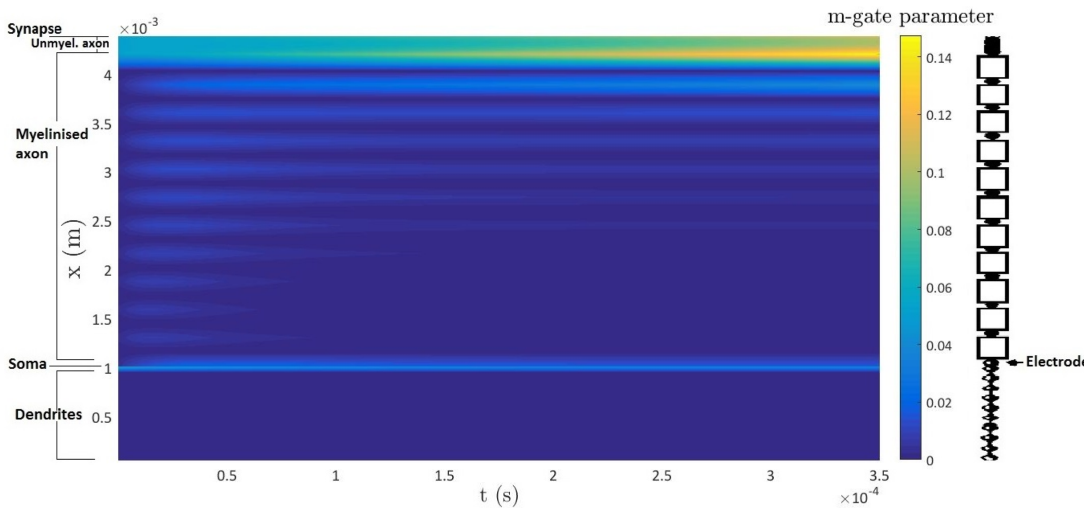

Figure A.14: Colour map of the m-gate parameter in time and space. The colours represent the value of m. The map is obtained by anode-make stimulation by a spherical electrode (10V) at 2mm from the soma of a straight neuron.

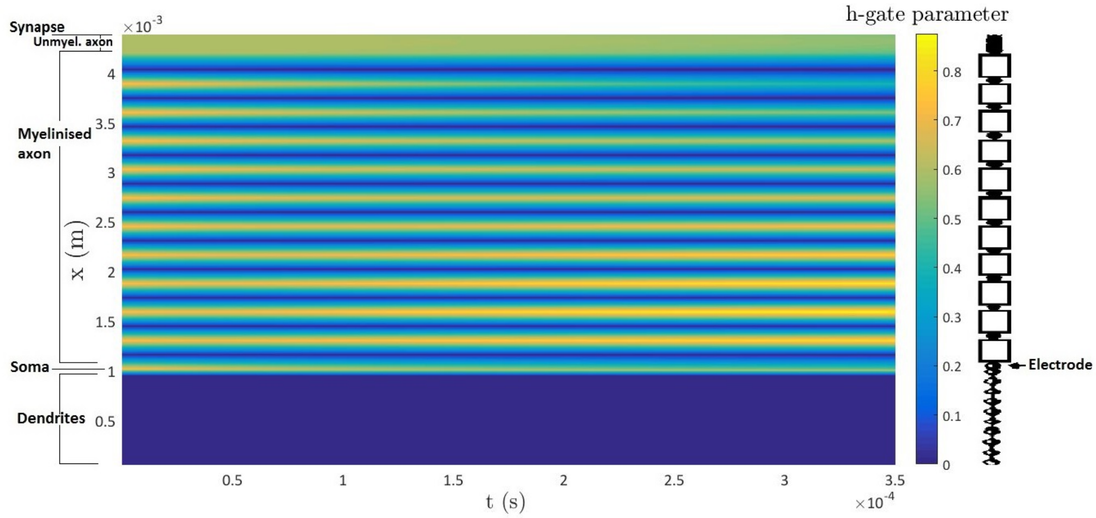

Figure A.15: Colour map of the h-gate parameter in time and space. The colours represent the value of h. The map is obtained by anode-make stimulation by a spherical electrode (10V) at 2mm from the soma of a straight neuron.

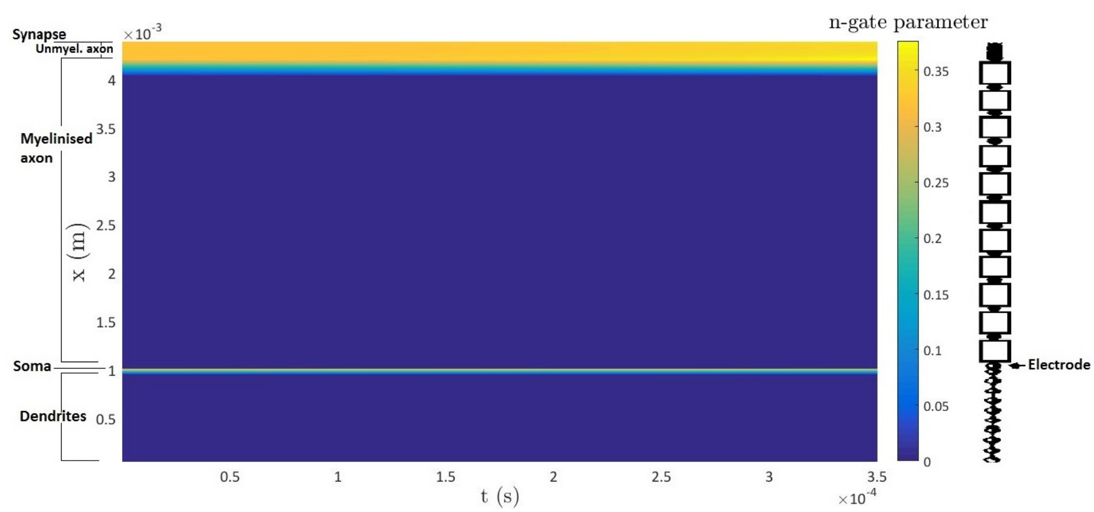

Figure A.16: Colour map of the n-gate parameter in time and space. The colours represent the value of n. The map is obtained by anode-make stimulation by a spherical electrode (10V) at 2mm from the soma of a straight neuron.

A.3 Anode-make stimulation by spherical electrode (40 V) at $2mm$ from soma

In this section, AM-stimulation by a spherical electrode at $40V$ at $2mm$ from the soma is discussed. In section A.2 and subsection 4.1.2, we discussed the same configuration, but at different electrode-potential ($10V$ and $60V$ respectively). In this section the neuron will be activated (table A.3), in contrast with section A.2 (electrode-potential at $10V$). Comparing with the results of subsection 4.1.2 shows that increasing the electrode-potential will not alter the shape of the spatial distribution of the membrane voltage, neither will it increase the strenght of depolarisation (an all-or-nothing principle applies for the generation of an actionpotential). Instead, a higher electrode-potential will lead to faster activation of the neuron.

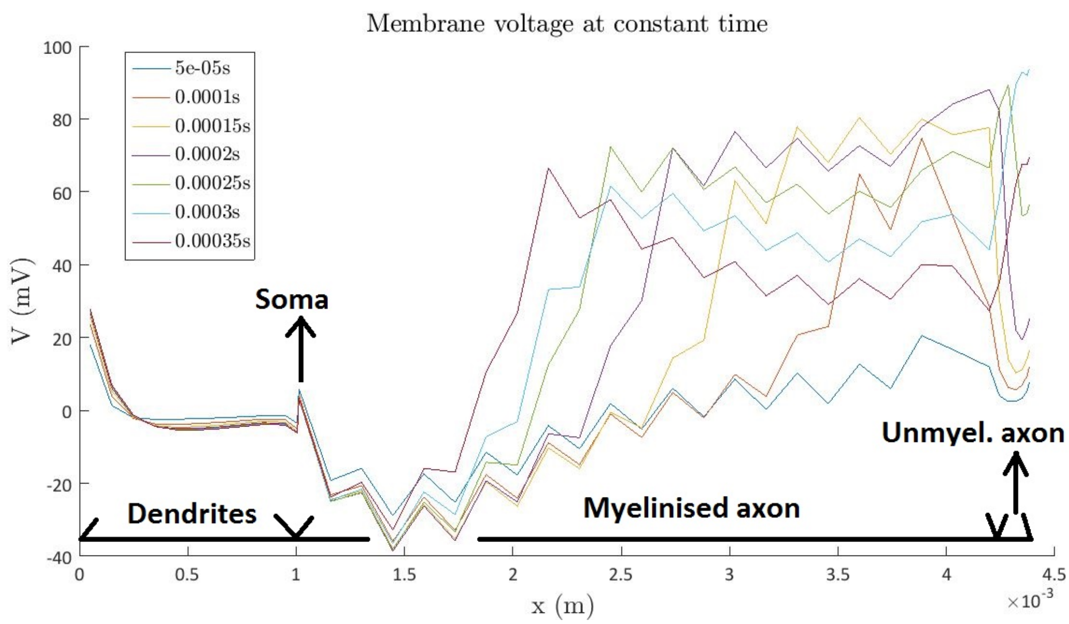

Figure A.17: Spherical electrode ($40V$) at $2mm$ from the soma. Spatial distribution of the reduced membrane voltage $\tilde{V}$ at 7 subsequent times is shown.

The reduced membrane voltage is shown in figures A.17 and A.18. We indeed observe that the neuron is activated. The activation function f is shown in figure A.19. Next, the gate-parameters are shown in figures A.20, A.22, A.21. For a discussion of the results, we refer to section 4.1.2.

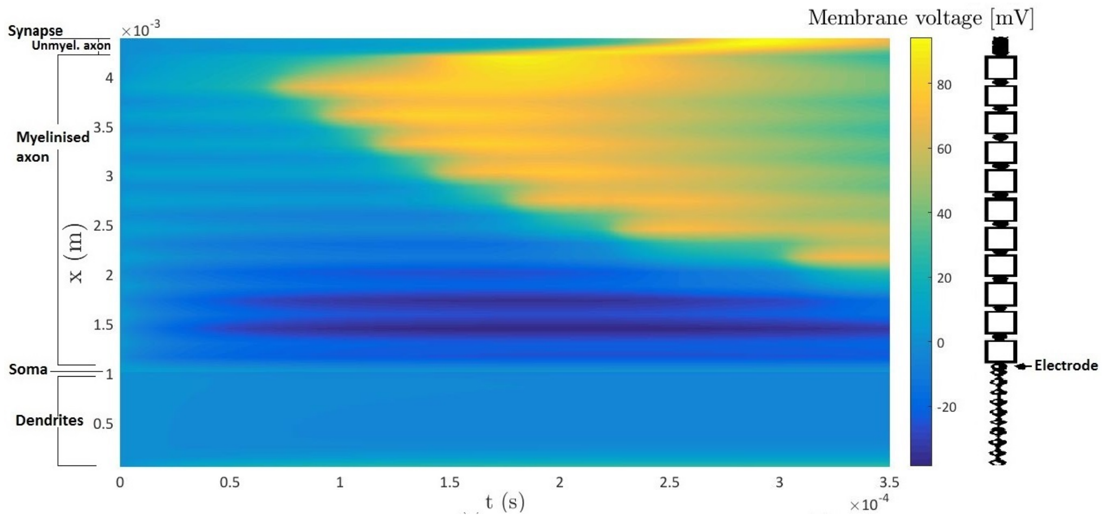

Figure A.18: Colour map of the reduced membrane voltage in time and space. The colours represent the value of $\tilde{V}$. The map is obtained by anode-make stimulation by a spherical electrode (40V) at 2mm from the soma of a straight neuron.

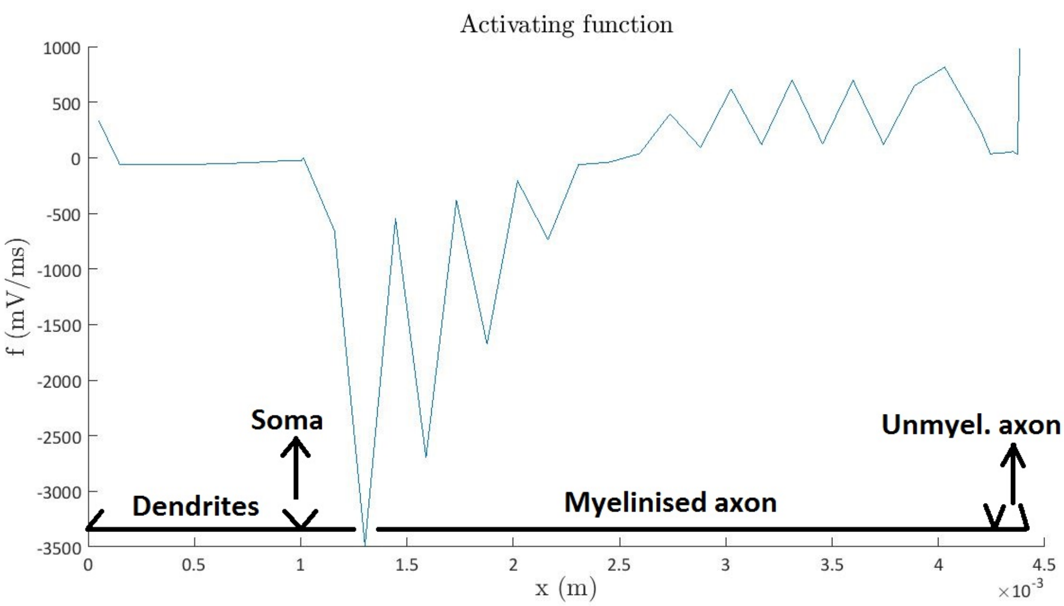

Figure A.19: Spherical electrode ($40V$) at $2mm$ from the soma. Spatial distribution of the activation function f is shown.

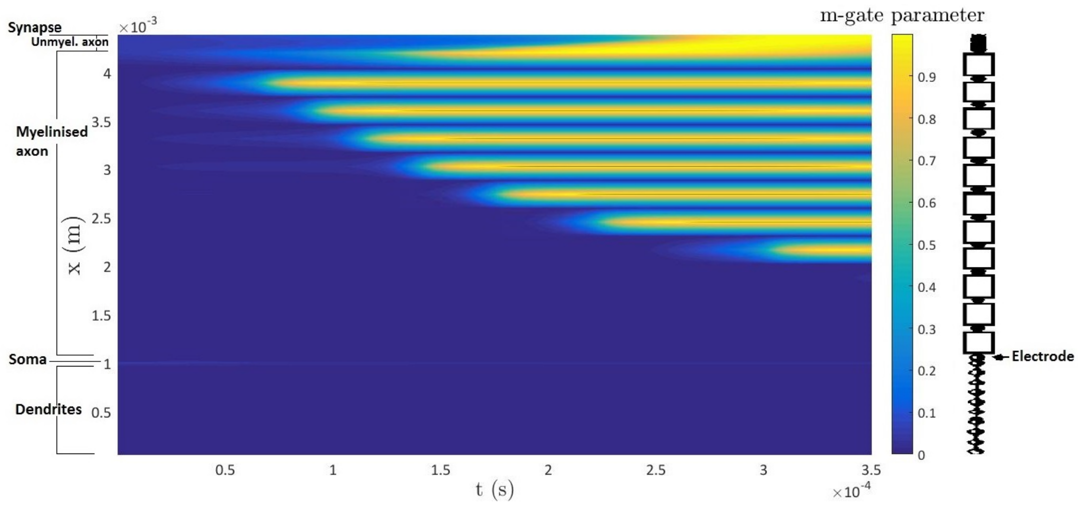

Figure A.20: Colour map of the m-gate parameter in time and space. The colours represent the value of m. The map is obtained by anode-make stimulation by a spherical electrode (40V) at 2mm from the soma of a straight neuron.

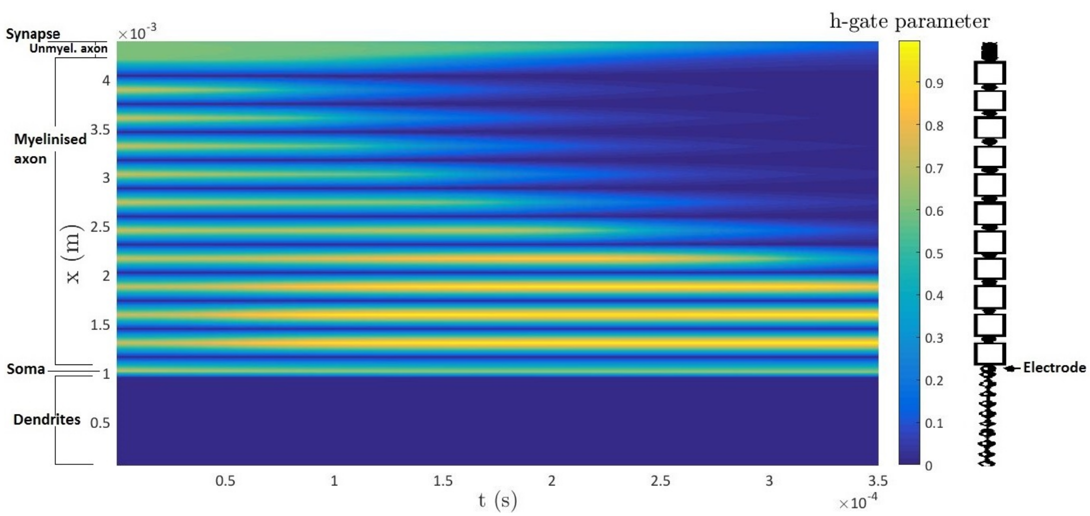

Figure A.21: Colour map of the h-gate parameter in time and space. The colours represent the value of h. The map is obtained by anode-make stimulation by a spherical electrode (40V) at 2mm from the soma of a straight neuron.

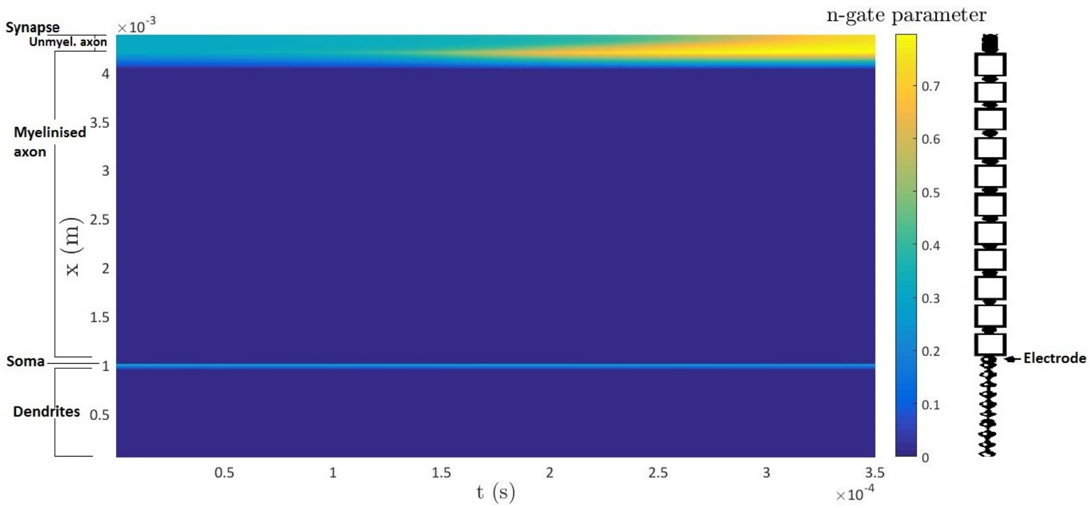

Figure A.22: Colour map of the n-gate parameter in time and space. The colours represent the value of n. The map is obtained by anode-make stimulation by a spherical electrode (40V) at 2mm from the soma of a straight neuron.

	Activated	Synapse activated	nr.	pos. (mm)	time (ms)	MSOAf (m/s)	MSOAb (m/s)
Config 1: anode-make (40 V)	yes	yes	1.	3.5985	0.1403	5.0124	7.5846

Table A.3: Activation table for a straight neuron, stimulated by a spherical electrode ($40V$) at 2 mm from the soma.

A.4 Additional results for simulation 3. Anode-make stimulation of voltage-clamped neuron by spherical electrode (60 V) at 2 mm from soma

In this section we expand on the results presented in subsection 4.1.3 for completeness. AM-stimulation of a voltage-clamped neuron by a spherical electrode ($60V$) at $2mm$ from the soma is considered. The colour maps for the h-gate parameter and n-gate parameter are shown in figure A.23 and figure A.24 respectively.

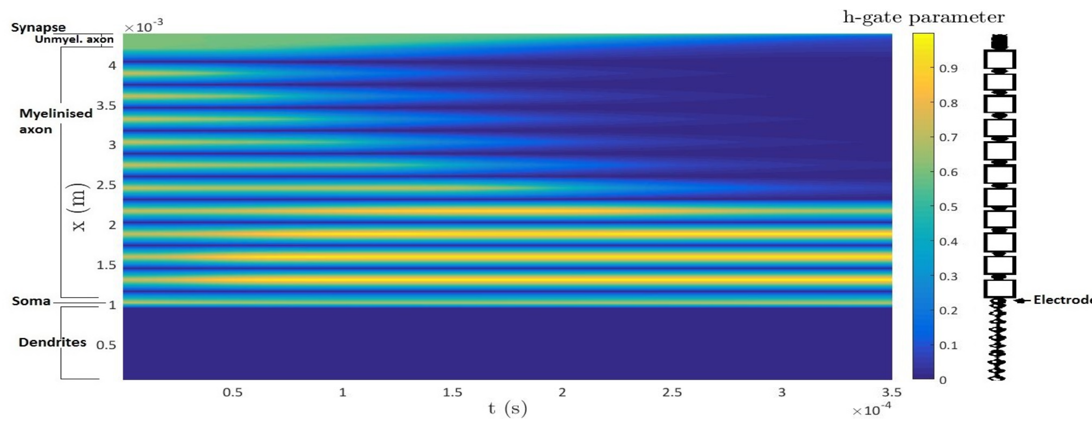

Figure A.23: Colour map of the h-gate parameter in time and space. The colours represent the value of h. The map is obtained by anode-make stimulation by a spherical electrode (60V) at 2mm from the soma of a straight, voltage clamped, neuron.

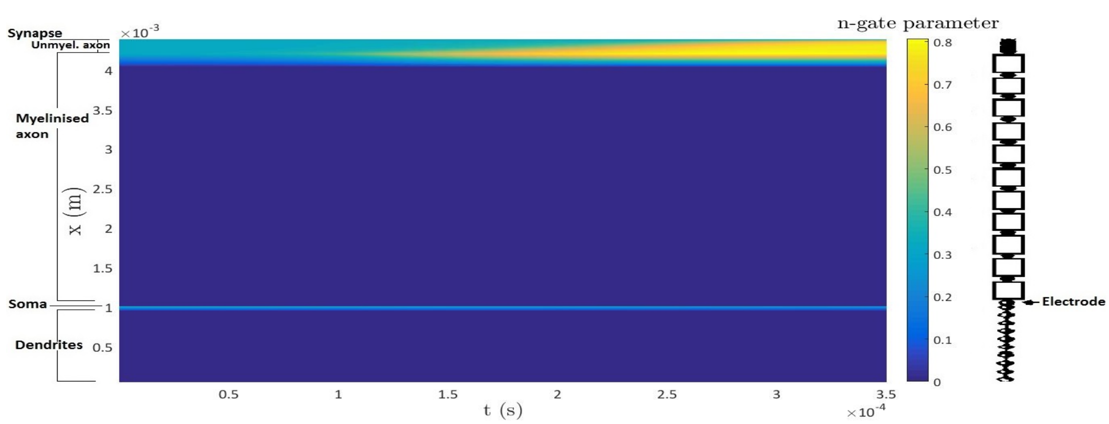

Figure A.24: Colour map of the n-gate parameter in time and space. The colours represent the value of n. The map is obtained by anode-make stimulation by a spherical electrode (60V) at 2mm from the soma of a straight, voltage clamped, neuron.

We compare the temporal distribution at the synapse of the h-gate parameter and n-gate parameter for sealed-end boundary conditions and voltage-clamped boundary conditions in figures A.25 and A.26.

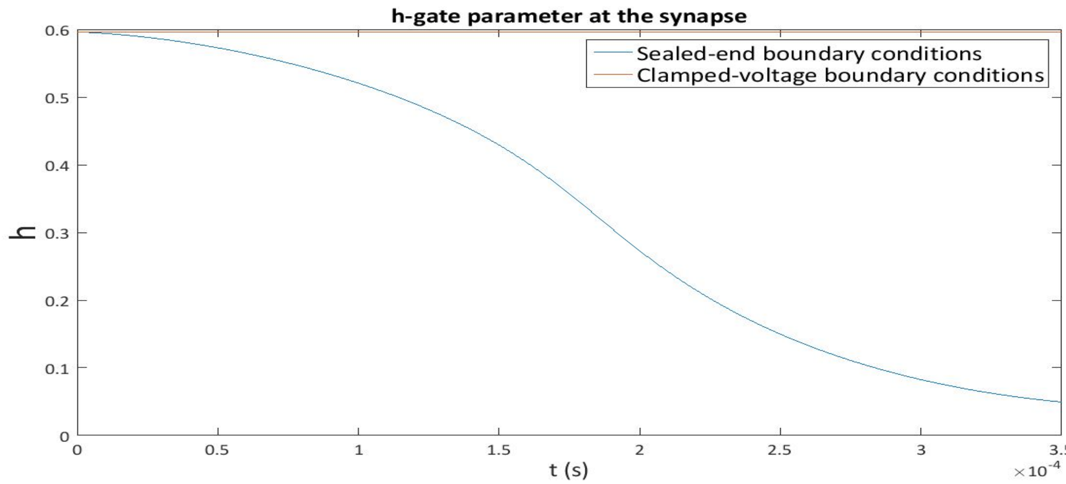

Figure A.25: h-gate parameter as function of time at the synapse for sealed-end conditions and voltage-clamped conditions

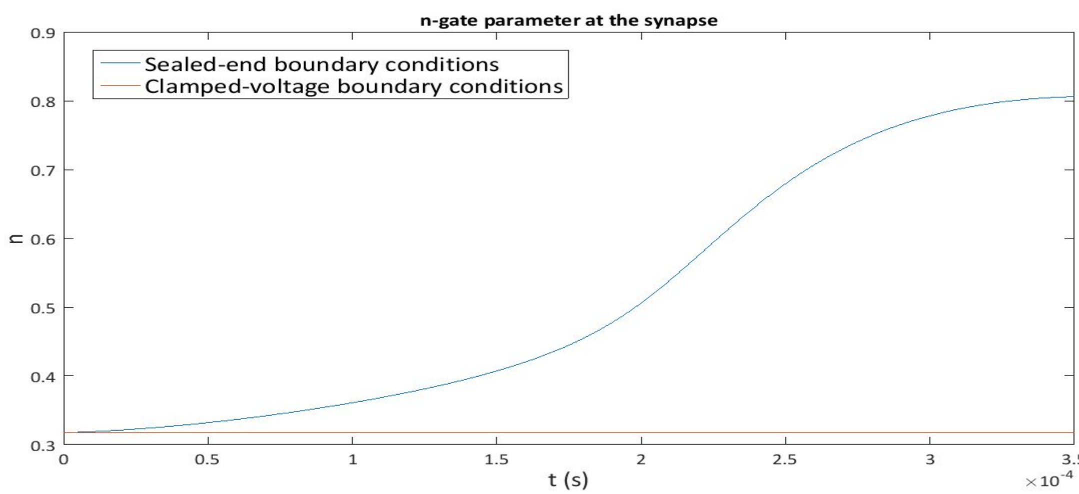

Figure A.26: n-gate parameter as function of time at the synapse for sealed-end conditions and voltage-clamped conditions

A.5 Additional results for simulation 4. Cathode-make stimulation by spherical electrode (-60V) at 2 mm from soma

In this section we expand on the results presented in subsection 4.1.4 for completeness. CM-stimulation of a straight neuron by a spherical electrode $(-60V)$ at $2mm$ from the soma is considered. The colour maps for the h-gate parameter and n-gate parameter are shown in figure A.27 and figure A.28 respectively.

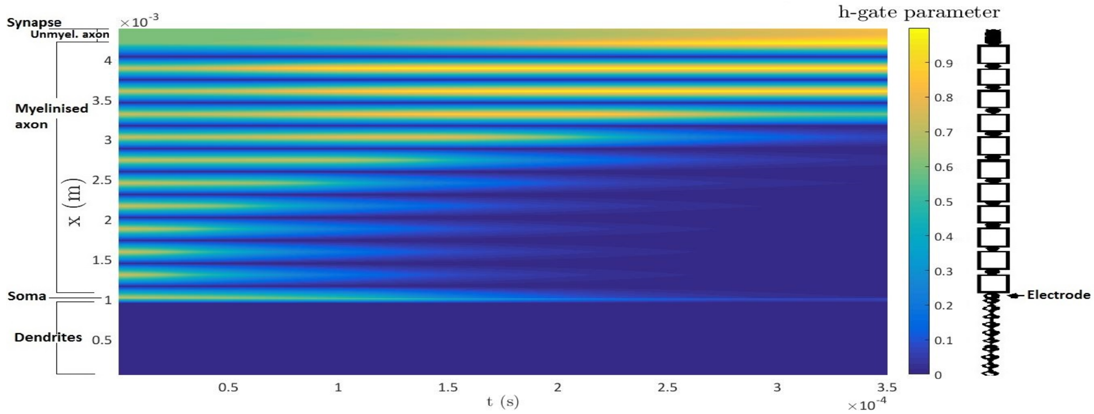

Figure A.27: Colour map of the h-gate parameter in time and space. The colours represent the value of h. The map is obtained by cathode-make stimulation by a spherical electrode (-60V) at 2mm from the soma of a straight neuron.

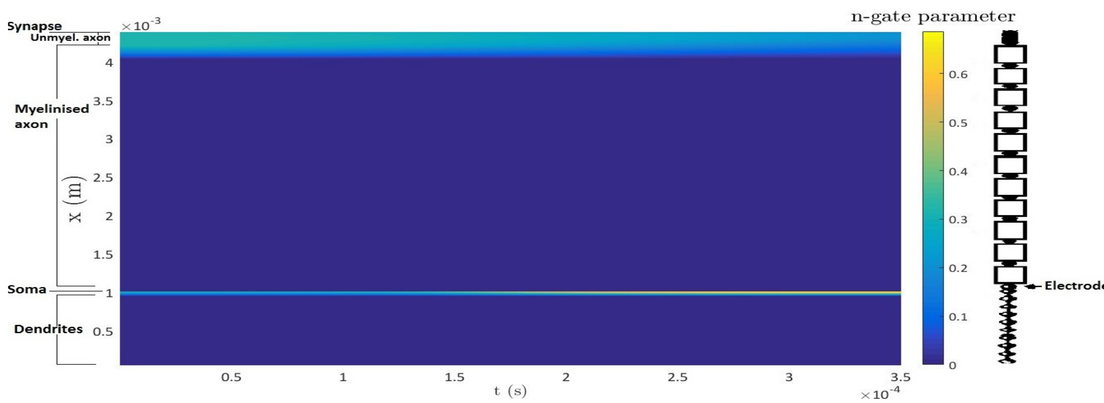

Figure A.28: Colour map of the n-gate parameter in time and space. The colours represent the value of n. The map is obtained by cathode-make stimulation by a spherical electrode (-60V) at 2mm from the soma of a straight neuron.

A.6 Additional results for simulation 5. Anode-make stimulation by spherical electrode (60V) at 2 mm from the centre of the neuron

In this section we expand on the results presented in subsection 4.1.5 for completeness. AM-stimulation by a spherical electrode ($60V$) at $2mm$ from the centre of the neuron is considered. The colour maps for the h-gate parameter and n-gate parameter are shown in figure A.29 and figure A.30 respectively.

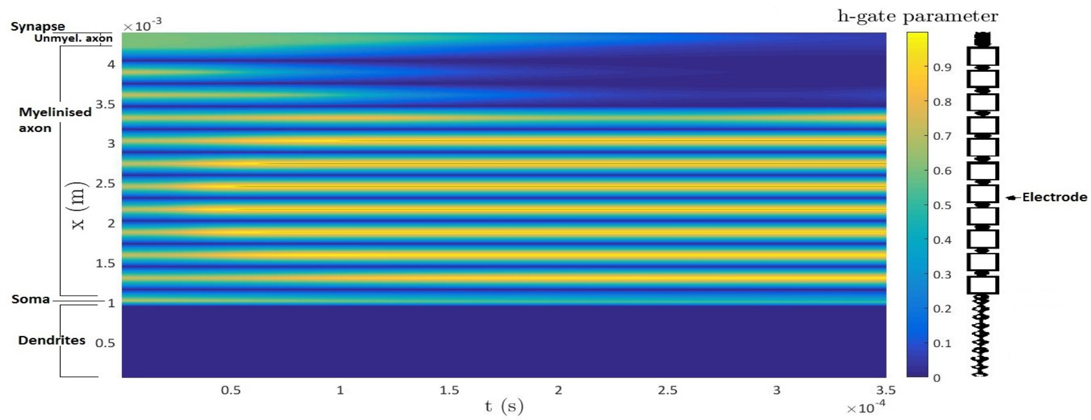

Figure A.29: Colour map of the h-gate parameter in time and space. The colours represent the value of h. The map is obtained by anode-make stimulation by a spherical electrode (60V) at 2mm from the centre of a straight neuron.

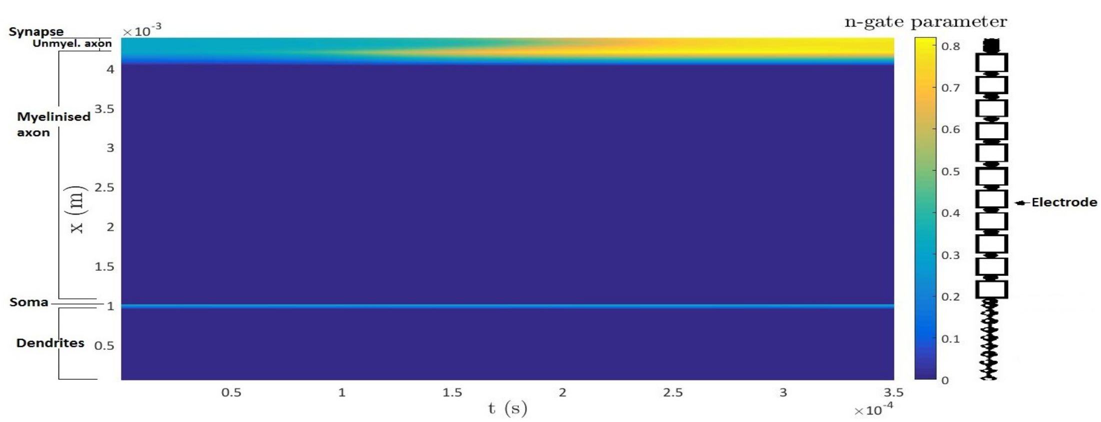

Figure A.30: Colour map of the n-gate parameter in time and space. The colours represent the value of n. The map is obtained by anode-make stimulation by a spherical electrode (60V) at 2mm from the centre of a straight neuron.

A.7 Additional results for simulation 6. Anode-make stimulation of neuron with central bending (15°) by spherical electrode (60 V) at 2 mm from soma

In this section we expand on the results presented in subsection 4.2.1 for completeness. AM-stimulation of a bend neuron (bending over 15°) by a spherical electrode ($60V$) at $2mm$ from the soma is considered. The colour maps for the h-gate parameter and n-gate parameter are shown in figure A.31 and figure A.32 respectively.

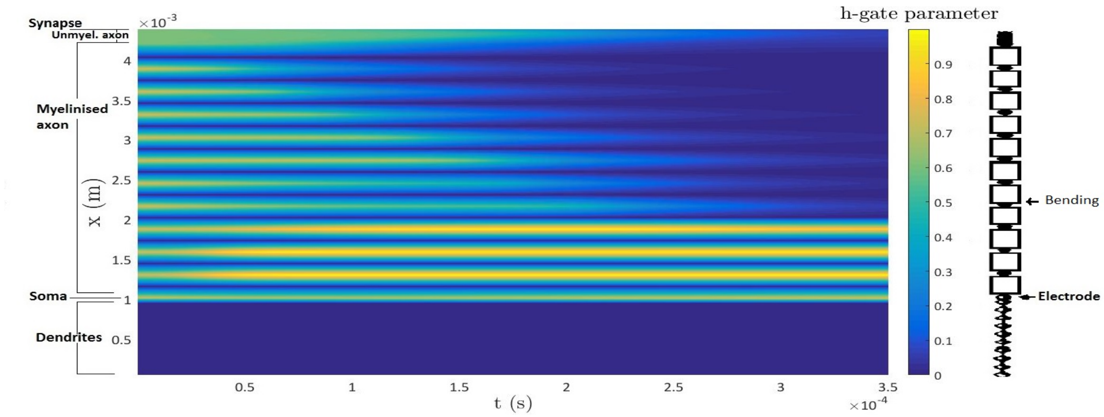

Figure A.31: Colour map of the h-gate parameter in time and space. The colours represent the value of h. The map is obtained by anode-make stimulation by a spherical electrode ($60V$) at $2mm$ from the soma of a bent ($15°$) neuron.

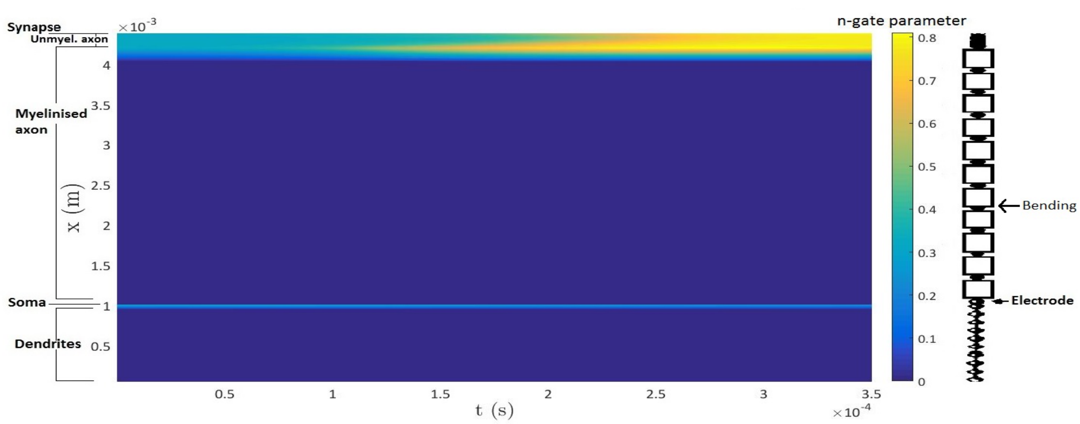

Figure A.32: Colour map of the n-gate parameter in time and space. The colours represent the value of n. The map is obtained by anode-make stimulation by a spherical electrode ($60V$) at $2mm$ from the soma of a bent ($15°$) neuron.

A.8 Additional results for simulation 7. Anode-make stimulation of neuron with central bending (15°) by spherical electrode at 2 mm from centre

In this section we expand on the results presented in subsection 4.2.2 for completeness. AM-stimulation of a bend neuron (bending over 15°) by a spherical electrode ($60V$) at $2mm$ from the centre of the neuron is considered. The colour maps for the h-gate parameter and n-gate parameter are shown in figure A.33 and figure A.34 respectively.

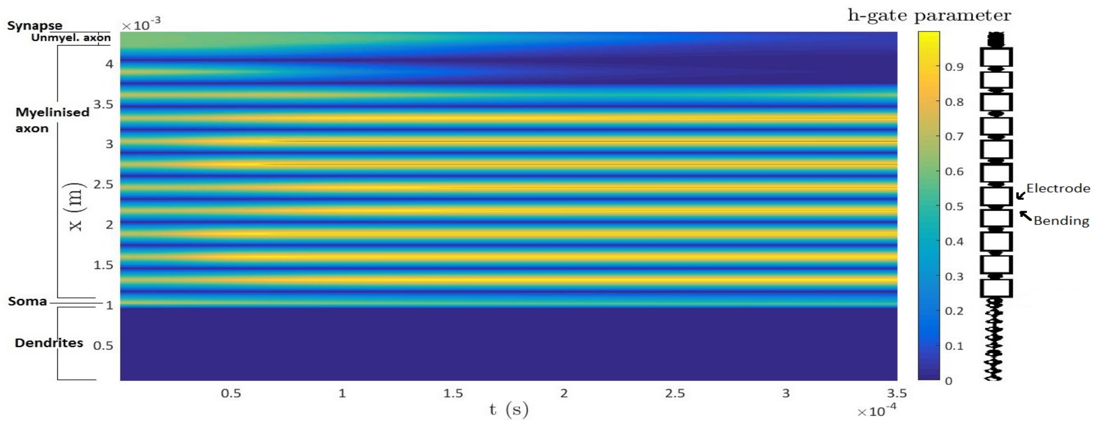

Figure A.33: Colour map of the h-gate parameter in time and space. The colours represent the value of h. The map is obtained by anode-make stimulation by a spherical electrode ($60V$) at $2mm$ from the centre of a bent (15°) neuron.

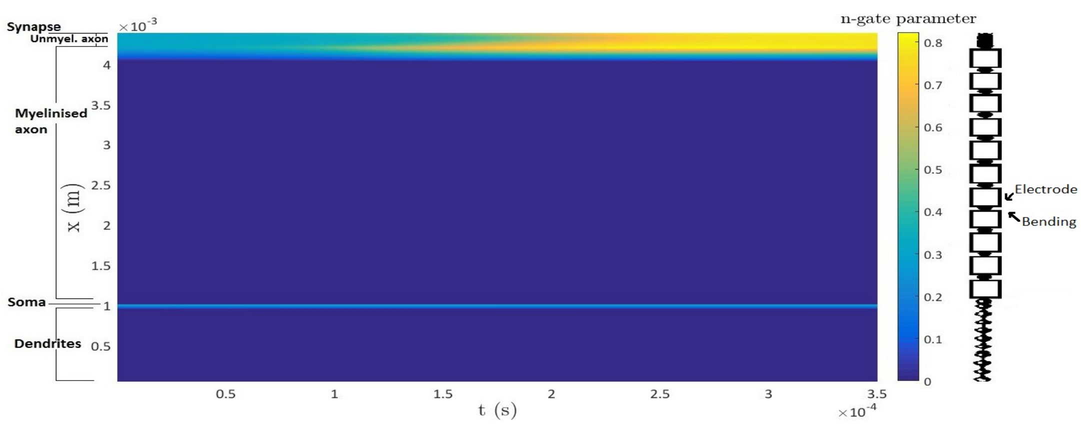

Figure A.34: Colour map of the n-gate parameter in time and space. The colours represent the value of n. The map is obtained by anode-make stimulation by a spherical electrode ($60V$) at $2mm$ from the centre of a bent (15°) neuron.

Part V

Bibliography

Bibliography

1. Benabid, A. L. Deep brain stimulation for ParkinsonâĂŹs disease. *Current opinion in neurobiology, Elsevier.*
2. Benabid, A. *et al.* Acute and long-term effects of subthalamic nucleus stimulation in Parkinson's disease. *Stereotactic and functional neurosurgery* **62,** 76–84 (1994).
3. Deuschl, G. *et al.* A randomized trial of deep-brain stimulation for Parkinson's disease. *New England Journal of Medicine* **355,** 896–908 (2006).
4. For Parkinson's Disease Study Group, D.-B. S. *et al.* Deep-brain stimulation of the subthalamic nucleus or the pars interna of the globus pallidus in Parkinson's disease. *The New England journal of medicine* **345,** 956 (2001).
5. Benabid, A. L. *et al.* Chronic electrical stimulation of the ventralis intermedius nucleus of the thalamus as a treatment of movement disorders. *Journal of neurosurgery* **84,** 203–214 (1996).
6. Kupsch, A. *et al.* Pallidal deep-brain stimulation in primary generalized or segmental dystonia. *New England Journal of Medicine* **355,** 1978–1990 (2006).
7. Vidailhet, M. *et al.* Bilateral deep-brain stimulation of the globus pallidus in primary generalized dystonia. *New England Journal of Medicine* **352,** 459–467 (2005).
8. Mayberg, H. S. *et al.* Deep brain stimulation for treatment-resistant depression. *Neuron* **45,** 651–660 (2005).
9. Nuttin, B. J. *et al.* Long-term electrical capsular stimulation in patients with obsessive-compulsive disorder. *Neurosurgery* **52,** 1263–1274 (2003).
10. Hodaie, M., Wennberg, R. A., Dostrovsky, J. O. & Lozano, A. M. Chronic anterior thalamus stimulation for intractable epilepsy. *Epilepsia* **43,** 603–608 (2002).
11. Iacono, M. I. *et al.* MIDA: a multimodal imaging-based detailed anatomical model of the human head and neck. *PloS one* **10,** e0124126 (2015).
12. Rattay, F. *Functional Electrical Stimulation of the Central Nervous System: Analysis of the Primarily Excited Structures* PhD thesis (Medical University of Vienna).
13. Maccabee, P., Amassian, V., Eberle, L. & Cracco, R. Magnetic coil stimulation of straight and bent amphibian and mammalian peripheral nerve in vitro: locus of excitation. *The Journal of Physiology* **460,** 201 (1993).
14. Nagarajan, S. S., Durand, M & Warman, E. N. Effects of induced electric fields on finite neuronal structures: a simulation study. *Biomedical Engineering, IEEE Transactions on* **40,** 1175–1188 (1993).

15. Roth, B. J. Mechanisms for electrical stimulation of excitable tissue. *Critical reviews in biomedical engineering* **22,** 253–305 (1993).

16. Chaturvedi, A., Foutz, T. J. & McIntyre, C. C. Current steering to activate targeted neural pathways during deep brain stimulation of the subthalamic region. *Brain stimulation* **5,** 369–377 (2012).

17. Schmidt, C. & van Rienen, U. Modeling the field distribution in deep brain stimulation: the influence of anisotropy of brain tissue. *Biomedical Engineering, IEEE Transactions on* **59,** 1583–1592 (2012).

18. Butson, C. R. & McIntyre, C. C. Role of electrode design on the volume of tissue activated during deep brain stimulation. *Journal of Neural Engineering* **3,** 1 (2005).

19. Sotiropoulos, S. N. & Steinmetz, P. N. Assessing the direct effects of deep brain stimulation using embedded axon models. *Journal of neural engineering* **4,** 107 (2007).

20. Yousif, N. & Liu, X. Investigating the depth electrode–brain interface in deep brain stimulation using finite element models with graded complexity in structure and solution. *Journal of neuroscience methods* **184,** 142–151 (2009).

21. Grant, P. F. & Lowery, M. M. Effect of dispersive conductivity and permittivity in volume conductor models of deep brain stimulation. *Biomedical Engineering, IEEE Transactions on* **57,** 2386–2393 (2010).

22. Butson, C. R., Maks, C. B. & McIntyre, C. C. Sources and effects of electrode impedance during deep brain stimulation. *Clinical Neurophysiology* **117,** 447–454 (2006).

23. Limousin, P. *et al.* Electrical stimulation of the subthalamic nucleus in advanced Parkinson's disease. *New England Journal of Medicine* **339,** 1105–1111 (1998).

24. Hamel, W *et al.* Deep brain stimulation of the subthalamic nucleus in ParkinsonâĂŹs disease: evaluation of active electrode contacts. *Journal of Neurology, Neurosurgery & Psychiatry* **74,** 1036–1046 (2003).

25. Nowinski, W. L., Belov, D., Pollak, P. & Benabid, A.-L. Statistical analysis of 168 bilateral subthalamic nucleus implantations by means of the probabilistic functional atlas. *Neurosurgery* **57,** 319–330 (2005).

26. Saint-Cyr, J. A. *et al.* Localization of clinically effective stimulating electrodes in the human subthalamic nucleus on magnetic resonance imaging. *Journal of neurosurgery* **97,** 1152–1166 (2002).

27. Starr, P. A. *et al.* Implantation of deep brain stimulators into subthalmic nucleus: technical approach and magnetic imaging-verified electrode locations. *Journal of neurosurgery* **97,** 370–387 (2002).

28. Voges, J. *et al.* Bilateral high-frequency stimulation in the subthalamic nucleus for the treatment of Parkinson disease: correlation of therapeutic effect with anatomical electrode position. *Journal of neurosurgery* **96,** 269–279 (2002).

29. Yelnik, J. *et al.* Localization of stimulating electrodes in patients with Parkinson disease by using a three-dimensional atlas-magnetic resonance imaging coregistration method. *Journal of neurosurgery* **99,** 89–99 (2003).

30. Zonenshayn, M., Sterio, D., Kelly, P. J., Rezai, A. R. & Beric, A. Location of the active contact within the subthalamic nucleus (STN) in the treatment of idiopathic Parkinson's disease. *Surgical neurology* **62,** 216–225 (2004).

31. Bossetti, C. A., Birdno, M. J. & Grill, W. M. Analysis of the quasi-static approximation for calculating potentials generated by neural stimulation. *Journal of neural engineering* **5,** 44 (2007).

32. Gimsa, J. *et al.* Choosing electrodes for deep brain stimulation experiments–electrochemical considerations. *Journal of neuroscience methods* **142,** 251–265 (2005).

33. Hasgall, P., Neufeld, E, Gosselin, M., Klingenböck, A & Kuster, N. ITâĂŹIS Database for thermal and electromagnetic parameters of biological tissues. *ITâĂŹIS Foundation website* (2012).

34. Geeter, N. D. *A Diffusion Tensor-Based Computational Model for Transcranial Magnetic Stimulation: from Macroscopic Fields to Neuronal Membrane Potentials* PhD thesis (University of Ghent, Technologiepark 913 9052 Zwijnaarde, Belgium, 2014-2015).

35. Commons, W. *Schematic representation of neuron* :File: `Neuron-no labels2.png`. <`https://upload.wikimedia.org/wikipedia/commons/thumb/b/bc/Neuron_Hand-tuned.svg/..2000px-Neuron_Hand-tuned.svg.png`> (2009).

36. Roth, B. J. & Basser, P. J. A model of the stimulation of a nerve fiber by electromagnetic induction. *Biomedical Engineering, IEEE Transactions on* **37,** 588–597 (1990).

37. Rattay, F. Analysis of models for extracellular fiber stimulation. *Biomedical Engineering, IEEE Transactions on* **36,** 676–682 (1989).

38. Varghese, A. Membrane models. *The Biomedical Engineering Handbook,* 139–161 (1995).

39. Hodgkin, A. L. & Huxley, A. F. A quantitative description of membrane current and its application to conduction and excitation in nerve. *The Journal of Physiology* **177.**

40. Nelson, M. E. Electrophysiological models. *Databasing the brain: from data to knowledge. New York: Wiley* (2004).

41. Chiu, S., Ritchie, J., Rogart, R. & Stagg, D. A quantitative description of membrane currents in rabbit myelinated nerve. *The Journal of Physiology* **292,** 149 (1979).

42. Sweeney, J., Mortimer, J. & Durand, D. *Modeling of mammalian myelinated nerve for functional neuromuscular stimulation* in *IEEE 9th Annual Conference of the Engineering in Medicine and Biology Society* **3** (1987), 1577–1578.

43. Frankenhaeuser, B. Sodium permeability in toad nerve and in squid nerve. *The Journal of physiology* **152,** 159 (1960).

44. Schwarz, J. R. & Eikhof, G. Na currents and action potentials in rat myelinated nerve fibres at 20 and 37 C. *Pflügers Archiv* **409,** 569–577 (1987).

45. Schwarz, J. R., Reid, G. & Bostock, H. Action potentials and membrane currents in the human node of Ranvier. *Pflügers Archiv* **430,** 283–292 (1995).

46. Koch, C. & Segev, I. *Methods in neuronal modeling: from ions to networks* (MIT press, 1998).

47. Rattay, F. Ways to approximate current-distance relations for electrically stimulated fibers. *Journal of theoretical biology* **125,** 339–349 (1987).

48. Ranck, J. B. Which elements are excited in electrical stimulation of mammalian central nervous system: a review. *Brain research* **98,** 417–440 (1975).

49. Fang, Z. P. & Mortimer, J. T. Selective activation of small motor axons by quasitrapezoidal current pulses. *Biomedical Engineering, IEEE Transactions on* **38,** 168–174 (1991).

50. Kandel, E. R., Schwartz, J. H., Jessell, T. M., *et al. Principles of neural science* (McGraw-hill New York, 2000).

51. Miranda, P. C., Correia, L, Salvador, R & Basser, P. Tissue heterogeneity as a mechanism for localized neural stimulation by applied electric fields. *Physics in medicine and biology* **52,** 5603 (2007).

52. Silva, S, Basser, P. & Miranda, P. Elucidating the mechanisms and loci of neuronal excitation by transcranial magnetic stimulation using a finite element model of a cortical sulcus. *Clinical neurophysiology* **119,** 2405–2413 (2008).

53. Salvador, R, Silva, S, Basser, P. & Miranda, P. Determining which mechanisms lead to activation in the motor cortex: a modeling study of transcranial magnetic stimulation using realistic stimulus waveforms and sulcal geometry. *Clinical neurophysiology* **122,** 748–758 (2011).

54. Tranchina, D & Nicholson, C. A model for the polarization of neurons by extrinsically applied electric fields. *Biophysical journal* **50,** 1139 (1986).

55. Amassian, V. E., Eberle, L., Maccabee, P. J. & Cracco, R. Q. Modelling magnetic coil excitation of human cerebral cortex with a peripheral nerve immersed in a brain-shaped volume conductor: the significance of fiber bending in excitation. *Electroencephalography and Clinical Neurophysiology/Evoked Potentials Section* **85,** 291–301 (1992).

56. Plonsey, R. & Altman, K. W. Electrical stimulation of excitable cells-a model approach. *Proceedings of the IEEE* **76,** 1122–1129 (1988).

57. Rubinstein, J. Axon termination conditions for electrical stimulation. *Biomedical Engineering, IEEE Transactions on* **40,** 654–663 (1993).

58. Altman, K. & Plonsey, R. Analysis of excitable cell activation: relative effects of external electrical stimuli. *Medical and Biological Engineering and Computing* **28,** 574–580 (1990).

59. Nagarajan, S. S. & Durand, D. *Determination of excitation sites during magnetic stimulation of nerve fibers* in *Engineering in Medicine and Biology Society, 1992 14th Annual International Conference of the IEEE* **4** (1992), 1426–1427.

60. Reilly, J. P., Freeman, V. T. & Larkin, W. D. Sensory effects of transient electrical stimulation-evaluation with a neuroelectric model. *Biomedical Engineering, IEEE Transactions on,* 1001–1011 (1985).

61. Reilly, J. Peripheral nerve stimulation by induced electric currents: exposure to time-varying magnetic fields. *Medical and Biological Engineering and Computing* **27,** 101–110 (1989).

62. Kumar, R *et al.* Double-blind evaluation of subthalamic nucleus deep brain stimulation in advanced Parkinson's disease. *Neurology* **51,** 850–855 (1998).

63. Kleiner-Fisman, G. *et al.* Subthalamic nucleus deep brain stimulation: Summary and meta-analysis of outcomes. *Movement Disorders* **21,** S290–S304 (2006).